Assessment of solvent capsule-based healing for woven fibre-reinforced epoxies

THÈSE N^{O} 6576 (2015)

PRÉSENTÉE LE 2 AVRIL 2015

À LA FACULTÉ DES SCIENCES ET TECHNIQUES DE L'INGÉNIEUR
LABORATOIRE DE TECHNOLOGIE DES COMPOSITES ET POLYMÈRES
PROGRAMME DOCTORAL EN SCIENCE ET GÉNIE DES MATÉRIAUX

ÉCOLE POLYTECHNIQUE FÉDÉRALE DE LAUSANNE

POUR L'OBTENTION DU GRADE DE DOCTEUR ÈS SCIENCES

PAR

Erica MANFREDI

acceptée sur proposition du jury:

Prof. A. Fontcuberta i Morral, présidente du jury
Prof. V. Michaud, directrice de thèse
Prof. I. Bond, rapporteur
Prof. I. Botsis, rapporteur
Dr F. Klunker, rapporteur

ÉCOLE POLYTECHNIQUE
FÉDÉRALE DE LAUSANNE

Suisse
2015

To Giuliana and Maria Michela

Au bonheur suisse

Acknowledgements

The present work was carried out at the Laboratoire de Technologie des Composites et Polymères (LTC) at the École Polytechnique Fédérale de Lausanne (EPFL, Switzerland) and funded by the Swiss National Science Foundation (SNF 200020-138213).

I would like to mention the most important people who have crossed my "Swiss path" during these years of research and whom without, everything would have been much more difficult. I believe that good science is also based on good human relationships and this is not simply expressed for the formality of the page.

First and foremost, I thank Prof. Jan-Anders Månson for giving me the precious opportunity to move to Switzerland four years ago to work at EPFL. I am grateful to have worked in such an important university with such an encouraging scientific environment. My significant appreciation then goes to my thesis director, Prof. Véronique Michaud: she has been able to simultaneously give me great freedom during my research and guide and supervise me in a very professional, friendly and honest way throughout this work. I would also like to thank Dr. Yves Leterrier, Dr. Christopher Plummer, Prof. Ioannis Botsis, Dr. Jericho Moll and Dr. Brennan Bailey for providing useful advice during the progress examination sessions. Moreover, I thank the members of the thesis committee Prof. Ian Bond, Dr. Florian Klunker and Prof. Anna Fontcuberta i Morral for the constructive discussions and corrections of the manuscript.

Much of this research would not have been possible without the participation of other EPFL laboratories, so I would like to send my acknowledgements to the Powder Technology Laboratory and Carlos Morais for allowing me to use the TGA and PCS, the Interdisciplinary Center for Electron Microscopy with Gregoire Baroz and Danièle Laub for use of the SEM and ultramicrotomy. I would also like to thank the Laboratory of Mechanical Metallurgy for the use of the capsule compression setup with the help of Jérôme Krebs and Suzanne Verheyden, the Laboratory of Biomechanical Orthopedics and Ulrike Kettenberger for X-ray micro-computed imaging, the Polymer Laboratory and Alessandra Apicella for AFM imaging, the Laboratory of Construction Materials and finally the Atelier de l'Institut des matériaux for their endless technical help.

Even more importantly, the outcome of this thesis could not be achieved without the great work and input of my collaborative "self-healing" laboratory mates Sam Neuser and Amaël Cohades. Together, we accomplished results in a quicker and more effective way.

I appreciate your commitment.

I am also grateful to all of the students including K. Markstedt, M. Ratte, M. Demierre, V. Lavanchy, I. Richard and C. Guidoux for their contribution to the work.

My time at LTC has been very pleasant thanks to old and new colleagues that provided such a good vibe in the lab and made my everyday life enjoyable, helped and advised me for technical troubles, and shared special moments with me, becoming, above all, my friends. I would like to specifically mention Robert W. and Azadeh as perfect office mates, Mr. Rob and Paul for their priceless help in the composite processing, Fabiane as my best week-flatmate, Fabien, Florian, Alessandra and Marina.

Finally, I feel extremely fortunate to be able to rely on my family and friends' continuous support, even more so from afar. For all your encouragements -and for many other things- I will never be able to thank you enough.

Abstract

Structural fibre-reinforced composites based on brittle matrices such as epoxy resins may be subject to short-term subcritical matrix damage that develops with time to the point where it may compromise the integrity of the structure. Currently, components that have been damaged at the microscale are usually inspected and, depending on the extent of the damage, repaired with patches or entirely replaced. Self-healing functionality would prevent development of such damage by repairing it as soon as it appears, thereby increasing the service life of the material.

Among the many potential methods for introducing self-healing capacity to epoxy resins, incorporation of solvent-filled capsules is particularly promising. Cracks cause the capsules to break, releasing a solvent that is able to swell the crack faces and induce reaction of residual monomer and/or crosslinkable functional groups intentionally left by under-curing the matrix. Thus, a model system based on ethyl phenylacetate (EPA) has been shown to provide up to approximately 90% efficiency in recovering fracture toughness, and to effectively block fatigue crack propagation in pure epoxy resin.

The present thesis focuses on the integration of a EPA solvent capsule-based healing system into a glass fibre-reinforced epoxy and the assessment of its effectiveness in repairing static interply damage.

EPA-filled capsules with diameters in the range of 90-250 μm were produced using an oil-in-water emulsion technique and characterized in terms of their thermal stability and mechanical properties. Pure urea-formaldehyde (UF) as well as polyurethane/urea-formaldehyde (PU/UF) double wall capsule shell materials were analysed, showing that the wall thickness of pure UF capsules is independent of their diameter, whereas that of PU/UF capsules is 4 to 6 times greater and scales with the capsule diameter until a saturation value. The modulus of these shell materials was quantified using compression test and an analytical model, and found to range from 1 to 4 GPa depending on the amount of PU content in the shell composition. Bursting forces varied from 5 to 25 mN depending on the shell composition and diameter, thus providing a range of shell compositions to select from in order to tune the capsule behaviour.

The integration of the capsules into the composite was carried out by dispersing them manually onto the reinforcement textile prior to processing. During this phase, the optimum capsule size range, position and concentration could be selected to fit in the inter-

stices and survive textile packing. Textile packing properties were tested in compression; the presence of capsules led to a decrease of the reinforcement volume fraction at a given applied load value, in particular at low packing loads, and affected the usual power law behaviour of a textile in compression, up to the rupture of the capsules. Longitudinal permeability was also increased by a factor of 6 to 8 in presence of capsules for a given reinforcement volume fraction, whereas the transverse permeability was not greatly affected.

A capsule-containing fibre-reinforced epoxy material was then produced using a suitably adapted processing protocol. Vacuum assisted resin infusion moulding (VARIM) was chosen as an industrially relevant, yet adaptable processing route. Priority was given to industrially relevant fibre volume fractions of approximately 50% and to optimizing processing parameters such as the lay-out and vacuum pressure difference. Healing assessment was carried out for cracks propagated in modes I and II and due to low energy impact loading. No crack healing was observed in the composites. This was mainly attributed to a combination of significant interfacial debonding, leaving fibre material that cannot react to the solvent apparent on the crack surface, and to a drop of 80-95% in solvent diffusion kinetics into the fibre-reinforced epoxy as compared with the unreinforced epoxy. However, the solvent-based system appeared promising for the repair of cracks in resin-rich joints between composites, where partial healing was shown to take place. A critical evaluation of healing systems adapted to composite materials concluded this study. Release of an adhesive system instead of a solvent seems better suited, although it also presents drawbacks and is often more costly to implement. Approaches based on the introduction of thermoplastics particles could provide better healing performance and be integrated within the composite using equivalent manufacturing protocols to those developed in the present work.

Keywords Self-healing, solvent healing, capsules, fibre-reinforced polymers, swelling, VARIM, DCB.

Résumé

Les composites fibreux structuraux comprenant une matrice fragile comme les résines époxydes peuvent être sujets à un endommagement sous-critique de la matrice, qui se propage avec le temps et peut finalement compromettre l'intégrité de la structure. Actuellement, les composants qui ont été endommagés à l'échelle microscopique sont inspectés et, selon l'étendue du dommage, sont réparés avec ajout de matière ou remplacés. Une fonctionnalité d'autoréparation permettrait d'empêcher la propagation d'un tel endommagement en le réparant dès son apparition, conduisant à une augmentation de la durée de vie de la structure. Parmi les méthodes disponibles pour introduire la capacité d'autoréparation au sein des matrices époxydes, l'incorporation de capsules remplies de solvant est particulièrement prometteuse. Les fissures entrainent la rupture de la capsule, relâchant un solvant qui peut faire gonfler les faces de la fissure et faire réagir le monomère résiduel et /ou les groupes fonctionnels laissés intentionnellement dans la matrice sous-réticulée. Ainsi, un système modèle basé sur le phénylacétate d'éthyle (EPA) a démontré environ 90% de recouvrement de la ténacité, et le blocage de la propagation de fissures de fatigue dans la résine époxyde pure. Le présent travail de thèse porte sur l'intégration d'un système auto-réparant à base de solvant EPA dans un composite renforcé de fibres de verre et à matrice époxyde, et sur l'évaluation de sa capacité à réparer un endommagement statique interlaminaire. Des capsules remplies d'EPA de diamètre entre 90 et 250 µm ont été produites avec une technique d'émulsion huile dans eau, et caractérisées en termes de leur stabilité thermique et leurs propriétés mécaniques. Des capsules en Formaldéhyde d'Urée (UF) et des capsules à double paroi en UF-Polyuréthane (PU) ont été analysées, montrant que l'épaisseur de paroi des capsules UF est indépendante de leur diamètre, alors que celle des capsules UF-PU est de 4 à 6 fois plus grande et augmente avec le diamètre des capsules jusqu'à une valeur de saturation. Le module des parois a été quantifié par des tests de compression associés à un modèle analytique, et se situait entre 1 et 4 GPa en fonction de la quantité de PU dans la formulation. Les forces d'éclatement se situaient entre 5 et 25 mN en fonction de la composition et de la taille des particules, fournissant ainsi une gamme de composition dans lesquelles sélectionner les capsules pour adapter leur comportement. Les capsules ont été intégrées dans les composites en les dispersant manuellement sur le textile de renfort avant la mise en oeuvre. Pendant cette phase, les gammes de taille de capsule, position et concentration ont été optimisées pour

que celles-ci puissent se loger dans les interstices du tissu et survivre à leur compression. Les propriétés de compression du renfort ont été testées; la présence de capsules conduit à une diminution de la fraction volumique de renfort à pression équivalente, en particulier aux faibles pressions, et affecte le comportement en loi puissance habituellement observé, jusqu'à la rupture des capsules. La perméabilité longitudinale augmente d'un facteur 6 à 8 en présence de capsules pour une fraction volumique de renfort donnée, alors que la perméabilité transverse n'est pas grandement affectée. Un composite fibreux à matrice époxyde a ensuite été produit, en utilisant un protocole de mise en oeuvre adapté. La mise en oeuvre par infusion assistée sous vide (VARIM) a été sélectionnée car c'est un procédé d'intérêt industriel, quoique facilement adaptable. En priorité, des factions volumiques de renfort d'environ 50%, intéressantes pour les applications pratiques ont été choisies, et les paramètres de mise en oeuvre comme l'empilement des couches et la pression de vide ont été optimisés. L'étude de l'autoréparation a été conduite sur les cas de fissures se propageant en mode I et mode II et après impacts. Aucune réparation des fissures n'a été constatée dans les composites. En effet, ceci résulte principalement d'une combinaison de délamination interfaciale importante, laissant de nombreuses fibres apparentes qui ne peuvent gonfler dans le solvant, avec une réduction drastique de 80 à 95% de la cinétique de diffusion du solvant dans le composite comparé à la matrice pure. En revanche, le système à base de solvant est plus prometteur pour réparer des fissures dans des joints riches en résine entre deux composites, où l'on a pu constater une réparation partielle. Une évaluation critique des systèmes d'autoréparation adapté aux composite fibreux a conclu cette étude. L'écoulement d'un système adhésif au lieu d'un solvant semble plus approprié, bien qu'il présente aussi des inconvénients et est souvent plus coûteux à implémenter. Les approches basées sur l'incorporation de particules thermoplastiques pourraient amener à une meilleure performance, et ces systèmes pourraient être intégrés en utilisant des protocoles de mise en oeuvre hérités de ceux de la présente étude.

Mots clef Autoréparation, matériaux auto-rèparants, capsules, polymères renforcés de fibres, gonflement, VARIM, DCB.

Riassunto

I compositi a matrice epossidica e fibre lunghe, destinati ad applicazioni strutturali, sono particolarmente soggetti a danneggiamenti subcritici, quali microfessurazioni della matrice, che possono propagare e di conseguenza compromettere l'integrità della struttura. Oggigiorno, i componenti che presentano micro-cricche sono di solito sottoposti ad ispezioni e, a seconda dell'entità del danno, riparati con speciali rattoppi o completamente sostituiti. Una capacità cosiddetta auto-cicatrizzante permetterebbe una riparazione del danno durante la fase stessa di formazione, evitandone il propagarsi. Questo consentirebbe un'estensione della vita del materiale.

Tra i numerosi approcci di auto-riparazione per le resine epossidiche si distingue il sistema a base di capsule contenenti solvente. Le capsule, il cui guscio viene fratturato da una cricca in propagazione, rilasciano un solvente che diffonde nel materiale attraverso il piano della cricca, innescandone il rigonfiamento e la consequente reazione di gruppi funzionali di monomero e indurente (appositamente lasciati nel materiale attraverso un'incompleta post-reticolazione). Facendo uso di etil fenilacetato (EPA) come solvente, per resine non rinforzate, sono state dimostrate efficienze di riparazione del 90%, calcolate sulla base del recupero delle proprietà di tenacità. Nondimeno, tale sistema si è rivelato efficace nel bloccare la propagazione di cricche di fatica.

Soggetto della presente tesi è l'integrazione di questo sistema di riparazione a base di solvente EPA in compositi a matrice epossidica e fibre lunghe di vetro. In particolare, viene valutata l'efficacia del sistema nel riparare cricche interlaminari indotte da carichi statici.

In una prima fase, le capsule contententi EPA (con diametri di 90-250 μm) sono state prodotte in emulsioni di tipo acqua-olio e sono state analizzate la loro stabilità termica e le loro proprietà meccaniche. In particolare, sono state analizzate capsule a guscio semplice di urea-formaldeide (UF) e guscio doppio di poliuretano/urea-formaldeide (PU/UF). E' stato dimostrato che lo spessore del guscio semplice è costante, mentre lo spessore del guscio doppio è proporzionale al diametro delle capsule, fino ad un valore di saturazione. Inoltre, il modulo dei gusci è stato quantificato tramite esperimenti a compressione con l'uso di un modello analitico. Valori tra 1 e 4 GPa sono stati misurati per capsule a guscio doppio, variabili a seconda della concentrazione di PU presente nel guscio. La forze massime a rottura di tali capsule sono state pure misurate variabili tra 5 e 25 mN,

a seconda della composizione del guscio e del diametro della capsula.

L'integrazione delle capsule nel composito è stata poi effettuata manualmente funzionalizzando i tessuti di fibra in una fase precedente al processo. Sono state selezionate in questa fase le dimensioni, la posizione e la concentrazione ottimali delle capsule, affinché queste possano inserirsi negli interstizi del tessuto e sopravvivere intatte alle fase di preparazione e processo. Si è in seguito dimostrato come le capsule modifichino le proprietà di impacchettamento dei tessuti di fibra; in particolare, la presenza delle capsule ha portato ad una diminuzione della frazione volumica di fibre per uno dato carico a compressione applicato, nonché ad una modifica della legge di potenza che di solito descrive le proprietà ad impacchettamento di tessuti non funzionalizzati. Nondimeno, la presenza delle capsule ha influenzato anche la permeabilità longitudinale dei tessuti, aumentandola da 6 a 8 volte, per una data frazione volumica di fibre. La permeabilità transversa, al contrario, è risultata indipendente dalla concentrazione delle capsule.

La produzione del composito contenente le capsule è stata poi ottenuta tramite un processo di rilevanza industriale quale l'infusione sotto vuoto (VARIM). Alcuni parametri di tale tecnica, quali la configurazione ed il grado di vuoto, sono stati ottimizzati allo scopo di considerare la presenza delle capsule durante le fasi di preparazione ed impregnazione. E' stato possibile ottenere compositi con valori realistici di frazioni volumiche di fibre (50 vol%). In seguito, è stata eseguita la valutazione delle capacità riparanti per cricche interlaminari modo I e II e dovute a impatti. Nel caso di delaminazioni modo I con significativo debonding interfacciale, tale sistema (basato su solvente) si é rivelato inefficace. La causa è stata attribuita principalmente alla presenza di significativo debonding e alla scarsa capacità di diffusione del solvente nel materiale epossidico rinforzato, nettamente inferiore (di circa l'80-95%) rispetto al materiale epossidico non rinforzato. Tuttavia, migliori risultati di riparazione sono stati dimostrati per cricche in giunti tra compositi.

Una ricerca bibliografica critica di sistemi di auto-riparazione alternativi, adatti per materiali compositi, ha concluso il presente lavoro. Questa è stata effettuata con l'intenzione di individuare approcci in grado di garantire efficienze di auto-riparazione maggiori e possibilmente integrabili nel composito attraverso protocolli di processo equivalenti a quelli qui sviluppati. Un esempio si è basato su sistemi basati su particelle termoplastiche.

Parole chiave Auto-riparazione, riparazione tramite solvente, capsule, polimeri rinforzati, rigonfiamento, VARIM, DCB.

Contents

Chapter 1

Introduction & objectives

1.1 Motivation

In the last century, composites have become predominant materials for high performance structures, often as substitutes to metals. In the case of composites with a thermoset polymeric matrix, their development has been driven by the need for stiff structural materials with lower weight than traditional metallic counterparts. Another important advantage lies in the possibility of a "flexible design" that enables tailoring of the material characteristics in order to achieve specific final properties, which can be anisotropic. Widespread applications of these materials mainly include aerospace, energy generation, sport and transportation (including automotive, marine and rail) engineering.

Although composites present these advantages, several technical drawbacks are still limiting their growth. First, fibre-reinforced thermosets are significantly brittle, are easily affected by delamination and other forms of matrix microcracking (due to low energy impact events), other types of thermomechanical loading and manufacturing flaws that may prematurely affect the material. These damaged areas are often difficult to detect (visually or via nondestructive testing techniques) and, if not repaired, they can propagate over further loading. Second, cost-efficiency is a crucial requirement: the processing steps should reduce cycle times and costs of special moulds and equipments (usually requested for high temperature and pressure techniques), the damage detection and the costs of maintenance-during-service should also be quantified and taken into account.

Currently, solving of these problems is the main driver for further research and improvements, related to (i) fast and possibly automated processing, (ii) low pressure and temperature processing routes, (iii) tolerant systems with high fibre volume fraction, (iv) manufacturing reproducibility, (v) monitoring techniques during both process and service, (vi) autonomous repair capabilities.

Concerning the latter, the concept of introducing an autonomous encapsulated repair capability into composite materials was born from these considerations approximately

15 years ago, when Kessler *et al.* presented the first structural fibre self-healing composite [1, 2]. The idea was taken from the previously developed self-healing thermoset neat polymers [3] and initial concepts of Dry *et al.* [4], which used hollow repair fibres. This category of new self-healing materials was named as *extrinsic*, meaning that the self-healing functionality was given by a system extrinsically introduced into the material. This concept was inspired from a "bleeding" biological approach to repair, which consists in actively carrying the healing agent to the site of injury and fix it to a certain extent. Many different studies followed, varying the healing system (*e.g.* capsule or microvascular-based), the type of processing or the targeted damage to heal. In parallel, another widely studied approach were *intrinsic* self-healing materials, mostly based on thermoplastics, with healing phenomena occurring at a molecular level, as initiated by Chen *et al.* [5], for instance. However, among these systems, few were used so far for composites.

Once the feasibility of the self-healing functionality is demonstrated on a matrix system, the challenge remains to improve the integration within fibre-reinforced materials without decreasing virgin properties, to adapt the processing routes to ensure it survives and remains in position during manufacturing and to verify its actual effectiveness.

1.2 Scope statement

In this work, specifically dealing with glass fibre-reinforced thermosets with approximately 50 vol% fraction reinforcement, we investigated an extrinsic capsule-based system, based on solvent-containing capsules that burst and lead to solvent diffusion and matrix swelling as well as on the presence of latent functionalities. The purpose consisted of achieving the integration of such a system within a fibre-reinforced material and assessing its effectiveness as autonomous repairing functionality for a certain type of damage, namely delamination. The present solvent-based healing system was chosen

- ▷ as a model, as it was widely studied for neat thermosets;
- ▷ since it represents a suitable system for achieving the most autonomous healing in structural composites.

Although a specific system was selected, most of the work resulted applicable to any other particle-based system.

The solvent healing system has been quite widely studied in the past years [6–13]. Specifically, recent work investigated whether the system was compatible with a thermoset matrix (epoxy), chemically stable during storage and service (high shelf life), able to withstand the high temperatures during curing and/or service, easily incorporated within the neat polymer and neither toxic nor too expensive. Last but not least, the influence of the incorporated healing system on the virgin mechanical properties was studied.

Here, the possible use of such a healing system for fibre-reinforced thermosets was investigated. New requirements and scope statements arose, in particular:

- ▷ the matrix and fibre reinforcement should be selected among those which are industrially and widely used, without unconventional features (*i.e.* weaving);
- ▷ the system should be easily integrated within the composite, through functionalisation of the fibre-reinforcement or of the impregnating matrix, without cumbersome steps;
- ▷ the system should not significantly modify the packing and permeability properties of a specific stack of fibre reinforcement, in the presence of the impregnating thermoset matrix;
- ▷ as a consequence, the system should be compatible with a standard, or only slightly adapted, processing technique, namely Vacuum-assisted resin infusion molding (VARIM). Applied temperatures and pressures and the reproducibility should be taken into account;
- ▷ the healing system should survive the processing step, be inert within the composite and not significantly alter the initial virgin properties;
- ▷ one type of damage being selected, the healing mechanism should be as effective in the presence of reinforcing fibres as it is for the neat polymer. Ideally, 100% healing efficiency should be reached for at least one damage event and in an autonomous way.

Moreover, research solutions, even in an embryonic step of "proof of concept", should be compatible with further larger scale industrial interests. Ideally, two requirements are essential: (i) the cost of the materials should equal that of standard structural composites (or possible increased costs due to added functionalities should be justified by a reduction in maintenance and repairing costs); (ii) the time for the manufacturing should be minimised, relative to conventional composites manufactured with the same technique.

1.3 Thesis methodology

Manufacturing a glass fibre-reinforced thermoset containing the selected healing functionality which is autonomously able to repair a certain damage was the final goal of the present work. Respecting the requirements stated above led to the workplan as reported in Figure 1.1.

In a first phase (1), a literature review was planned; moreover, the fibre-reinforcement and the processing technique were selected. A reproducible open-mould processing, belonging to the category of Liquid Composite Molding technique, such as VARIM, was

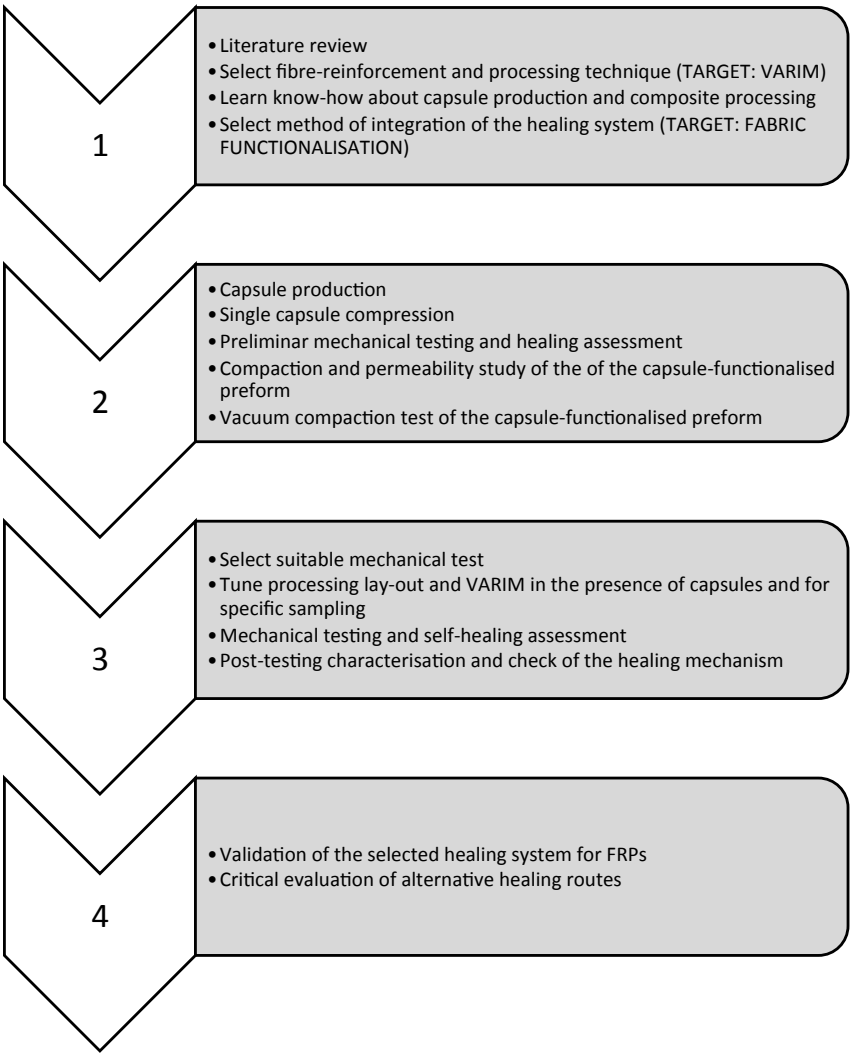

Figure 1.1: Workplan of the thesis.

targeted. The know-how about capsule production and composite processing had to be learnt. A method to introduce the healing system within the composite prior or during processing was then investigated and validated. A functionalisation of dry fabrics with the encapsulated healing agent was targeted, rather than the introduction of capsules into the matrix prior to the impregnation process, which might lead to an increase of matrix viscosity and poor wetting, as well as a change of the fabric compressibility and permeability.

A second step (2) consisted in preliminary studies mainly dedicated to understand different properties. Namely, investigations were carried out about (i) which robustness the encapsulated healing agent presents (for other capsule characterisation we referred to [14]), (ii) whether and how the presence of the healing agent modifies the compaction behavior of the selected dry fabrics as well as the permeability towards the selected impregnating matrix, (iii) which level of vacuum during manufacturing should be applied to ensure the survival of the healing system. Concurrently, preliminary investigations

concerning the effectiveness of the healing system for repairing damage induced through compression-after-impact (CAI) test was also carried out.

Therefore, once these informations were gained, (3) an appropriate mechanical test was selected in order to assess the healing performance in a more adapted way than by CAI test. First, tuning the processing lay-out, the technique and selecting the matrix system suitable with the presence of the healing agent was necessary prior to carry on the manufacturing step. The processing had then to be adapted to the case of capsule-functionalised preforms. Once the panels were produced, mechanical testing was performed by following an adapted procedure for investigating the influence of the healing system on the virgin properties and for assessing the healing efficiency. According to the results achieved, post-testing characterisation such as fracture surface analysis and swelling tests were carried out in order to probe the healing mechanism.

This led to (4) an assessment of the limitations of such a healing concept for composite materials and to a critical evaluation of alternative routes for better healing performances.

1.4 Outline

The present manuscript will first offer a literature overview (§ 2) concerning existing extrinsic healing systems for polymers, in particular capsule-based ones. After that, materials and methods used for the present work will be detailed in § 3. Three main chapters describing the obtained experimental results will follow. Specifically, § 4 will present the results related to the characterisation of solvent-filled polyurethane/urea-formaldehyde (PU/UF) core-shell capsules, § 5 to the preliminar assessment of healing through CAI testing, § 6 to the packing and permeability properties of woven fabrics functionalised with those capsules and § 7 to the assessment of the solvent healing for VARIM-processed composites. The final chapters § 8 and 9 will convey conclusions on the present solvent capsule-based system and perspectives on alternative healing routes applicable to fibre-reinforced polymers using equivalent manufacturing routes and aiming at the improvement of the efficiency.

Chapter 2

State of the art

The aim of this chapter is to present a literature review concerning the domains relevant to this work: Section 2.1 will be dedicated to briefly describe damage mechanisms in fibre-reinforced polymers (FRPs), Section 2.2 will give an overview of extrinsic self-healing materials, with a particular focus on the capsule pioneering system and on the solvent capsule system, which is the object of study in the present work. Finally, Section 2.3 will explore how the healing efficiency is usually characterised and Section 2.4 which are the key points when a healing system has to be integrated in FRPs rather than in neat polymers.

2.1 Damage in fibre-reinforced polymers (FRPs)

Despite the advantages of structural composites (such as lightweight, high strength and stiffness), some limitations remain mainly in the case of brittle thermoset matrices, in particular the susceptibility to various forms of microcracking. This damage arises when the composite is subject to excessive loading (tensile or low energy impact, static or fatigue), or to changes in temperature or both. The material is not able to plastically deform and reacts to stresses only by energy absorption via damage creation. Most common observations of microcracking, as shown in Figure 2.1, are detailed as follows.

Interlaminar cracks (delamination) They occur when a gap forms between two plies of different fibre orientation. They are often due to faulty bonding between plies, related to (i) weak interfaces between the matrix and the fibres, due to poor wetting and impregnation and unclean manufacturing conditions [16, 17], (ii) the matrix strength and its void content [18,19], as well as the thickness of the resin-rich areas, (iii) residual stresses linked to the manufacturing process and (iv) the ply stacking sequence. Delaminations have an unique orientation, which depends on many factors such as the type of loading. This field has been widely investigated [20–22].

Intralaminar (or ply) cracks The are either longitudinal or transverse. Their presence might lead to the composite failure and compromise the integrity of the structure, as a consequence of (i) degradation of the composite thermomechanical properties (moduli, Poisson ratio and thermal coefficients) and (ii) nucleation of worse forms of damage, such as delaminations, fibre breaks, creation of pathways for corrosive liquids [23,24]. A feature of longitudinal intralaminar fracture is the presence of large-scale bridging.

Translaminar cracks The main form consists in the fibre rupture, mainly occurring when loading is in the fibre direction and depending on the fibre properties and, at some extent, on the energy transfer between the fibre and the matrix [15]. Translaminar cracks commonly translate into a high amount of energy dissipation compared to intralaminar and interlaminar ones.

Localised subsurface damage It is commonly named barely visible impact damage (BVID) and is a specific form of intralaminar microcracking which can be found in the case of impact loading for fibre-reinforced materials, often carbon fibre-reinforced toughened epoxy. This kind of damage originates from low energy impact loads, whereas the material is able to bear high energy loads under gross failure conditions [25].

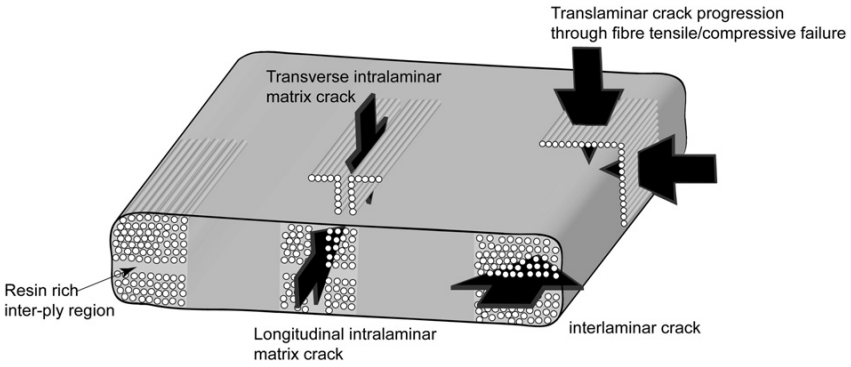

Figure 2.1: Different modes of laminate failures [15].

Main types of delaminations and intramatrix cracking can be listed as shown in Table 2.1 [26].

Moreover, an exhaustive review by Prof. J. A. Nairn [23] examines features of intralaminar microcracking as the most common form of damage in cross-ply laminates, according to the fact that cracking in 90° plies during axial loading (either tensile, fatigue or thermal [27]) in the 0° direction is the most frequent experimental observation. For a certain cross-ply laminate $[0_n/90_m]_s$ or $[90_n/0_m]_s$, several factors influence initiation and propagation of one or multiple cracking phenomena:

- ▷ 90° PLIES THICKNESS: as 90° plies thickness decreases, the strain to initiate microcracking increases (Figure 2.2); for thick 90° plies (in comparison with 0° supporting

Delaminations	**Matrix cracks**	**Holes**
Bearing surface damage	Bearing surface damage	Bearing surface damage
Blistering	Contamination	Crushing
Corner/Edge splitting	Corner/Edge crack	Cuts and scratches
Corner radius delamination	Cracks	Fastener holes
Delamination	Edge damage	Fibre kinks
Unbond or debond	Matrix cracking	Fracture
Edge damage	Matrix crazing	Holes and penetration
Fastener holes	Porosity	Reworked areas
Fibre/matrix debond	Translaminar cracks	Surface damage
Holes and penetration	Voids	
Pills or fuzz balls		
Surface swelling		

Table 2.1: Composites defects types categorised by Bull [26].

plies) microcracks are fracture events with an instantaneous propagation over the entire cross-section, for thin plies microcracks propagation is controlled or could be entirely suppressed. This phenomenon is not predicted by the "first-ply failure theory" (the first ply cracks or fails as soon as the strain in that ply reaches its strain to failure), for which the strain to failure seems independent of the ply thickness.

▷ STACKING SEQUENCE AND SUPPORTING 0° PLIES THICKNESS: in case of multiple microcracking, crack density is a function of the applied stress and it increases as the stress increases, until reaching a saturation value, which is inversely proportional to the 90° plies thickness (Figure 2.3). However, the onset of the curve, which represents the crack initiation, increases as the 90° plies thickness decreases (in thin 90° ply groups, as mentioned before, microcracking might also be suppressed). Furthermore, the initial rate depends on manufacture defects and statistical inhomogeneities of the material and its broadening has been associated with the statistical variability of the laminate. These curves have also been found influenced by the stacking plies sequence and by the 0° supporting plies thickness, that is:

- microcracking starts sooner in $[90_n/0_m]_s$ than in $[0_n/90_m]_s$, but $[0_n/90_m]_s$ laminates eventually develop more microcracks at saturation (Figure 2.3);
- $[0_n/90_m]_s$ laminates have one ply group which cracks and it develops a roughly periodic array of aligned microcracks, while $[90_n/0_m]_s$ have two ply groups which develop staggered cracks, resulting in a different microcracking pattern depending on the stacking sequence of plies. Furthermore, at high crack densities, curved cracks may appear near straight ones, due to the interactions between existing cracks which cause the maximum stress shift to a location

near the 0/90 interface and close to an existing crack instead of midway between two (Figure 2.4).

▷ LOADING MODE AND CONDITIONS: microcracking phenomena consequent to bending loading are quite similar to those to which tension loading usually leads. Biaxial loading (*i.e.* residual stresses due to changes of temperature, thermal shrinkage, presence of moisture), instead, can be treated as two uniaxial loadings, one on a $[0_n/90_m]_s$ laminate and one on $[90_n/0_m]_s$, and can induce cracks both in central and surface plies, then a relative amount of them depending on the ratio n/m. Moreover, other non-uniform stress states need to be taken into account besides uniform stress states, especially in the case of holes or other laminate defects. Fatigue loading, then, introduces some more variables, such as the amplitude of the fatigue stress ΔK, the distance of a microcrack to the neighboring existing ones, and ΔT in the case of thermal fatigue.

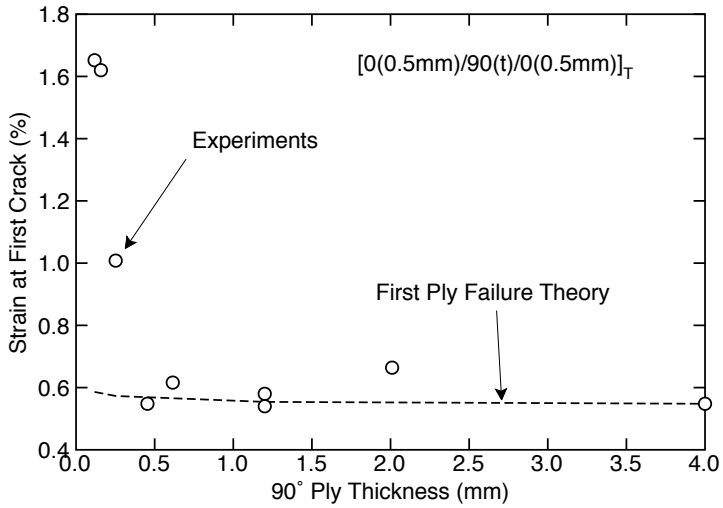

Figure 2.2: The strain to initiate microcracking in glass reinforced laminates $[0/90]_s$ as a function of the total thickness of 90° plies, which are supported by 0° plies with a thickness of 0.5 mm [23].

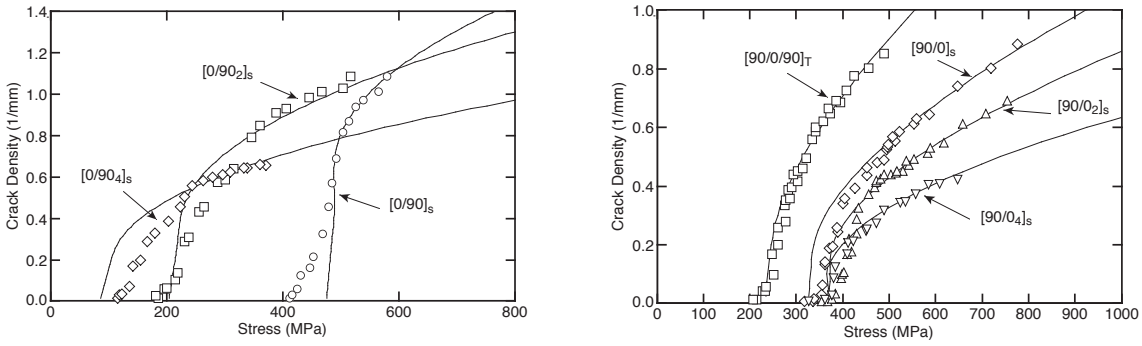

Figure 2.3: Microcrack density as a function of applied stress for several different $[0/90_n]_s$(left) and $[90/0_n]_s$ (right) carbon/epoxy laminates [23].

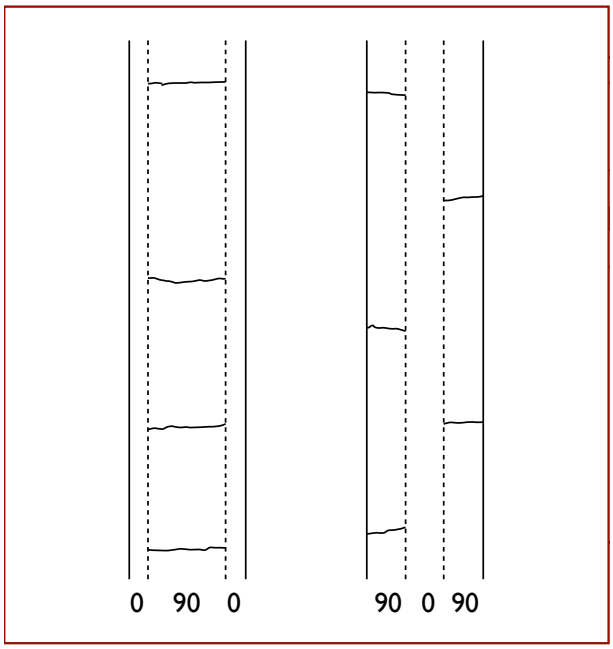

Figure 2.4: Roughly periodic array of aligned cracks in a $[0/90_4]_s$ laminate (left); staggered cracks in a $[90_4/0_2]_s$ laminate (right) [23].

- ▷ MATRIX AND FIBRES PROPERTIES, STRENGTH OF INTERFACE: volume fraction of the matrix is usually low, since fibres constitute the most significant part of the composite, thus matrix contributes less to load bearing in comparison with fibres. The fibre toughness and their statistical defects, but especially their distribution and their interface within the matrix, play a fundamental role in the fracture mechanics of composites. For carbon-FRPs, several reviews [28, 29] summarise the research work about the carbon fibre-epoxy interface.

In summary, the interply cracks (delaminations) often start from the debonding of transverse fibres and the intraply cracks (within 90° plies as the most frequent, as main evidences of damage) are the locations where the self-healing system should effectively operate. Moreover, the increase of 90° ply thickness decreases the strain for microcracking (also in relation with the stacking sequence of plies): this should be considered when new components are introduced in the material (as healing microcapsules), since their presence could have a significant influence on the damage mechanisms. Finally, knowing how loading modes are related to consequent damages should be harnessed to select proper healing assessment methods: this means choosing a reference material property and a specific testing protocol in order to calculate the healing efficiency.

Considerable research efforts were devoted in order to control and solve damage in composites, thus increasing the material life-time. Besides trying to reduce the material ageing, general approaches consist of:

- ▷ PREDICTION: In general, failure models have been studied and improved for damage prediction. In particular, theoretical analysis methods have been developed to pre-

dict the effective thermomechanical properties of a laminate with a given amount of already existing microcracks, the conditions for which those microcracks formed and, by the mean of some failure modes, how the microcracking will evolve [23]. Both the initiation and propagation of the crack take place into composite materials according to failure mechanics models which are more complex than those for traditional materials. Both fibres and matrix failure, and the presence of a complex system of crack deflection mainly due to interfaces, have to be taken into account [30]. Most successful models are energy-based (finite or non-finite), rather than strength-based (*non*-fracture mechanics) [27]: they are able to predict the next microcrack when the total energy released by its formation (G_M) reaches the critical energy release rate for microcracking (G_{MC}) [31].

- ▷ Detection: In order to localise the damage and quantify its extent (damage mapping), several non-destructive evaluation (NDE) techniques are employed, such as ultrasonic inspection, X-rays tomography, low-frequency vibrations method, thermography and vibro-thermography, acoustic emission techniques. These can be applied during maintenance steps and during processing too, during which the application of a high control for detecting the formation of defects is of great importance. Besides these conventional approaches, the concept to incorporate a damage self-detection capability into the material itself has been recently also developed, through the use of optical fibres (with Bragg gratings or distributed sensing), piezoelectric sensors/actuators, magnetostrictive materials, bruisable paintings. All these embedded components should be sufficiently miniaturised not to disrupt the structural integrity of the component and they should allow a health monitoring both during fabrication and in service. One of the main goals is to achieve a complete damage detection without the need of conventional NDE during service or, even worse, the interruption of service [30, 31].

- ▷ Repair: Depending on the damage extent and composite system, the component is removed from service and replaced entirely or it is repaired by manual intervention. An effective repair expertise is then necessary for providing the possibly full restoration of the initial mechanical properties. During the last decade, the concept of an autonomic repairing response which the material should be able to intrinsically give has been increasingly developed. This feature for synthetic materials is inspired from living biological systems, which are able to provide an autonomic healing at the site of damage, and should allow extended lifetime and reliability.

- ▷ Prevention: Examples of damage prevention are for example the application of high safety margins and the creation of specific type of structures able to prevent a known damage. For instance, in order to improve interlaminar properties of the 2D laminates, three dimensional (3D) textile preforms have been developed during

the past 30 years by using different manufacturing techniques like weaving, knitting, braiding, stitching, and non-woven manufacturing [32–34]. With 3D woven composites, it is possible to produce complex shape preforms, less expensive then the same shapes made of 2D laminates and also easier to manufacture. They also have good through thickness properties, higher delamination and ballistic damage resistance and better impact damage tolerance. Using 3D fabrics permits the creation of reinforcement geometries that can be extremely complicated in all three dimensions. To add to the complexity, the internal structure of a 3D preform can be further distorted when compressed and shaped into the mould with consequent loss of their potential [35].

In summary, exploiting effective prediction methods, detection strategies, expert repair techniques or autonomic healing capability proper of the material, and prevention approaches, a new concept for damage management can emerge and the material life-time could be substantially elongated.

2.2 Extrinsic self-healing approaches

The present chapter is intended to give an overview about how and when a specific category of self-healing approaches first appeared, namely the extrinsic ones (§ 2.2.1). Two subsections of this chapter will highlight: (i) a pioneering approach, extrinsic and based on the presence of capsules, which will herein viewed as a reference for presenting other similar systems (§ 2.2.2), (ii) a specific variant of the pioneering system, namely the solvent capsule-based approach, also extrinsic and developed as a non-toxic alternative (§ 2.2.3). As mentioned, the present work investigated healing by using this latter approach.

2.2.1 The birth of self-healing

The idea of a material which is able to self-heal, that means repair itself in an autonomous way, dates back to '80. This concept came out from the scientific aim of extending the lifetime of polymers thanks to the ability of autonomically healing forms of damage that develop in the material, whenever and wherever: this can prevent their worsening and eliminate the need of the usual repair steps. Repair steps would not be external (manual or not) interventions anymore, but they would rely on an intrinsic functionality of the material itself, able to recover from injuries. The self-healing approach is inspired by nature, since it mimics the ability of many living biological systems which are capable of reacting to external stresses and damage thus providing an autonomic healing response at the site of interest (our skin is an outstanding example).

Self-healing materials can be polymers, metals and ceramics; moreover, auto-repairing mechanisms can be used both in neat and in composite materials; as yet, however, more

efforts have been dedicated to research on neat materials rather than composites.

The first efforts in this field refer to the University of Illinois at Urbana-Champaign (USA), where they started to apply their engineering and chemical know-how to impart a native self-healing functionality to a polymeric material. In 1993, Prof. C. Dry, in collaboration with Prof. N. Sottos, developed a FRP with an embedded healing system constituted of hollow repair fibres filled with a reactive fluid [4]. Some years later, in 2001, a variant of this first system appeared, developed by Prof. S. White and N. Sottos, again in Illinois: they used microcapsules instead of hollow fibres, filled with a healing agent and embedded within a neat thermoset material (unreinforced), and they successfully demonstrated the healing capability for both static fracture and fatigue healing [3]. Figure 2.5 shows a scheme of these two "pioneering" systems. In both cases, the healing mechanism was taking place thanks to the rupture of the hollow fibres or of the microcapsules caused by a propagating crack, and the consequent delivery and polymerisation of the healing agent to the damage site (crack). The two different approaches can be seen as leading models for the two categories of extrinsic self-healing materials as they will be defined later on: microvascular and microcapsule-based. Many other variants followed inspired to those and developed by a large number of research groups.

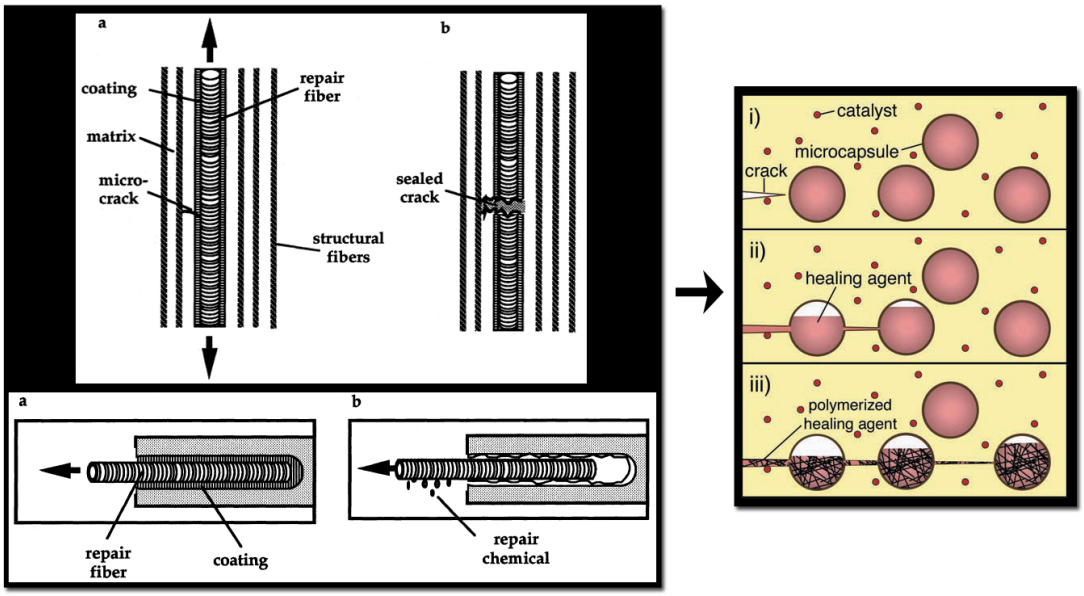

Figure 2.5: Schematics of the first self-healing systems: (left) FRP with hollow repair fibres [4] and (right) neat polymer with microcapsules [3], developed at the University of Illinois in 1993 and 2001 respectively.

2.2.2 The pioneering capsule-based self-healing system and its alternatives

A detailed description of the system developed by White *et al.* at the Beckman Institute for Advanced Science and Technology (University of Urbana-Champaign), starting from 2001 [3], is given here. Features of the system are listed and variants developed by other research groups are reported. A summary is given in Figure 2.6. In particular, the pioneering healing system is here defined as (a) extrinsic, (b) irreversible, (c) capsule-based, it is (d) contained in an epoxy material and (e) based on two components, namely capsule and catalyst (f). Specifically, the first component is composed of dicyclopentadiene (DCPD) capsules (g) and the second one of a Grubbs' catalyst. Finally, the healing phenomenon (i) relies on the ring-opening metathesis polymerisation (ROMP) and (j) is pseudo-autonomous.

a) Extrinsic system The system was defined by Yuan *et al.* [36] as extrinsic, because it contained a specific new phase that releases the healing agent which wets the crack faces and rebonds them at a macroscopic level. It differs from intrinsic systems, where atomic- or molecular-level interactions (chain mobility or entanglement, reversible polymerisation, melting of thermoplastic phases, hydrogen bonding, etc.) allow the healing mechanism. Different strategies exist [37]:

- ▷ reversible bonding based on the reversibility of specific chemical reaction;
- ▷ chain re-entanglement based on the chain mobility enhanced by a thermal trigger;
- ▷ non-covalent bonding healing related to hydrogen bonding and ionic clustering where the reversibility of the polymer cross-link is observed.

We omit herein the description of the wide number of intrinsic systems developed throughout the years, since it would go beyond the scopes of the present thesis.

b) Irreversible system The self-healing mechanism was irreversible [38]; the healing event can occur just once in a certain position, because the healing phase is used and consumed after the repairing event. This differs from reversible systems, in which the healing event can take place several times at the same location, thanks to the reversible characteristics of the chemical (or physical) healing process. Extrinsic systems are usually irreversible, whereas intrinsic ones are in general reversible, even if there are some exceptions.

c) Capsule-based system The systems was based on the segregation and storage of the healing agent in capsules, later embedded within the material, until they are ruptured by damage phenomena or dissolved. The rupture triggers the release of the capsule

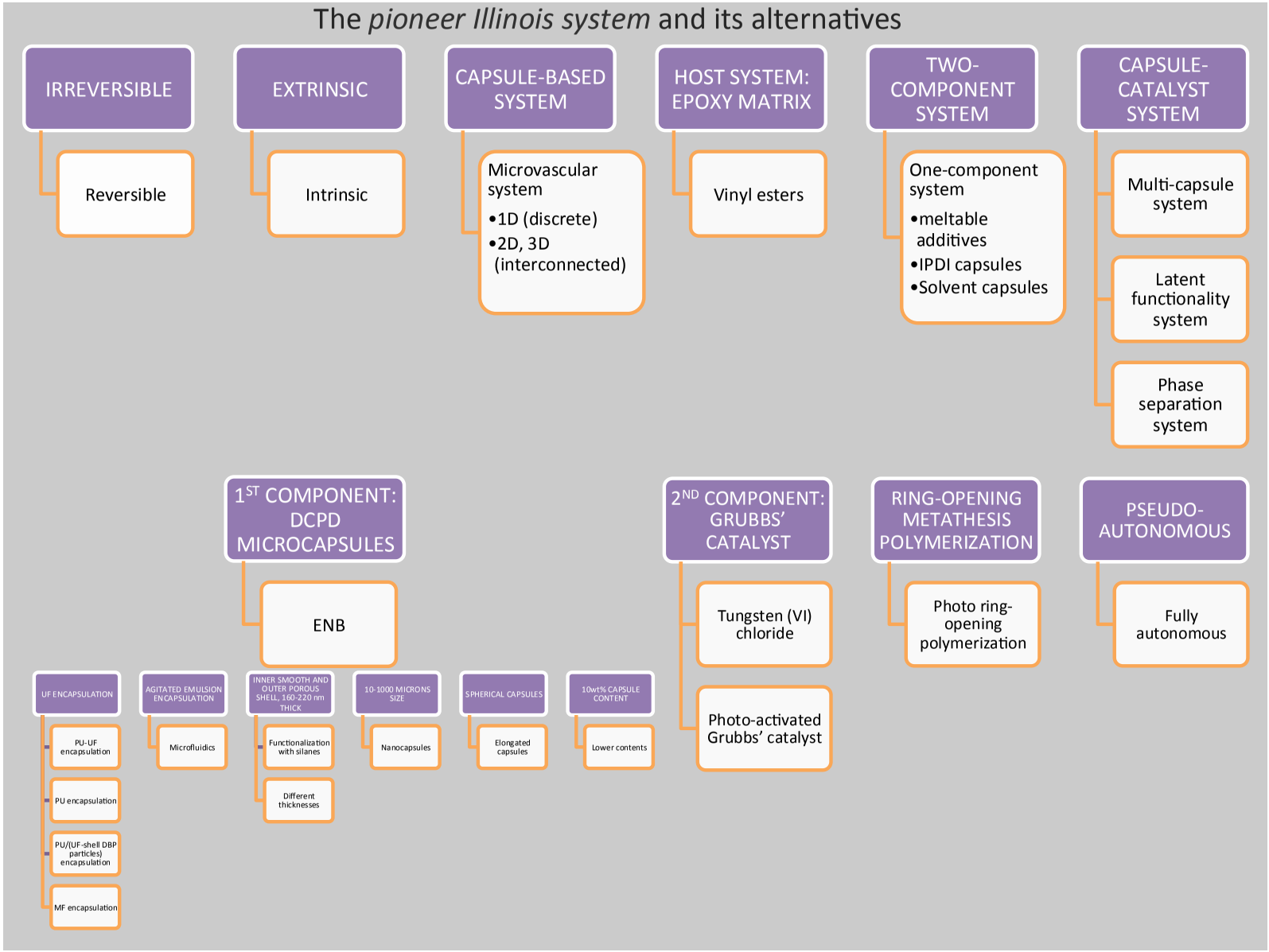

Figure 2.6: The features of the pioneering "Illinois system" and variants developed by other groups.

content, which then reacts somehow with the matrix or with a second component. Several microencapsulation techniques are currently used for food science, medical, industrial and agricultural applications, although the most used ones in the case of self-healing materials are *in situ*, interfacial and meltable dispersion. A detailed review by Blaiszik *et al.* [37] distinguished five steps in which the design cycle process for capsule-based self-healing materials can be divided.

1. SEQUESTRATION: the healing agent is stored in capsules by encapsulation or phase separation with specific parameters adapted to the physical and chemical characteristics of the healing agent, as solubility, viscosity, volatility, pH, reactivity. So obtained capsules are usually characterised from a mechanical/physical/chemical point of view before integrating them within the matrix.

2. INTEGRATION: the capsules are carefully incorporated into the material (neat or reinforced), paying attention to their reactivity with the matrix, induced shear forces and temperatures during manufacturing, size scale and dispersion/distribution issues.

3. MECHANICAL CHARACTERISATION: the material is mechanically characterised to verify whether the embedded capsules have modified strength, fracture toughness, elastic modulus, etc., depending on their content, mechanical properties and bonding characteristics with the matrix.

4. TRIGGERING: the healing agent is released on the crack plane and takes effect in a certain way; this is usually validated through different kind of *in situ* or postmortem observations.

5. HEALING EVALUATION: this last step evaluates the effectiveness of the healing system; we cross-refer to § 2.3 for a detailed illustration about how the healing efficiency can be quantified.

As aforementioned, the capsule-based system constitutes one between two main existing approaches to develop extrinsic self-healing materials (Figure 2.7). It differs from the microvascular approach, which currently employs either discrete or interconnected capillaries integrated within the material and containing the healing agent, which is released when a damage event occurs and passes through these channels. Compared to capsule-based systems, a higher probability of the healing agent "containers" to be intersected by a propagating crack, a higher agent volume per crack area and the possibility of multiple healing events are known advantages of microvascular-based approaches.

Discrete channels (1D) can be fabricated independently and can be loaded with the healing agent prior to incorporation. They can be placed into a material in an array with an appropriate spatial distribution in order to distribute the healing agent throughout the

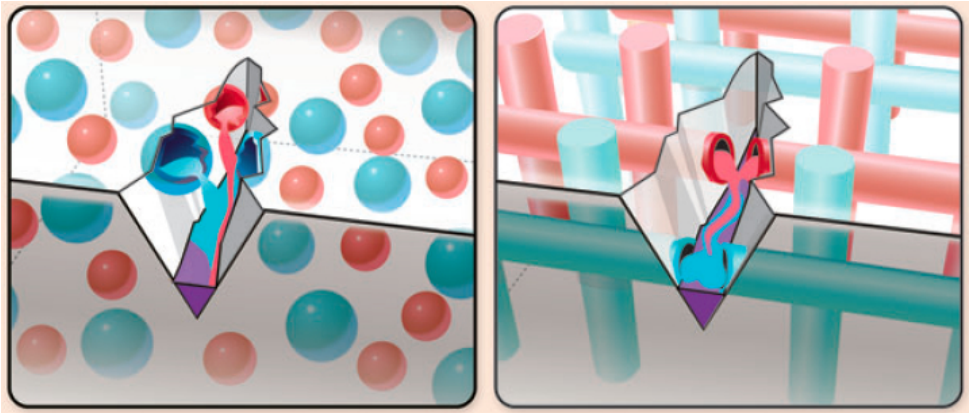

Figure 2.7: The two main extrinsic healing approaches: microcapsule-based (left) and 3D microvascular-based (right) systems [37].

material. Early attempts were performed by Dry and coworkers [39], who explored the healing ability of epoxies containing mm-diameter glass pipettes pre-loaded with either cyanoacrylate or a two-part epoxy system. Glass and carbon FRPs have been widely studied for incorporation of discrete channel arrays, since their integration can be easily done during the laminate assembly process. The use of glass pipettes quickly shifted to the use of hollow glass fibres (HGFs) by Motuku *et al.* [40], Bleay *et al.* [41] and later by Pang and Bond [42, 43]. Improved results were obtained later by Trask *et al.* [44, 45] and Williams *et al.* [46, 47]. Key issues of these systems began to be addressed such as the channel method of incorporation and (pre)filling, the effects of the channels on the material properties due to their large diameter, the effectiveness of the fluids contained in the channels and the ability to reach damaged areas and lead to property recovery. The potential for discrete channel arrays for use in damage healing (reduction) is significant, but limited by the difficulty in replacing fluid to depleted channels. Also, the need for each channel to fill specific damage volumes for complete self-healing dictates constraints on how sparsely the channels can be distributed, which affects mechanical properties. Reductions of initial damage strength up to 16% [44] and flexural strength up to 8% [45] were demonstrated for HGFs, with variations depending on the channel spacing. However, the evaluation of the quantitative influence of the healing system on the mechanical properties is still absent in many works.

On the other hand, interconnected channels (2D and 3D) requires simultaneous fabrication with the surrounding material. This certainly increased the process complexity. Moreover, in this case, the choice of the healing agents requires chemical compatibility tests with the matrix due to their direct contact at the channel surface. Several techniques have been developed to fabricate these networks. Micromachining has been extensively used and consist in creating channel grooves at the microscale with traditional machining principles (such as electrical discharge or laser), while chemical etching limits to specific applications. Both techniques, however, are more versatile for 2D networks, while they

suffer the limitation of requiring stacking in order to build 3D structures. Other approaches are based on direct ink writing (DIW), which involves the controlled extrusion of fugitive viscoelastic inks through a fine nozzle to build 3D structures, which are later infiltrated with the matrix material. These structures are then liquefied and removed from the matrix via vacuum, leaving a 3D microchannel network. Examples of use in the literature include the early work by Toohey *et al.* (coatings with 3D channels filled with DCPD [48, 49]), Williams *et al.* [50, 51], Patrick *et al.* (foam sandwich core with channels filled with two-part chemistry based on PU [52]) and Hamilton *et al.* [53] An alternative method consists in the use of sacrificial fibres which are then thermally depolymerised [54]. For DIW-based techniques, some authors found negligible influence of the channels on the mechanical properties [50, 51], while some others showed a reduction of stiffness and fracture toughness up to 11%, varying with the channel orientation.

A recent approach developed by Bond and coworkers in Bristol (UK) relied in coupling the self-healing mechanism with damage redirection. The use of interleaves and vascules in the structure (without affecting the global mechanical properties) is able to provide a successful damage steering and visualisation, as well as healing, although research is still on going.

d) Host material: epoxy matrix A thermoset epoxy resin was selected as matrix for the self-healing system. In the beginning, the resin was neat (*i.e.* was not reinforced with any glass or carbon fibre to make a composite). Most articles proposed the epoxy as it is structural, and specifically brittle, material that could easily show how damages can be repaired through the self-healing mechanism. A variant could be vinyl esters, used for example by Cho *et al.* [55] employing PDMS-based healing chemistry and by Wilson *et al.* [56] employing the pioneer DCPD/Grubbs' system. For more realistic studies which could represent more what is used in industrial applications, toughened thermoset must also be studied.

e) Two-component healing system The initial system was based on two components: the first consisted of microcapsules filled with the monomer dycyclopentadiene (DCPD) and with a shell composed of urea-formaldehyde (UF), which are dispersed within the polymeric matrix; the second was a Grubbs' first generation catalyst, also incorporated into the matrix. The healing phenomenon takes place thanks to the ring-opening metathesis polymerisation (ROMP) of DCPD, activated by the catalyst, which is an essential ingredient. Two-components systems differ from those with one component, which is the healing agent as itself; for the healing to occur, any additional reactant is needed or, if it is, the reactant does not constitute a second component, as it is a matrix latent functionality, for instance. A brief description of some one component-systems follows.

- ▷ Several studies have been conducted on one-component systems based on the introduction of a meltable additive, usually thermoplastic, under the form of microcapsules. These approaches usually belong to the category of intrinsic systems based on chain re-entanglement. Typical thermoplastic additives include polycaprolactone, poly(ether sulfone), poly(methyl methacrylate), poly(sulfone), polyetherimide [5, 57–68].

- ▷ Yang *et al.* [69] developed a specific type of healing agent intended to be embedded as a single-component, as it does not need any catalyst. It consists of an isophorone diisocyanate (IPDI) encapsulated via interfacial polymerisation of polyurethane (PU). This agent is effective in humid conditions at ambient temperature, but its healing behavior in a matrix has not yet been tested.

- ▷ Caruso *et al.* [6, 7] developed a new concept of single-component healing system for epoxies, which relies in encapsulated polar solvents as healing agents, such as chlorobenzene and less toxic aromatic esters as phenylacetate (PA) and ethyl phenylacetate (EPA). This repair system is based on the swelling of the epoxy crack faces in the presence of the solvent released by the ruptured capsules and on the subsequent reaction of the residual epoxy and hardener functionalities of the under-cured matrix. This enables the healing of the fracture plane, by reptation and chain interlocking. More exhaustive informations about the features of this system will be detailed in § 2.2.3.

f) Capsule-catalyst system The pioneer system was defined as a capsule-catalyst system [37], meaning that one of the two components (DCPD in this case) is encapsulated, whereas the other (Grubbs' catalyst) is not (even if it can be protected by an external wax layer). A similar example of capsule-catalyst system was proposed by Coope *et al.* [70], who presented a system based on a epoxy/EPA solvent mixture encapsulated in a polyUF shell, that undergoes a ring-opening polymerisation when it reacts with a Lewis acid, such as scandium(III) triflate under the form of dispersed solid particles, which acts as curing initiator for the epoxy monomer. Autonomous self-healing experiments demonstrated healing efficiencies up to about 80%. In a more recent work [71], Coope *et al.* reported on self-healing of the above epoxy/catalyst system in FRP samples. The epoxy/EPA healing agent was introduced to the crack zone through small vascules and healing efficiencies close to 100% were observed. Furthermore, it was reported that the healed material showed brittle or ductile behavior as a function of solvent to epoxy ratio in the healing agent. Nevertheless, a pressurized pumping system was required to achieve a self-healing effect as capillary forces were insufficient to fill the crack gaps.

This capsule-catalyst approaches differ from:

▷ MULTICAPSULE SYSTEMS: both the healing agent and the "polymeriser" are encapsulated. In Table 2.2 some examples are reported with respective references.

1st encapsulated component	**2nd encapsulated component**	**Matrix**	**Catalyst**	**Ref.**
PDMS resin	PDMS resin	elastomeric	Pl	[72]
PDMS resin	DMDNT catalyst	epoxy vinyl ester coating	/	[73]
PDMS resin	DBTL catalyst	PDMS layer	/	[74]
epoxy resin	mercaptan	epoxy	/	[75]
epoxy resin	boron trifluoride diethyl etherate	epoxy	/	[76]
epoxy resin	amine	epoxy	/	[77]

Table 2.2: Multicapsule self-healing systems.

▷ LATENT FUNCTIONALITY SYSTEMS: whatever the healing agent is, either encapsulated or dispersed, the polymeriser is a "latent" residual functionality present in the matrix or an environmental stimulus; the most appropriate example is the approach developed by Caruso *et al.* [6, 7], as described above, where the latent functionality consists in the unreacted amines of the under-cured matrix. Thus, we can define that a latent functionality system is usually single-component (and not always vice-versa). Other examples can be found in the literature: it is worth mentioning Zako and Takano [78], who introduced encapsulated thermally polymerizable epoxy in a glass fibre/epoxy composite, and healing was initiated by a thermal stimulus, and Sauvant-Moynot *et al.* [79], who used water-soluble self-curing epoxy-amine adduct particles, the polymerisation of which was triggered by an aqueous environment, for a coating with anti-corrosion properties. Also, Yin *et al.* [80] proposed $CuBr_2$(2-MeIm)$_4$ (the complex of $CuBr_2$ and 2-methylimidazole) as a dispersed latent hardener to polymerise the epoxy contained in 30-70 μm diameter capsules. In the case of 10 wt% epoxy microcapsules and 2 wt% latent hardener, the self-healing epoxy exhibited a 111% recovery of its original fracture toughness and a healing efficiency of 68% in a plain weave glass fabric epoxy laminate.

▷ PHASE SEPARATION SYSTEMS: the healing agent and the polymeriser are phase-separated in the matrix, as it happens in the anti-corrosion self-healing coatings developed by Cho *et al.* [73].

g) 1st component: DCPD-microcapsules As mentioned, the healing agent used by White *et al.* was DCPD, a liquid monomer which is available in the shape of two stereoisomers, *endo*- and *exo*-DCPD. Since the beginning, White *et al.* used *exo*-DCPD, thanks to its better polymerisation kinetics. Another diene monomer, the 5-ethylidene-2-norborene (ENB), was investigated by Lee *et al.* [81] and by Guadagno *et al.* [82], and

compared to DCPD: ENB has a faster reaction rate in the presence of much lower amount of catalyst (consequently lower cost), low viscosity (enabling full infiltration in the crack volume), no melting point and resulted in a cured resin with higher T_g, whereas it had similar thermal resistance and shape.

UF encapsulation The encapsulation of the DCPD monomer in a urea-formaldehyde shell was performed by an agitated emulsion technique. This method consisted in forming an oil-in-water emulsion, in which the oil part is the healing agent that needs to be encapsulated and the water part is an aqueous medium. The immiscibility of the two phases and the continuous mechanical stirring of the emulsion enable the formation of healing agent droplets: their stabilisation is achieved by the shell formation. The components of the shell, urea and formaldehyde, are contained in the aqueous medium, as they are soluble in it. They start to polymerise depending on chemical conditions such as temperature and pH: the growing polymer shell is hydrophobic and forms at the interface between the healing agent droplets and the aqueous medium. This kind of encapsulation gave good results over the past years and most authors used it, but some variants have been developed in order to achieve specific characteristics:

- Caruso *et al.* [83] developed the so called double-shell wall encapsulation: in order to produce double-shell capsules, they dissolved a polyisocyanate precursor (Desmodur L75) in the healing agent, which then reacted with water and formed a PU inner shell under the usual UF outer one. The capsules were so constituted of two shells PU/UF and they showed higher mechanical resistance and higher shell thickness.

- Yang *et al.* [69] formed capsules with PU-only shells, for the encapsulation of IPDI, as explained above.

- Mookhoek *et al.* [84] produced original binary capsules, constituted of a core of liquid DCPD with a PU wall which contained small capsules of UF-shell dibutylphthalate (DBP, as catalyst).

- Sun *et al.* [85] investigated an encapsulation with melamine-formaldehyde (MF) shell and compared it to the standard UF one. Measurements of the capsule mechanical properties showed superior yield points and deformations at bursting, meaning an higher resistance for surviving during their integration within the matrix, but a lower probability of rupture over load transfer from the matrix, during the crack initiation/propagation.

- Hu *et al.* [86] also performed a MF-shell encapsulation and showed the direct proportionality between rupture stress and capsule diameter.

Agitated emulsion techniques can be easily adapted to encapsulate liquid phases, whose viscosity is not too high and which are not reactive; controlling pH, temperature and agitation rate results in a change of capsule properties, such as strength, shell thickness and morphology, dimensions and shape. An alternative technique is producing capsules through microfluidics [87–92]. This approach is based on the production of capsules drop wise, using microdevices composed of hydrophobic and hydrophilic microchannels, that deliver the liquid components and enable the formation of different emulsions. The great potentiality of microfluidic techniques relies in the fact that new capsules characteristics can be achieved: nanodimensions, non-spherical shapes, monodisperse size distribution, UV curable shells, different core materials.

Shell morphology As a common feature of UF microcapsules [93], their shell has an inner smooth layer, 160-220 nm thick [13] (depending on manufacturing parameters), with low porosity and permeability, and an outer layer which is porous and rough instead (Figure 2.8). The shell thickness increases up to 1.3 μm when the shell is composed of two layers (inner polyurethane and outer UF) [13, 83]. The surface properties of microcapsules influence their adhesion (interfacial bonding strength) to the matrix, thus the load transfer; therefore, an accurate control of the emulsion parameters is directly linked to the achievement of desired surface characteristics [94]. Li *et al.* [95] and Jackson *et al.* [96], in order to enhance the interfacial bonding between capsules and matrix, attached different types of silanes to the surface of UF capsules, thus obtaining improved tensile strength and impact resistance of material (composites in their case). Moreover, the shell thickness also plays an important role since the capsules should be thick enough in order to "survive" during handling, and thin enough to be ruptured by the propagating crack.

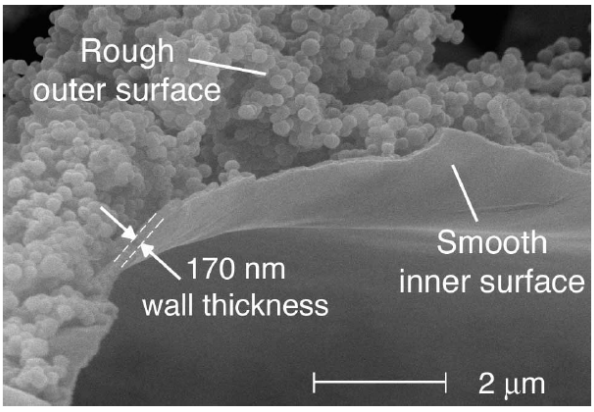

Figure 2.8: Surface morphology of microcapsules, showing the inner smooth surface (170 nm thick) and the outer rough one (up to 60 nm thick) [94].

Capsules size The average capsule size is controlled by the agitation rate of the emulsion bath, *i.e.* it is possible to obtain microcapsules of 10-1000 μm by adjusting the

agitation rate in the range 200-2000 rpm. The linear correlation between agitation rate and diameter (log-log scale) is supposed to respect the dependence between droplet size and shear rate described by Taylor in 1932, even if the fluid flow is not laminar but turbulent [94]. The mean capsule diameter using a stirring rate of 550 rpm is 200 μm, as also reported by Brown *et al.* Smaller capsules were obtained in 2007 by Rule *et al.* [97] with the traditional technique (just increasing the stirring rate) and in 2008 by Blaiszik *et al.* [98], who used a modified protocol and obtained capsules with diameters down to 220 nm. The microcapsule diameter directly influences the performance of self-healing materials, since it is related to the amount of healing agent they contain. For instance, Rule *et al.* [97] showed that, if a sufficient amount of healing agent is delivered to fill the crack volume, the healing performance is maximised, while it falls off when the crack volume exceeds the amount of available healing agent.

Yields Yields of the encapsulation was defined by Brown *et al.* [94] by the ratio of the mass of retained capsules to the total mass of core and shell constituents. Typical yields of 79–92% were obtained at 550 rpm agitation rate. These values could be lower because of phenomena such as capsule breakage due to too high shear conditions or non-recoverable fractions over high agitation rates.

Capsules shape As yet, capsules were obtained with a spherical shape. More recently, research studies were conducted in order to investigate non-spherical shapes and their influence on self-healing properties:

- ▷ Mookhoek *et al.* [84], through geometrical simulations, compared spherical and elongated capsules in terms of probability of being intersected by a crack plane and amount of deliverable healing agent, at a fixed content of microcapsules in the matrix, *i.e.* 10 vol%. Elongated capsules showed a greater healing potential, taking into account that, as far as considering liquid-based self-healing material systems, the average crack opening rather than the crack length governs the healing potential. Indeed, spherical capsules (volume = 15.7 μm, diameter = 3.11 μm) released an amount of healing agent capable of filling a crack volume with an uniform crack opening distance of maximum 0.317 μm, whereas cylindrical capsules (randomly oriented, aspect ratio (AR) = 5, volume = 15.7 μm) released a larger amount, meaning a larger maximal opening distance, *i.e.* 0.448 μm. Elongated capsules have also been compared in term of aspect ratio, orientation and influence on the elastic modulus.

- ▷ Bon *et al.* [99] investigated how to process non-spherical capsules, by forcing spherical capsules in narrow capillaries which imparted to capsules elongated shapes with ARs up to 10. The use of a synthetic clay Pickering agent was crucial for the capsule shape stabilisation after the capillary exit. No quantitative results were provided

about the fill content and the size distribution and the capsules produced were poorly resistant.

- ▷ Xu *et al.* [100] produced monodispersed cylindrical capsules using a microfluidic flow-focusing device (MFFD) and stabilised their shape through direct UV or thermal polymerisation, convalidating the idea that encapsulation methods through microfluidics may represent new and effective routes for capsule-based self-healing materials.

Shelf-life After processing, microcapsules must survive before the introduction within the matrix, which means that the core content and the initial mechanical properties must be kept. Thus, leakage, diffusion phenomena or breakage must be avoided in order to keep the healing agent contained in the core. An average fill content decrease of 2.3% after 30 days of exposure to ambient laboratory conditions were judged acceptable [94]. Blaiszik *et al.* checked the capsules thermal stability by TGA, showing less than 5% capsule weight loss below 100°C (mainly due to residual water), then a significant weight drop in the range 150-220°C, corresponding to the vaporisation of DCPD [98]. As a consequence, the presented system is not suitable for applications with manufacturing and service temperatures higher than 120°C.

Other issues which reduce the capsule shelf-life might arise from ageing, as explained in § 2.2.3 for solvent-filled capsules. An elegant solution for the ageing problem can be found in healing systems with encapsulated epoxy and amine by Jin *et al.* [77]: the healing efficiency, in this case, was tested to be stable up to six months ageing, only except an initial drop in the first month.

Mechanical properties Keller and Sottos [101] investigated the microcapsule mechanical properties early in 2006. A Young's modulus of 3.7 ± 0.2 GPa was obtained from a single-capsule compression test and it was found to be independent of the capsule diameter (capsules with different diameters were tested) whereas failure behavior was found to be dependent (smaller diameters, lower failure loads but higher normalised failure strength).

Content within the matrix In the first studies, the capsule concentration was kept at 10 wt%, in order to achieve at the same time maximal DCPD delivery and maximal virgin fracture toughness. Then, it was showed that reducing the concentration to 5 wt% decreased the virgin toughness but did not have a significant effect on the healed one; this enabled to get quasi-complete healing. Figure 2.9 summarises the results by Brown *et al.* [102] concerning the effect of the capsule concentration (given the size) on the fracture toughness and the healing efficiency.

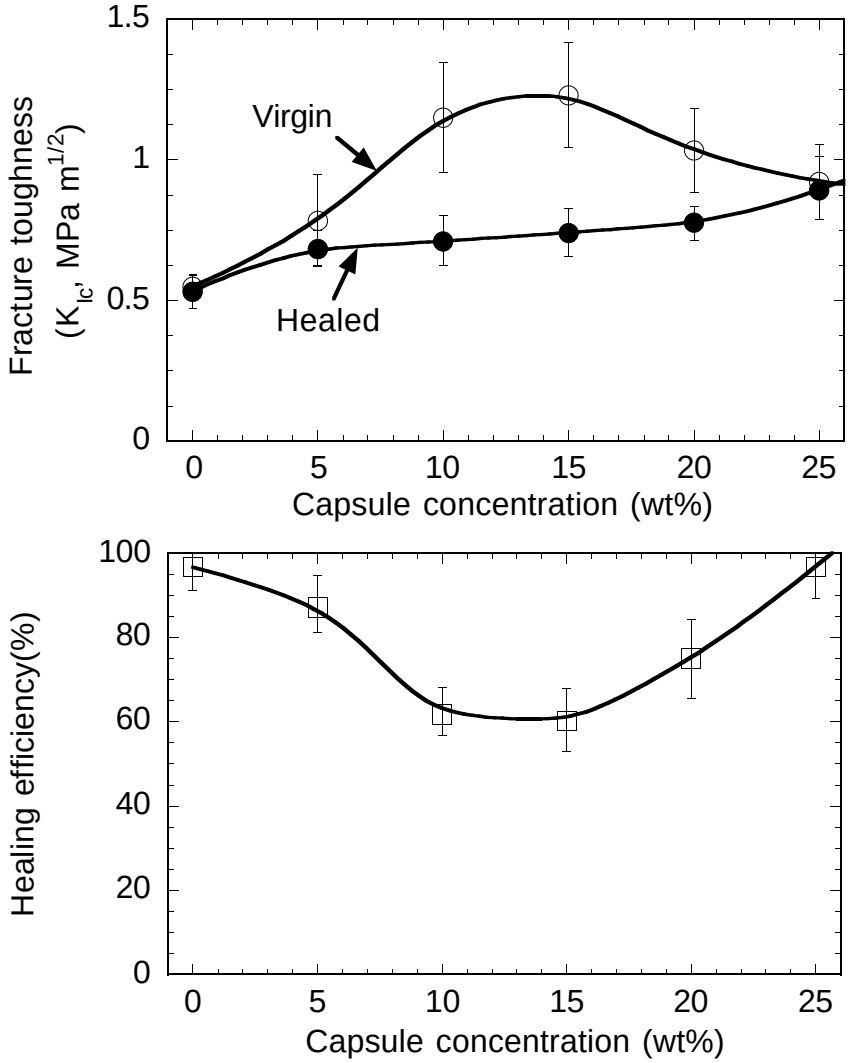

Figure 2.9: Virgin and healed fracture toughness as a function of capsule concentration (capsule diameter around 180 μm) [102].

h) 2nd component: Grubbs' catalyst As mentioned, the polymerisation of DCPD takes place in the presence of a transition metal-based catalyst. A 1st generation Grubbs' catalyst, namely bis (tricyclohexylphosphine) benzylidine ruthenium(IV) dichloride, was chosen as it shows high cross metathesis activity towards olefins, being tolerant to a wide range of functional groups as well as oxygen and water, and being often used for ROMP and RCMP (ring-closing metathesis polymerisation) [103]. The initial idea consisted in dispersing the catalyst as itself within the matrix, with relatively large loadings (2.5 wt%); it was supposed that, once DCPD microcapsules were broken by the propagating crack, the released liquid monomer, flowing in the crack plane, would have undergone ROMP by contact with the embedded catalyst and the curing would have provided structural continuity across the crack plane. However, different issues arose:

- ▷ Poor dispersion: the catalyst did not disperse well in the epoxy and tended to clustering; this led to lack of catalyst in certain matrix regions and, consequently,

to incomplete healing [1].

- ▷ Deactivation by amines: the epoxy's curing agent, diethylentriamine (DETA) in the present system, was found to deactivate the catalyst as the epoxy initially cures. In 2005 Rule *et al.* [97] proposed to encapsulate the catalyst with wax, in order to create an insoluble barrier between catalyst and amine, thus preventing catalyst deactivation and clustering. For the polymerisation to occur, the wax had to be dissolved by DCPD, though. It was showed that wax encapsulation was effective since it increased the catalyst's resistance to the amine, while decreasing the catalyst's reactivity by 9% only (quantified in term of ROMP kinetics). Moreover, wax encapsulation also enabled a better distribution of the catalyst within the epoxy, with a 10 times lower overall catalyst loading. Thus, healing efficiencies were improved thanks to wax encapsulation. Moreover, self-healing induced with wax microspheres exhibited non-linear elastic behavior: the ductility was explained with the fact that polyDCPD is plasticised by the wax that dissolved in the DCPD prior to curing. The problem of the catalyst deactivation was also solved by using alternative curing agents as tertiary amines, that showed lower chemical interaction with Grubbs' catalyst, or adjusting the mixing order and curing time [2].

- ▷ Time-dependent dissolution kinetics: an effective polymerisation of DCPD depends on the catalyst dissolution in the monomer phase; the dissolution rate must be faster than the polymerisation rate, otherwise lack of catalyst could lead to incomplete coverage, partial polymerisation and poor mechanical recovery. This was investigated in 2006 by Jones *et al.* [104], who also studied the influence of the two crystal polymorphs (one purchased by Sigma-Aldrich and another by Strem Chemicals) of Grubbs' catalyst on the ROMP efficiency.

- ▷ Crystallite size-dependent catalyst efficiency: since smaller crystallites have an higher surface area/volume ratio, very fine Grubbs' catalyst crystal size are found to be better. Indeed, the importance of the surface area for self-healing applications consists in the fact that the effective catalyst concentration in the material corresponds to the amount of exposed catalyst in the fracture plane. Thus, it seems crucial to decrease the dimensions of catalyst crystallites before use. Jones *et al.* [104] demonstrated that catalyst recrystallisation after dissolution is better than grinding. Among three distinct methods of recrystallisation, the precipitation from CH_2Cl_2/acetone presented the best results, but freeze/drying presented the best yield.

- ▷ Prohibitive cost: at the present time the cost of the chosen catalyst makes the system unsuitable for large-scale production (131 CHF per 100 mg [103]), even if low loadings (0.25 wt%) are sufficient for achieving high healing efficiencies.

- ACUTE TOXICITY (oral, dermal, inhalation), category 4 [103].

- RELATIVELY LOW DECOMPOSITION TEMPERATURE: Jones *et al.* [104] checked by DSC the catalyst's thermal stability, which resulted 190°C in nitrogen atmosphere and 140°C in air. In this context, care should be taken concerning cure and post-cure schedules for the polymeric material.

An alternative use of the catalyst was performed by Skipor *et al.* together with Motorola Inc. (United States patent No. 7108914 B2 [105]). The catalyst was attached on the outer surface of the microcapsules, as shown in Figure 2.10: a raised overall healing efficiency was claimed. The functionalisation was performed by a chemical reaction able to create a molecular bridge unit.

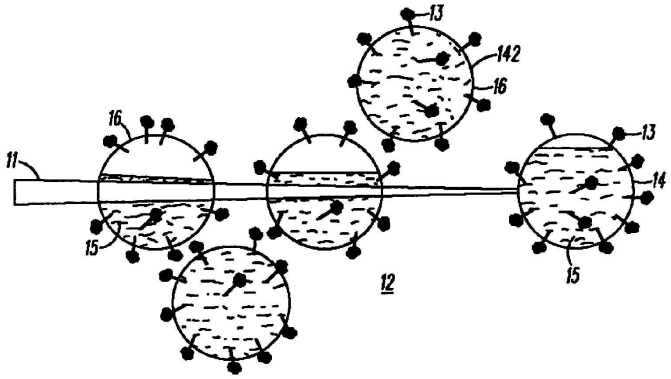

Figure 2.10: Schematic drawing representing a crack rupturing microcapsules on which the polymerisation catalyst is directly chemically attached [105].

Alternative catalysts for ROMP of DCPD were used:

- tungsten (VI) chloride (WCl_6) as catalyst precursor for the polymerisation of *exo*-DCPD: both "as received" and recrystallised forms of this cheaper catalyst resulted in promising results, even if the catalyst needed a co-activator to initiate the ROMP (phenyl acetylene, 0.5 wt%) and a dissolution agent to dissolve WCl_6 in DCPD (nonylphenol, 1 wt%) [106]. Further investigations about catalyst protection, catalyst/matrix interfacial bonding improvements by silanes [96], alternative co-activators and better catalyst dispersion are still on going.

- Grubbs' catalysts of other generations (first, second and Hoveyda-Grubbs' second) were studied and compared by Wilson *et al.* [107, 108] and Liu *et al.* [109], showing contrasting results.

- photo-activated catalysts: in this case the reaction was a photo-induced ring-opening metathesis polymerisation (PROMP) that took place at room temperature, was extremely fast, simple and environmental friendly. Sriram *et al.* [110] suggested

this with both DCPD and ENB monomers, although they did not perform any experimental tests.

i) Ring-opening metathesis polymerisation The reaction between DCPD and catalyst provides the monomer ring to open, forming a polyDCPD network, which is tough, highly cross-linked and not too sensitive to chemical shrinkage; the polymerisation is highly exothermic, it works at room temperature (even if it has slow kinetics), it is stoichiometric independent (10000:1 as monomer/catalyst ratio is the minimum) and it does not need thorough mixing. Referring to DCPD ring-opening metathesis polymerisation (ROMP) in the presence of the Grubbs' catalyst, Rule and Moore [111] and Mauldin *et al.* [112] found out that different DCPD stereoisomers correspond to different polymerisation kinetics. Exo-DCPD has a 20 times faster polymerisation rate and a shorter gelation time, compared to the other stereoisomer; this is usually considered as an advantage, but it could be an issue at low catalyst weight fraction (0.25 wt%), because the fast gelation impedes the complete catalyst dissolution, thus leading to inferior degrees of cure in comparison with *endo*-DCPD. Nevertheless, appropriately blending of *exo*/*endo* DCPD could lead to optimal compromises. Moreover, Kessler and White [113] performed a detailed research to investigate the cure kinetics of DCPD in the presence of the Grubbs' catalyst: they showed that the activation energy for the reaction strongly increases for degrees of cure greater than 60% and that the catalyst concentration influences the cure kinetics (a specific and unexpected dependence of the reaction rate on the square of the catalyst concentration was found by Aldridge *et al.* [114]).

j) Pseudo-autonomous system An optimal self-healing system is able to recover 100% of its original properties without any human intervention. External stimuli able to increase the self-healing ability may consist in applying a clamping pressure and/or heating the system. The system by White *et al.* is considered as pseudo-autonomous, as the self-healing takes place mostly with a clamping pressure to reduce crack volume.

2.2.3 The solvent capsule-based self-healing system

A more detailed explanation of the latent functionality system as initially investigated by Caruso *et al.* [6, 7] is here given, as such a system will be used for the purposes of this thesis.

Before 2007, healing/sealing through the use of solvents was investigated only for thermoplastic polymers. Caruso *et al.* aimed at demonstrating, for the first time, healing of cracks in thermosets. The healing mechanism, in both cases, was based on the polymer surface wetting and the swelling of the bulk polymeric material, that induced reptation and interlocking of the chains across the crack plane.

A screening of different organic solvents (Figure 2.11) was performed in 2007 in order to verify their healing ability (the tests were performed using tapered double cantilever beam (TDCB) samples and manually injecting the solvent). It was found that the effectiveness in terms of healing was somehow related to the solvent polarity, meaning that polar aprotic solvents (such as nitrobenzene, N-methyl pyrrolidone, dimethylacetamide, dimethylformamide and dimethyl sulfoxide) worked better than protic solvents. Solvents with electric constants between 5 and 38 were found ideal. However, the relationship between polarity and healing efficiency remained unclear. On the other hand, it was found that the high polarity of such solvents prevented their successful encapsulation in UF, so they had to be discarded. Chlorobenzene, the encapsulation of which was possible, although giving a lower healing efficiency, was selected as the best option for the "proof of concept". Control systems with hollow capsules and capsules containing non polar solvents (xylene, hexane) were also tested as control experiments showing no healing. No detailed explanation about the healing mechanism was given at that time; however, possible hypotheses were indicating that the solvent released from the fractured capsules was able to wet and swell the crack faces, enabling an intimate contact between them; moreover, healing appeared to be inversely related to the crosslinking density (maximal with the stoichiometric ratio of 100:12 for EPON 828/DETA, as shown in Figure 2.12), suggesting that the healing mechanism was based on the further curing reaction of unreacted functionalities, promoted by the matrix plasticisation in the presence of the solvent [6].

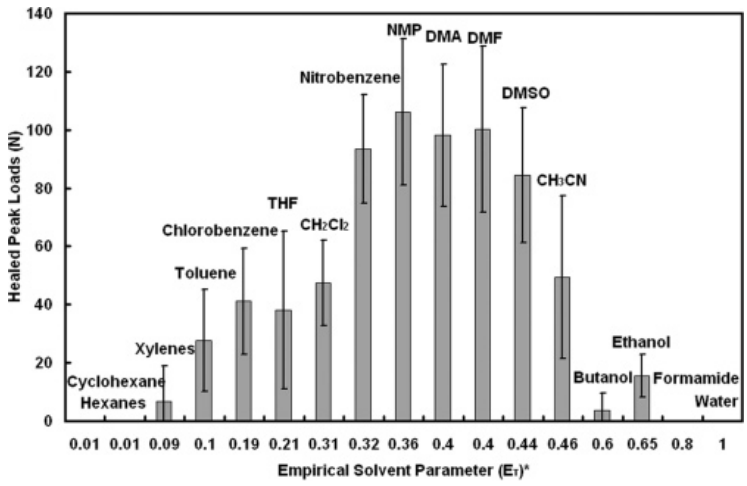

Figure 2.11: Solvent screening for their healing effectiveness [6].

Given the toxicity of chlorobenzene, in 2008 the investigations moved to greener solvents, such as PA and EPA, and hexyl acetate (HA) for control experiments. Moreover, given the proposed mechanism that healing was occurring thanks to the curing of residual amine functionalities transported in the matrix sol, it was believed that co-encapsulating epoxy functionalities could increase the healing efficiency. However, by keeping the stoichiometric ratio of EPON 828/DETA fixed in the matrix, it was found that adding too

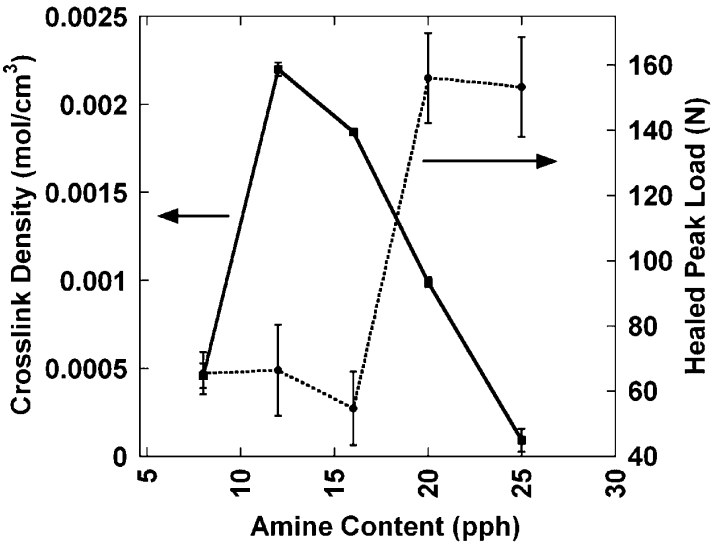

Figure 2.12: Healed peak loads as a function of amine content thus crosslinking density [6].

much epoxy (20 wt%) in the capsule core decreased the healing efficiency from 82 to 30%. Thus, a core formulation with 5 wt% epoxy dissolved in the solvent was considered as optimal and provided efficiencies of 100% indeed. In other terms, the amount of epoxy delivered to the crack plane (function of epoxy content in the core, capsule loading and diameter) was also calculated and the maximal healing was found to occur for 0.1 mg/cm^2. The healing efficiency also was found to depend on the capsule content; complete recovery was obtained at 15 wt% capsule loading and above. Furthermore, up to 3-5 multiple healing events were observed and attributed to the rupture of new capsules by the propagating deviated crack. Preliminary ageing studies demonstrated that the healing efficiency decreased by approximately 30% after storing the samples at room temperature during a month [7].

The encapsulation procedure of EPON 828 (DGEBA) and EPON 862 (DGEBF) diluted in chlorobenzene, PA and EPA was fine tuned by Blaiszik *et al.* in 2009, adapting the standard protocol of Brown *et al.* [94]. Yields, size distributions, stirring rate/capsule size dependence, thermal properties and shell morphology were studied. Concerning EPON 828/EPA capsules, yields were approximately 92%, the dependence between agitation rate and capsule diameter was found as indicated in Figure 2.13, the capsules were thermally stable up to 180°C (only 20% of mass loss). Moreover, a new protocol to produce capsules with diameters smaller than 10 μm was investigated [8].

More recently, the solvent-based healing chemistry so developed for bulk polymers was applied by Jones *et al.* for repairing the debonded interface between an epoxy matrix and a glass fibre. A single glass fibre was isolated and functionalised with EPON 862/EPA capsules, in order to integrate them specifically at the site of damage. Microbond specimens consisted then in the functionalised fibre embedded in an epoxy droplet. Healing effi-

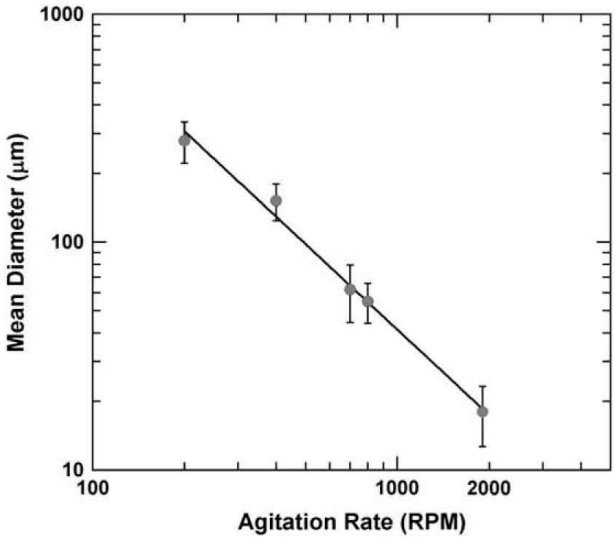

Figure 2.13: Mean diameter of EPON 828/EPA capsules (15 wt% epoxy) as a function of the emulsion stirring rate [8].

ciency was calculated from the ratio of the recovered interfacial shear strength (IFSS) to the virgin value. Nearly full recovery was achieved; with increasing the capsule coverage, the virgin IFSS was only slightly reduced and higher efficiencies were obtained. Moreover, a critical volume of EPON 862 of 300 μm^3 was required for a maximal recovery [11].

Further investigations on the mechanism of the solvent healing were then presented by Neuser *et al.* between 2012 and 2014. The main conclusions that arose were:

- ▷ it was confirmed that healing is firstly based on the matrix swelling due to the diffusion of the solvent molecules into the matrix: the mass gain as a function of time was quantified in an ideal case of epoxy cylinders immersed in EPA and the swelling thickness was calculated assuming a Case II diffusion (Figure 2.14). It was estimated that the maximum crack face separation that can be healed in 24 h corresponded to 31 μm [9];

- ▷ it was found that the EPA diffusion into the matrix causes a decrease of the matrix T_g by approximately 30°C, enabling the reaction of the unreacted functionalities present in the matrix [9]. The presence of unreacted functionalities is a necessary condition without which the system cannot be effective; however, it represents an unstable state for the material, since the degree of polymerisation can evolve over time leading to the loss of the healing functionality;

- ▷ ageing studies demonstrated that the healing efficiency could drop from 77 to 13% after 77 days ageing at room temperature (Figure 2.15), due to the solvent diffusion through the capsule shell, that led to a decreased residual heat of reaction of the matrix. This confirmed the previous observations of M. Caruso [115], who showed

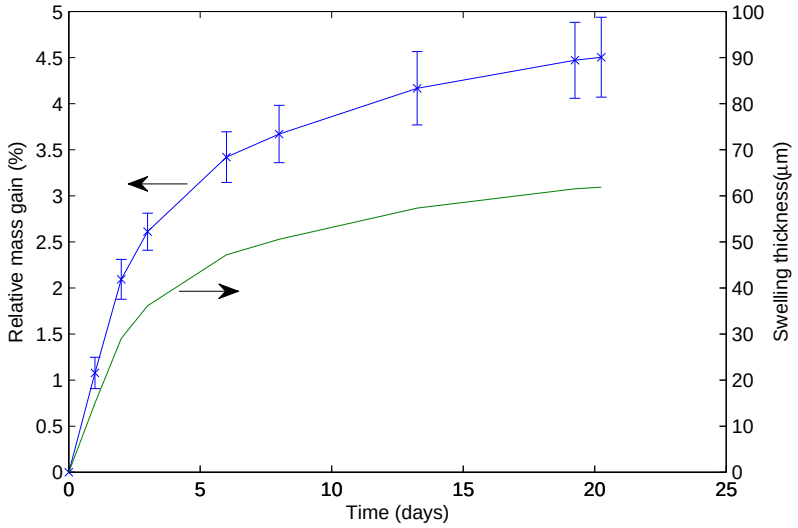

Figure 2.14: Average weight of epoxy cylinders immersed in EPA solvent over 3 weeks and corresponding swelling thickness [9].

that 30 days ageing of the capsules caused a decrease of healing efficiency, that dropped down to zero after 1.5 years, due to the completion of the polymerisation thus the lack of residual functionality within the matrix (Figure 2.16). Moreover, it was noticed that water absorption was another reason for a decrease in healing efficiency, as the hydrophobic solvent diffuses less successfully in the presence of moisture. Thus, in order for the solvent system concept to be viable, the solvent diffusion must completely be avoided and the moisture controlled [10];

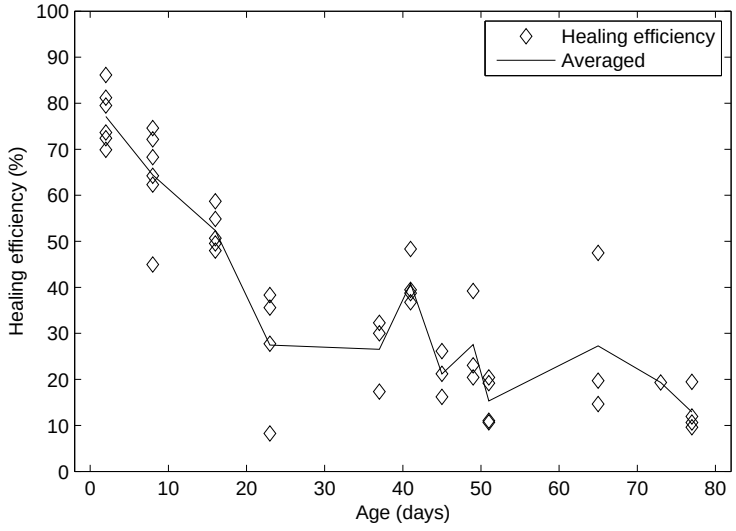

Figure 2.15: Effect of TDCB samples ageing at room temperature on autonomic healing efficiency of EPON 828/EPA capsules [10].

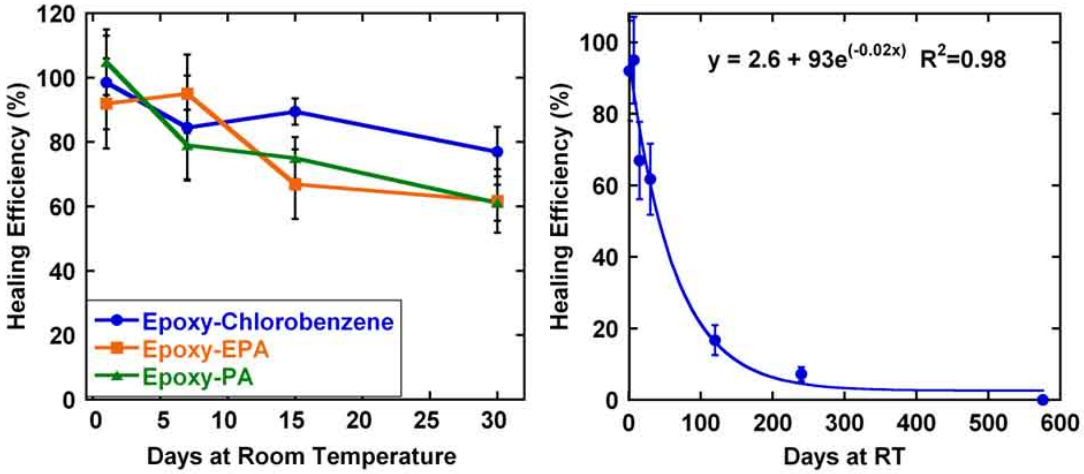

Figure 2.16: Short and long term ageing studies on EPON 828-solvent capsule systems (15 wt% loading) with 24 h healing time and short-groove TDCB specimens [115].

- ▷ the solvent healing system works for specimens subject to fatigue loading, since the stresses at the crack tip can be reduced due to the solvent diffusion. Indeed, in an under-cured epoxy matrix loaded with solvent microcapsules, a crack arrest is achieved after a lower number of cycles if compared with the plain matrix (Figure 2.17) [12]. However, for cracks propagated under static loading, healing efficiencies only up to approximately 30% were achieved using long-groove TDCB samples. These values could increase to 90-100% when using short-groove TDCB specimens or when placing Shape Memory Alloy (SMA) wires perpendicular to the crack plane in order to enable crack closure [9].

- ▷ for fully cured epoxy, the solvent system neither repairs statically fractured crack planes (due to low solvent diffusion rate and low residual functionality concentration), nor enables crack arrest during fatigue testing (due to inhibited solvent diffusion) (Figure 2.18) [12]. The evolution of the conversion for the initial under-cured system must thus be avoided since it can lead to complete loss of the healing properties.

2.3 The assessment of the healing efficiency

2.3.1 What does healing efficiency mean?

All the results in the field of self-healing materials are consistent if an evaluation of the healing efficiency they are able to achieve is provided. This parameter enables the comparison of results in a quantitative way and the deduction of the quality of the performance that a certain healing system is able to show. The assessment of the healing efficiency is always carried out through the following steps:

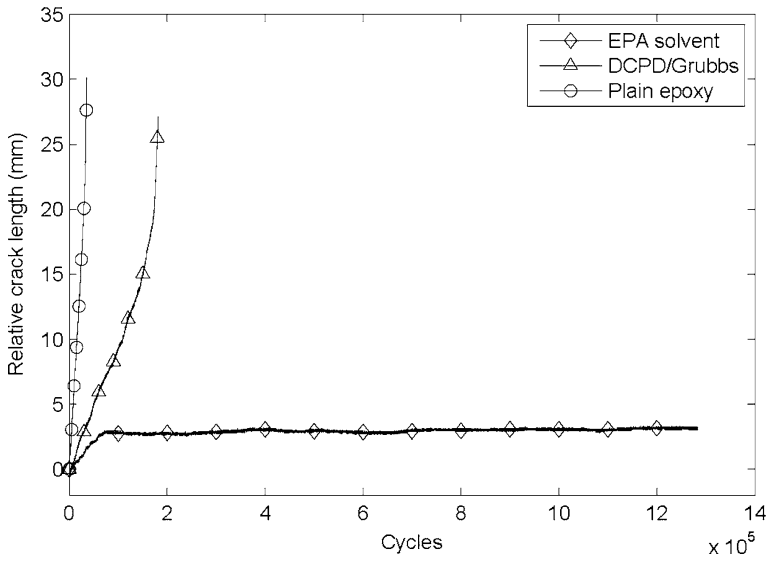

Figure 2.17: Crack evolution for plain epoxy and epoxy loaded with DCPD/Grubbs' and EPA capsules [12].

1. choice of a material property, thus a suitable method of testing in order to obtain the value of this property;

2. testing of the *virgin* material and extraction of the value of the property in the virgin state (P^{virgin}); thus, a certain damage is induced in the material, resulting in a loss of the chosen property;

3. concurrently on the same or different sample(s):

▷ testing of the *damaged* material and extraction of the value of the property in the damaged state ($P^{damaged}$);

▷ healing step of the material, in specific conditions of temperature, time, etc. and testing of the *healed* material with extraction of the value of the property in the healed state (P^{healed}).

If we define *Loss* the amount of the property lost between the virgin and the damaged state (no healing occurred) and *Recovery* the amount of the property recovered in the healed state (compared to the damaged state), we can define the healing efficiency η with Equation 2.1

$$\eta = \frac{Recovery}{Loss} = \frac{P^{healed} - P^{damaged}}{P^{virgin} - P^{damaged}} \cdot 100 \tag{2.1}$$

Figure 2.19 helps to understand the concept of efficiency.

The approach that leads to Equation 2.1 takes into account that the property in the damaged state could not be entirely lost, so $P^{damaged}$ might be not zero . Healing efficiencies calculated on samples that are catastrophically failed, *i.e.* with $P^{damaged} = 0$,

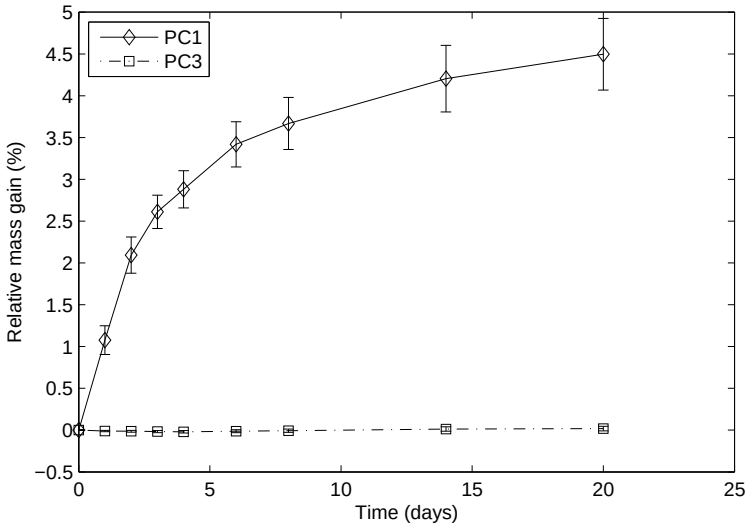

Figure 2.18: Mass increase of under-cured (PC1, curing of 24 h at 25°C and post-curing of 24 h at 35°C) and almost fully cured (PC3, curing of 24 h at 25°C and post-curing of 6 h at 45°C and 45 min at 75°C) epoxy cylinders immersed in EPA solvent [12].

are probably more rigorous, since the control on the virgin failure and the subsequent healing event can be along a single fracture path. On the other side, causing only partial damage may be a more realistic way to simulate failure conditions such as microcracking and delaminations (that is what the self-healing concept was originally thought for).

Such a definition results to be more precise in comparison with the first one given by Woll & O'Connor in 1981 [116]: a specific property was considered (fracture toughness in mode I K_{Ic}) and $P^{damaged} = 0$:

$$\eta = \frac{K_{Ic}^{healed}}{K_{Ic}^{virgin}} \cdot 100 \tag{2.2}$$

First results of White *et al.* [3] were based on this last definition, adopting P_C as critical load at fracture in quasi-static fracture tests and again $P^{damaged} = 0$:

$$\eta = \frac{P_C^{healed}}{P_C^{virgin}} \cdot 100 \tag{2.3}$$

This was allowed since (i) in quasi-static fracture the fracture resistance in damaged state is zero and (ii) the fracture toughness K_{Ic} depends only on the applied load and is independent of the crack length, which is true for specimens where compliance changes linearly with crack length during testing ($K_{Ic} = \alpha P_C$ where α is function of geometry and material properties).

Moreover, the virgin property could refer to the *neat* material or to the material which contains the healing system. These two values can be different, meaning that the healing additives may increase or decrease the virgin properties. For instance, Brown *et al.* [117] showed that microcapsules increase virgin fracture toughness because they

constitute a crack deflection system (depending on their morphology), whereas they decrease the stiffness and the ultimate strength. This clarification is crucial especially when comparing healing efficiencies at different contents of healing additives (and, even more, when comparing beneficial with detrimental additives). By using this approach, a useful extra information, that is the increase or reduction of the virgin property in the presence of the healing system, could be calculated [112]. Nevertheless, while evaluating healing efficiencies, it should be noted that both increasing the healed material property and decreasing the virgin properties in the presence of the healing system may lead to increase η: obviously, the latter is not a promising option.

Another crucial aspect is the existence of multiple healing efficiency values. This could happen when the measured property, both in the virgin and in the healed state, may vary due to simple property anisotropy in the virgin state, uneven coverage of fracture plane with the healing agent or contaminations of the fracture plane. In these cases, an average healing efficiency and a maximum healing efficiency should be defined [2], as in Equation 2.4 and Equation 2.5, respectively

$$\eta_{avg} = \frac{Average[P^{healed}]}{Average[P^{virgin}]} \cdot 100 \tag{2.4}$$

$$\eta_{max} = \frac{Max[P^{healed}]}{Average[P^{virgin}]} \cdot 100 \tag{2.5}$$

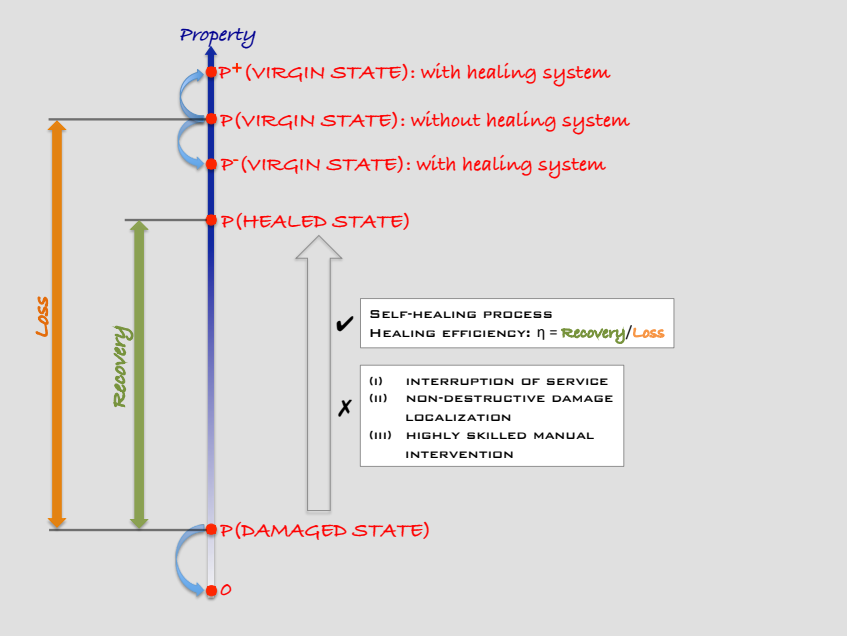

Figure 2.19: Schematic representation of the concept of self-healing referred to a specific material property.

Many factors influence healing efficiency, as identified by Wool & O'Connor [116]:

▷ TIME: at constant temperature, in general, increasing the healing time increases the efficiency; an empirical formula, without any microscopic physical foundation, based on a kinetic theory of healing, exists.

▷ TEMPERATURE: at constant time, given two healing temperatures T_1 and T_2, and the glass transition temperature of the healing phase T_g, the temperature dependence on η is given by Equation 2.6

$$\eta(T_1) \begin{cases} > \eta(T_2) & T_1 > T_2 > T_g \\ = \eta(T_2) & T_2 < T_1 < T_g \end{cases} \tag{2.6}$$

It is worth noting that the healing temperature, which takes into account the curing temperature of the healing agent, must not be higher than the glass transition of the matrix, in the case of amorphous thermosets.

▷ HEALING LAY-OUT*:* until an optimal autonomous self-healing system will be developed, external or internal interventions can increase the healing performance. For instance, some examples are the use of external clamps to manually decrease the crack volume and bridge the crack faces closer together (*e.g.* [1, 2]) or the use of shape memory alloys (SMA) wires (*e.g.* [9, 12]).

▷ CAPSULES DISTRIBUTION AND SIZE*:* in the case of microcapsules, the efficiency depends on how many capsules are broken by the crack and, consequently, on how much healing agent could be delivered. Dispersion and distribution of microcapsules (together with their size) play a critical role. In order to simulate an ideal healing at a laboratory scale, some authors placed a given amount of microcapsules just in the zone where crack was expected to propagate.

▷ STIFFNESS RATIO AND FRACTURE TOUGHNESS RATIO: in addition, one of the most important key issues of the microencapsulation approach is the requirement that cracks passes through capsules. The crack propagation route depends on the stiffness ratio between an inclusion on the path (a capsule in this case) and the matrix. In order to make sure the crack does not deviate away from the capsule, but encounters it instead, the capsule modulus must be lower than the matrix modulus, otherwise the crack would tend to round the capsule [3]. Some simulation experiments showed that also the fracture toughness difference between matrix and capsule should be less than 0.11 MPa $m^{1/2}$, otherwise the crack would not be attracted from the capsule [118].

2.3.2 Healing efficiency evaluation methods

As mentioned, the evaluation of healing requires the choice of a damaging mode. Many different damage methods have been applied, since a unifying standard is lacking. The extent of damage that these methods provoke ranges from microcracking and thin delamination to catastrophic failure of specimens.

A brief overview of different damage procedures, and consequently healing assessment methods, follows [37]. Various evaluation methods can be grouped in five main categories: quasi-static, fatigue, impact, indentation and barrier tests. Every damage method enables to extract a specific mechanical property, based on which the evaluation of healing is done.

Quasi-static fracture Quasi-static tests are the most common ones and they generally cause small damage volumes, with small crack separation. Healing efficiency is calculated with Equation 2.1, in which $P^{damaged}$ is zero since the fracture resistance in the damaged state is zero. The mechanical property which is usually extracted from these types of tests is the fracture toughness, but sometimes it is replaced by the peak fracture load. For tearing mode tests, the property is the tear strength, for bending the flexural strength. Quasi-static tests can be divided in:

- ▷ Mode I (tensile fracture): the most common specimen (for polymers rather than composites) is the TDCB, first introduced by Mostovoy *et al.* [119] and extensively adopted in the self-healing literature (firstly by White *et al.*), since it allows the crack to grow along the centerline in a controlled way and the compliance (and consequently the fracture toughness) to be length-independent and to depend only on the applied load, avoiding to measure the crack length *in situ*. The specimens are usually pre-notched with a razor blade. From the measured force vs. crack opening displacement (COD) plot one extracts the peak load P_C and then calculates K_{IC} with Equation 2.7 (or others existing), both in the virgin and in the healed specimen

$$K_{IC} = 2P_C \frac{\sqrt{m}}{\beta} \tag{2.7}$$

  where β is a geometrical factor depending on sample geometry, $m = \frac{Eb}{8}\frac{dC}{da}$, E is the Young's modulus, b is the specimen width, a is the crack length and C is the compliance (which is constant over different a values). Healing efficiencies obtained over the last years were between 75 and 93% [3, 97, 102, 117]. Other sample geometries are the double-cantilever beam (DCB), width-tapered double cantilever beam (WTDCB), compact tension (CT) (which cause a larger crack separation and it is therefore modified with a crack arrest hole to prevent complete failure), single-edge notched beam (SENB), 3-point bend, 4-point bend (preferred to 3-point bend because it does not cause an indentation effect) and double cleavage drilled

compression (DCDC). Figure 2.20 summarises the different specimen geometries.

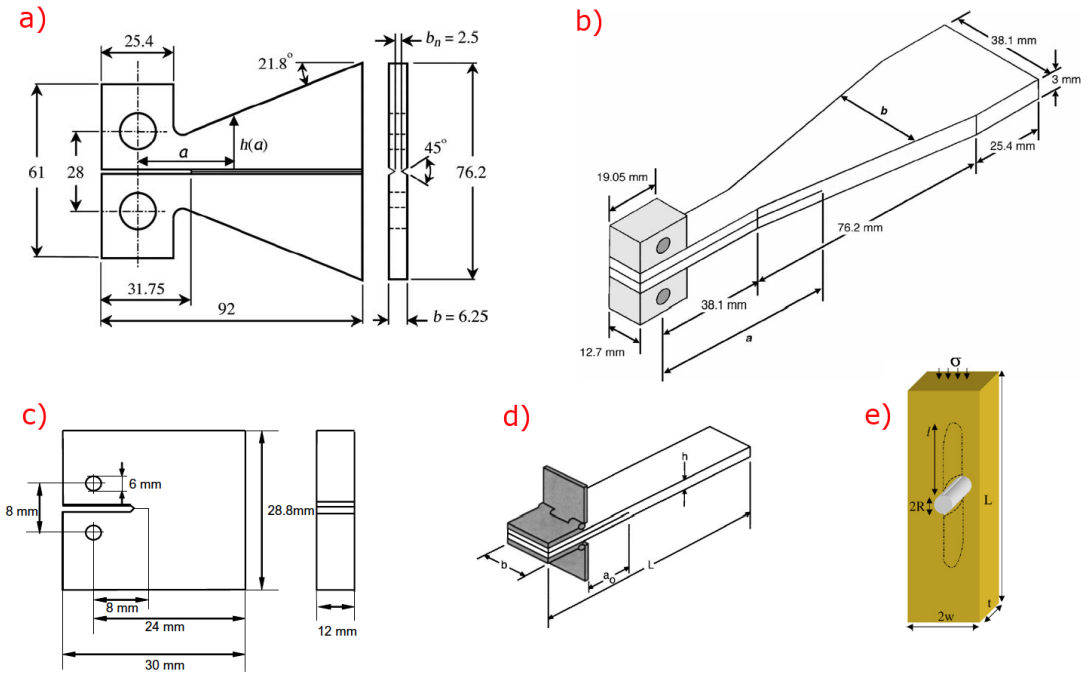

Figure 2.20: Different specimen geometries for thermo-mechanical tests: a) TDCB, b) WTDCB, c) CT, d) DCB, e) DCDC [3].

- ▷ Mode II (shear fracture): not being used as widely as Mode I, this damaging mode makes the crack propagate in shear mode and the fracture toughness K_{IIC} can also be calculated. No traces are found in literature related to self-healing assessment.

- ▷ Mode III (tearing fracture)*:* this mode makes use of the trouser test specimen; some work has been done by Keller *et al.* with capsule-based PDMS-Pt catalyst healing system [72].

- ▷ Cutting*:* this is a qualitative method to evaluate the healing efficiency, since it is based on cutting the sample with a blade and optically evaluating the crack closure after the healing event. It is however useful for ductile samples.

Fatigue Cyclic tests are very important because they simulate common and frequent failure modes in structural materials. In this case, the reference property is the fatigue life (in term of number of cycles) and the fatigue life extension λ (Equation 2.8) as a measure of healing efficiency

$$\lambda = \frac{N^{healed} - N^{control}}{N^{control}} \tag{2.8}$$

where $N^{healed}$and $N^{control}$ are the total number of cycles to failure for the healed sample and for the sample without healing, respectively. As yet, fatigue experiments have been

performed by Brown *et al.* [120] and later by Jones *et al.* [121], showing different results depending on the applied stress intensity factor ΔK_I. Neuser *et al.* [12], also, used fatigue testing for observing the crack arrest related to the diffusion of the solvent capsule core. A certain amount of life extension was obtained thanks to toughening mechanisms acted by microcapsules, crack tip shielding and crack closure due to the polymerisation of the healing agent. The latter was observed only if some rest periods during the experiment were inserted, to allow the healing to happen. Jones *et al.* obtained encouraging results thanks to the wax encapsulation of the catalyst and to the consequent higher polymerisation rate of the healing agent. More recently, Ye *et al.* [122] also used fatigue testing to assess the time of the healing phenomenon.

Impact Some tests on composite panels subject the material to low-velocity impacts. The reference property, in this case, was the residual (*i.e.* after impact) compressive strength, being evaluated with and without healing time after impact. These tests are referred as compression-after-impact (CAI) tests and the procedures are explained with two ASTM standards [123, 124]. Patel *et al.* [125] used this damaging test for fibre-reinforced microcapsule-based self-healing composites. The main issues concerning this type of test consist in (i) the perfect alignment conditions required for the compressive test, that mean the need of very accurate grinding of the sample edges and compression frame alignment procedures, (ii) the need of thick samples (*e.g.* 5 mm) so the adaptation of the liquid manufacturing techniques [120].

Others Indentations tests are useful to reproduce impact tests but with a lower amount of damage. Up to date, all these experiments have been done on composites with a microvascular self-healing system, rather than capsule-based [42–46].

Moreover, barrier properties are usually deteriorated if a crack passes through the thickness of a material, which can enable the diffusion of some fluid avoiding a correct seal. The idea to extend self-healing properties to materials used for barrier purposes (some examples in [126–128]) has come concurrently with the results of Moll *et al.* [129], who tested healing performances of a 4 mm-thick epoxy composite loaded with capsule-based self-healing system.

Other properties that can be recovered are the corrosion resistance (critical in coatings for the protection of metallic components that operate in aqueous and saline environments, for instance) and electrical conductivity (in solders). Corrosion resistant polymeric or organic coatings able to self-heal harnessing either capsule-based or intrinsic systems have been recently developed [79, 130, 131] and first microcapsule systems for the restoration of conductivity in mechanically damaged electronic devices, in which the repairing agent is not conductive until its release, have been also investigated [132].

2.4 Integration of self-healing systems in FRPs

Self-healing approaches have been applied to FRPs starting from the last decade, both for polymers reinforced with glass and carbon fibres; however, both cases were only scarcely investigated despite the great potential they could offer. Incorporating in FRPs an added functionality such as self-healing is very promising and it could be a great benefit for these materials, since they often manifest types of damage difficult to visually detect and that can grow further, as matrix intra-ply microcracking or inter-ply delaminations.

2.4.1 Integration of capsule-based extrinsic healing systems

The concept of introducing an encapsulated self-repair functionality into composite materials was born about 15 years ago, when Kessler *et al.* presented a first structural fibre self-healing composite [1, 2], taking the cue from the previously developed self-healing thermoset polymers [3] and from initial concepts of Dry *et al.* [4], which used hollow repair fibres.

Kessler *et al.* manufactured self-healing composites by hand lay-up and compression molding, the matrix was a toughened epoxy resin cured with a secondary or tertiary amine, the woven reinforcement was satin or plain E-glass, or plain carbon; the healing system belonged to the extrinsic capsule-based category of systems [37] and exploited the reaction between the core of microcapsules (DCPD) and a second generation Grubbs' catalyst, both dispersed within the matrix of the central layers. The DCB test was initially used to assess the healing efficiency, taking into account the initiation and propagation strain energy release rate, while the WTDCB test was used later on considering the average critical load to propagate the crack. For self-activated samples (embedded catalyst and injected healing agent), healing efficiencies did not exceed 20% in the first article; the authors attributed the reason to (i) the presence of catalyst clusters, that lowered the fracture toughness and contributed to unstable crack propagation; (ii) an incomplete coverage of the fracture plane with the injected healing agent, due to the slow polymerisation rate and the subsequent diffusion of the monomer into the matrix; (iii) the interfacial debonding as dominant failure mode. For a fully integrated system (both catalyst and healing capsules embedded in the matrix), the second article presented healing efficiencies up to 45% (room temperature healing) and to 80% (80°C healing), thanks to a higher capsule loading although to the detriment of a 21% lower virgin toughness of the capsule/catalyst-loaded thick layer.

The healing of other failure modes was explored later by Sanada *et al.* [133–135], to repair the interfacial debonding of unidirectional carbon/epoxy composites occurring during tensile tests using the same DCPD/Grubbs' catalyst system and by Yin *et al.* [136], who employed a new healing system (30 wt% embedded epoxy capsules and 2 wt% latent hardener) and used CAI tests.

Furthermore, Patel *et al.* [125] investigated the healing of low-velocity impacts-induced delaminations through CAI tests. The manufacturing route and healing system were the same as Kessler *et al.* Very thick glass reinforcements were used and a bimodal size distribution of capsules was employed. Results indicated that healed specimens exhibited a decreased crack length and a partial recovery of residual compressive strength.

Concerning the solvent-based healing system proposed by Caruso *et al.* [6, 7] and further investigated by Blaiszik *et al.* [8] and Neuser *et al.* [9, 10, 12], it has not been investigated yet for FRPs.

2.4.2 Key points of self-healing for FRPs

Transitioning from neat self-healing resins to fibre-reinforced composites implies some complications, that are summarised below.

Rheological properties of the matrix The viscosity of the resin becomes fundamental for FRPs since they are usually manufactured by liquid transfer molding techniques, where the resin flow and the fibres impregnation are key points. The option of adding a viscosity modifier exist in order to have a better impregnation, however with the possible implication of increasing the matrix fracture toughness, thus the crack growth stability. Nevertheless, the introduction of the healing agent might also lead to a viscosity increase.

Introduction and survival of the healing agent Introduction and survival of the healing system is one of the major issues in the manufacturing of such composites. Concerning microcapsule-based extrinsic healing systems, two techniques for incorporating the healing agent have been proposed so far. Kessler *et al.* [1, 2] and Patel *et al.* [125] simply mixed capsules with the epoxy resin prior to hand lay-up; this solution leads to two side issues, typically the increase of the matrix viscosity, with consequent risk of poor impregnation, and the possible retention of capsules through the fabrics. Sanada *et al.* [134] slightly modified this methodology performing a dip-coating of the reinforcement (carbon fibre strands) in a strongly capsule-loaded resin, followed by partial curing and further impregnation with the same resin. A second strategy consisted instead in functionalising the fibre reinforcement rather than the matrix. Blaiszik *et al.* [137], although dealing with single glass fibres, used a dip-coating technique in order to couple catalyst particles first and then 1.5 μm diameter healing capsules; the dipping medium was in this case a liquid destined to evaporate. This procedure is undoubtedly elegant but might become significantly time-consuming. Jones *et al.* [11] also functionalised single fibres by dipping them in an aqueous solution of capsules, with the aim of further embedding them in epoxy droplets and testing the healing mechanism of the epoxy-fibre interface through a microbond test. An alternative method of fabric functionalisation consists in the manual dispersion of capsules by hand sieving, which ensures an acceptable degree of

capsule dispersion and distribution, although is not indicated for non-flat shapes. In literature, such a technique can be found for the functionalisation of preforms with binders or tackifiers [138], and it lends itself to scale-up using the same automatised methods as for binder deposition on fabrics directly following the weaving process.

Healing agent dimensions and dispersion Care should be taken when selecting the size of the healing agent. In the case of capsule-based healing systems, large capsules might disrupt the yarns network and create resin-rich areas, thus weakening the composite. Nevertheless, they might lead to increase the the composite ply thickness thus decreasing the virgin interlaminar fracture toughness. Moreover, the presence of capsules, depending on their size, could affect the compressibility of the preform and, not least, change its permeability. On the other hand, the use of too small diameter capsules would mean smaller amount of healing agent available, thus possibly delivered.

In the case of catalyts, smaller sizes are preferred since they can infiltrate narrow interlaminar regions; however, the efficiency of the catalyst protection by wax, necessary to avoid catalyst deactivation and clustering, decreases with size, since the ratio surface area/volume concurrently increases.

New processing routes Producing self-healing FRPs rather than self-healing neat polymers implies the choice and the adaptation of new processing routes. Hand lay-up, resin transfer molding (RTM), VARIM and compression molding constitute available options. Their adaptation in terms of processing/cure/post-cure temperatures, pressure or vacuum level, etc., is necessary in the presence of the healing agent. An important key point is also the achievement of specific fibre volume fraction in the presence of the healing agent.

New assessment methods New assessment methods, for example new specimen geometries, may be more adapted for testing the healing efficiency of self-healing FRPs. As mentioned, the DCB test was first used by Kessler *et al.* (and then by Yin *et al.* [136]) by using the initiation and propagation strain energy release rate as assessment property, while the WTDCB test was used later on considering the average critical load to propagate the crack [1, 2].

Alternatively, Patel *et al.* [125] investigated low-velocity (up to 45 J) impact damages, since composites are relatively vulnerable of damage from out-of-plane impact events, which lead not only, eventually, to fibre breakage, but especially to matrix delamination and transverse cracks, subsurface or more widespread located. They measured the efficiency with the already mentioned CAI testing protocol with a large curvature of the impact head and a precise range of impact energies (in order to avoid relevant fibres rupture). The efficiency was expressed in term of recovery of residual compressive strength

(RCS): this property has been found sensitive to impact damages, since a great reduction in compression is observed after the impact event, due to laminae buckling in the delaminated areas [139].

Moreover, an example of testing the healing efficiency through pure Charpy impact as assessment method can be found in the publication by Hayes *et al.* [58].

Tensile tests were used by Sanada *et al.* [133–135], to check the repair of interfacial debonding of unidirectional carbon/epoxy composites.

2.5 Summary

This chapter gave an overview of the literature review on the main points of interest of the present work. First, common forms of damage for FRPs were explored, in order to understand a suitable strategy to heal them. Interlaminar, intralaminar and translaminar cracks, as well as barely visible impact damage, most commonly occur in composites, due to different loading types, namely tension, compression and impact. Furthermore, a literature study about extrinsic healing approaches was presented; the pioneering approach based on DCPD capsules and Grubbs' catalyst was described and taken as reference for reviewing all alternative systems. A deeper investigation on the solvent capsule-based system was carried out, since it is the approach of interest. This system represents an evolution from the pioneering approach, being also extrinsic, irreversible, capsule-based, pseudo-autonomous, but one-component. Also, it is unique system -among the extrinsic category- since the healed material does not differ from the virgin one.

Finally, a general review about the assessment of the healing efficiency, in terms of formula used and evaluation methods (mechanical tests) performed, was presented. Not least, a final description about how self-healing concepts apply to fibre-reinforced rather than neat polymers, was given.

Chapter 3

Materials and methods

3.1 Epoxy resin

Two epoxy resins were used for this work:

- EPON 862 (Momentive), a diglycidyl ether bisphenol F (DGEBF) resin, cured with diethylentriamine (DETA, Sigma Aldrich) in a 100:12 weight ratio for 24 h at room temperature and post-cured for 24 h at 35°C (if not otherwise defined);

- EPON 828EL (Momentive), a diglycidyl ether bisphenol A (DGEBA) resin, also cured with diethylentriamine (DETA, Sigma Aldrich) in a 100:12 weight ratio for 24 h at room temperature and post-cured for 24 h at 35°C (if not otherwise defined).

Epoxy resins rather than other thermoset materials were chosen for the present thesis for the main reason of comparing the results with the work previously carried out related to the study of healing in the neat epoxy (specifically EPON 828EL) [14]. Also, epoxy resins give quite brittle thermoset polymers which are suitable for studying healing and are commonly used for processing techniques such as liquid composite molding. EPON 862, thanks to a slightly different chemical structure compared to EPON 828EL (differing by two methyl groups), presents a 4 times lower viscosity, thus is more versatile for fabric impregnation. DETA was chosen as hardener since it allows low-temperature curing. Note that the resin/hardener ratio used herein corresponds to the stoichiometric ratio [6]. No additional hardener was introduced as compared to the stoichiometric ratio, thus the healing mechanism was based on the presence of unreacted functionalities obtained by under-curing the matrix. This represents a known intrinsic drawback for the selected healing system, since the under-cured system can evolve over time thus the healing efficiency can be lost. Nonetheless this system represents a good model system for the develop of a self-healing composite, provided that the samples are stored for limited time and at low temperature and controlled humidity.

3.2 Fibre reinforcement

The fibre reinforcement was a standard woven twill 2 × 2 E-glass purchased by Suter Kunststoffe AG (Figure 3.1). The nominal construction of the fabric corresponded to 6 end/cm for warp fibres and 6.7 pick/cm for weft fibres. As indicated by the manufacturer, both warp and weft fibre diameters were 9 μm, yarn thickness 0.45 mm (in unloaded conditions), warp and weft tex 68 × 5 and 272 respectively [140]. The fabrics presented a nominal areal weight of 390 g/m^2, with a fluctuation which was measured on 100 × 100 mm samples to be ± 2.7% over the nominal value (Figure 3.2). If not otherwise defined, a stacking sequence of 16 layers of fabric with $[(+45/\text{-}45)/(0/90)]_{4s}$ was used. A fibre volume fraction V_f of 50 vol% was targeted.

The choice of a woven fabric rather than unidirectional has been related to the aim of having a surface ply morphology that could provide interbundle spaces where the healing capsules could fit being more protected and safe compared than laying onto the reinforcement tows. Moreover, investigating the use of carbon reinforcements rather than glass ones was out of the scopes of the present work, although we believe similar results could be obtained.

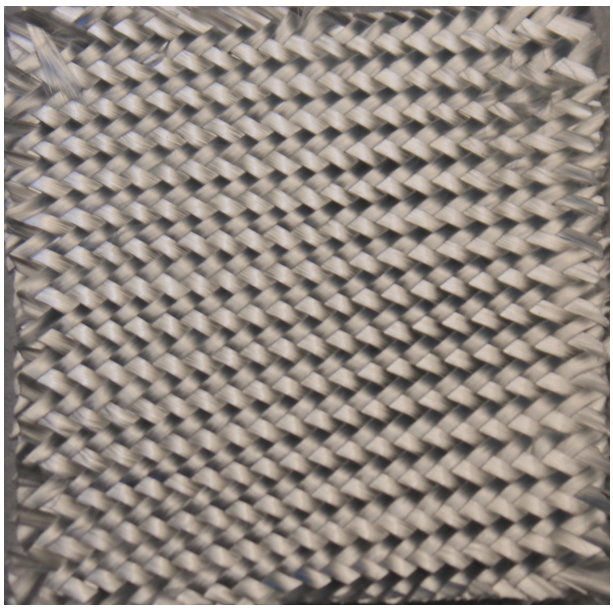

Figure 3.1: Picture of the selected glass fabric reinforcement.

3.3 Capsule production

The preparation of microcapsules was carried out using an oil-in water emulsion technique, following the protocol established by Blaiszik *et al.* [8]. First, 100 ml distilled water and 25 ml of a 2.5% wt/v ethylene maleic copolymer solution (2.5%, Sigma Aldrich) were poured in a 600 ml beaker. Then 2.5 g urea (Acros Organics), 0.25 g ammonium chloride

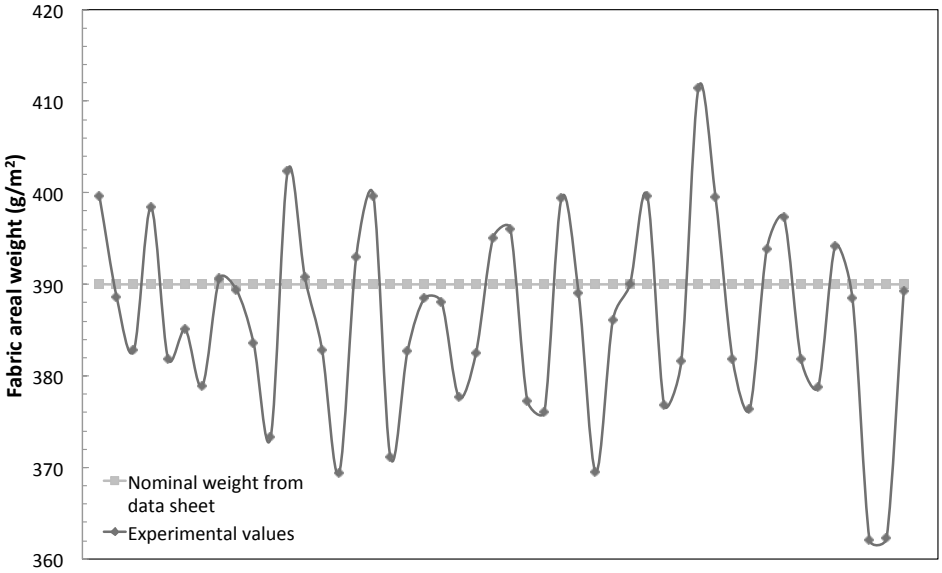

Figure 3.2: Fluctuation of the fabric nominal areal weight.

(Fluka) and 0.25 g resorcinol (Sigma Aldrich) were added in that order. When required, capsules were dyed in order to make them more visible when functionalising the glass fabrics; in those cases, a few mg of red dye (Oil Red O, Sigma Aldrich) was added to the formulation. The pH was tuned to 3.5 using sodium hydroxide (20%, Acros) and stirring at 400 rpm was started, with an expected mean capsule diameter of approximately 150 μm, as shown by Blaiszik *et al.* At this point, 60 ml of the core material were added and left for 10 min in order to have a stable agitated emulsion before adding 6.33 g formaldehyde (37%, Sigma Aldrich) and covering the beaker with aluminum foil. At this point, heating was started (55°C at 1°C/min). After 4 h, the capsules were left to cool down to room temperature for at least 24 h and washed with approximately 500 ml of distilled water while filtering under vacuum using a coarse fritted glass filter with a porosity grade 2 (P2, 40-100 μm). The capsules were then allowed to dry for 48 h under a chemical hood before they were stored at room temperature. For all batches, size fractions of <90, 90-125, 125-180, 180-250 and 250-355 μm were separated by manual sieving and retained for use.

Different types of capsules were produced, differing in the combination of their shell and core. Two types of capsule core were prepared, with two different solvents, which differ in their polarity, thus their ability to diffuse into the composite matrix and initiate the healing process:

- ▷ solution of 2.5 vol% of EPON 828EL (Momentive) in ethyl phenylacetate (EPA, 99% Acros Organics), for *healing* capsules;
- ▷ hexylacetate (HA), for *control* capsules.

Two types of shell were produced, in order to investigate how the capsule mechanical

properties can change:

- ▷ urea-formaldehyde for pure-UF (or mono-wall) capsules, following the procedure indicated above;

- ▷ urea-formaldehyde/polyurethane for PU-reinforced (or double-wall or PU/UF) capsules; for this type of capsule, different concentrations (2.5, 5 and 7.5 g) of a PU precursor solution was previously added to the core formulation. Such a solution is called Desmodur L75 (Bayer) and is a prepolymer solution in ethyl acetate with an equivalent weight of 315 g and an isocyanate content of 13.3 ± 0.4 wt%. Before use, the contact between the solution and moisture must be strictly avoided. Caruso *et al.* reported a successful encapsulation of EPA/EPON 828 with different amounts of dissolved Desmodur L75 for obtaining a double-shell PU/UF. It was found that the addition of the PU prepolymer solution leads to an encapsulation via combined *in situ* poly(UF) microencapsulation with an interfacial polyurethane microencapsulation and does not affect the mean size/stirring rate dependence [83].

3.4 Capsule characterisation

3.4.1 Thermogravimetric analysis (TGA)

The thermal stability of microcapsules was tested using TGA on a Mettler Toledo SDTA 851e, available at the Powder Technology Laboratory (LTP) at EPFL. In general, the samples were kept at ambient conditions for several days before testing and 10-15 mg were transferred to alumina crucibles which were then subject to a temperature ramp at 10°C/min from 30°C to 400°C or 600°C, under nitrogen. The relative mass loss was then computed to investigate the critical temperatures of the microcapsules, relative to the boiling temperatures of their core.

3.4.2 Optical microscopy (OM) and scanning electron microscopy (SEM)

An optical microscope (Olympus BH-2) was used to acquire images of the capsules. For better imaging, capsules were dispersed in mineral oil. The capsule diameters were measured on optical images (50 measurements per image) and the average number length diameter was calculated for a specific size fraction. The same microscope was also used to investigate the aspect of the slices for atomic force microscopy (AFM) measurements (§ 3.4.4).

Furthermore, SEM analysis was used in order to characterise the diameter-dependent shell thickness of microcapsules. The tests were carried out on the XLF-30 FEG, FEI

available at the Interdisciplinary Center for Electron Microscopy (CIME) at EPFL. For each type of capsules, five different size fractions (<90, 90-125, 125-180, 180-250 and 250-355 μm) were analysed. Prior to imaging, capsules were slit using a razor blade, washed with acetone several times and dried with compressed air followed by 2 h storage in vacuum. A layer of carbon coating of approximately 10 nm was then deposited onto the samples. On the micrographies, a total of 35 thickness measurements were taken on 5 different capsules within each diameter fraction and averaged. Particular care was taken to acquire images of the shell sections at a perpendicular angle in order to limit the error due to an oblique observation angle. SEM was also used for imaging the slices for AFM measurements (§ 3.4.4).

3.4.3 X-ray micro-computed tomography

X-ray micro-computed tomography was used for an effective imaging of the fabric cross-sections, with the specific aim of investigating the fabric interstice dimensions. Such an analysis was particularly useful for the measurements of the interstice dimension along the z-coordinate, since OM is not able to provide such an information. The tests on one layer of the selected fabric (approximately 1 × 3 cm) were performed at Laboratory of Biomechanical Orthopedics (LBO, EPFL) using the SkyScan1076. The analysis parameters were set as follows: source voltage 80 kV, source current 120 mA, filter Al 0.5 mm, resolution 9 mm, exposure 1600 ms, rotation step 0.560 deg. The images were reconstructed with the software NRecon and then converted to binary images using ImageJ with the thresholding algorithm "Minimum" [141] (this enabled to set a threshold for transforming images into a binary format).

3.4.4 Atomic force microscopy (AFM)

Atomic force microscopy (Multimode Nanoscope, Veeco), available at the Polymers Laboratory (LP) of EPFL, was used in tapping mode in order to acquire images of the shell morphology. Through phase contrast imaging, the capsule shell compositions were investigated for pure-UF and PU/UF capsules. Samples were prepared by mixing 5 wt% of healing pure-UF and PU/UF capsules in a resin/hardener mixture composed of EPON 862 and diethylenetriamine in a 100:12 weight ratio; the compound was then degassed for 10 min and poured into a silicone mold for ultramicrotomy samples. Curing at room temperature for 24 h and post-curing at 35°C for 24 h then followed. These samples were then cut into 300 nm thin slices by using an ultramicrotome device (PowerTome X, Cordouan Technologies), available at the Interdisciplinary Centre for Electron Microscopy (CIME) of EPFL. The slices were collected in water and then put onto glass slides for drying and further imaging. Slices consisted in sheets of matrix with holes corresponding to sectioned embedded capsules, as depicted in Figure 3.3. Images of a folded slice acquired by SEM

after sputter coating with carbon, as well as an optical image, are shown in Figure 3.4(left) and (right), respectively. The shell could then be observed at the air/matrix interface.

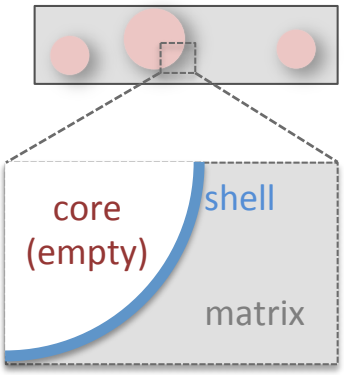

Figure 3.3: Schematic showing the morphology of the 300 nm thick slices, used for further AFM imaging.

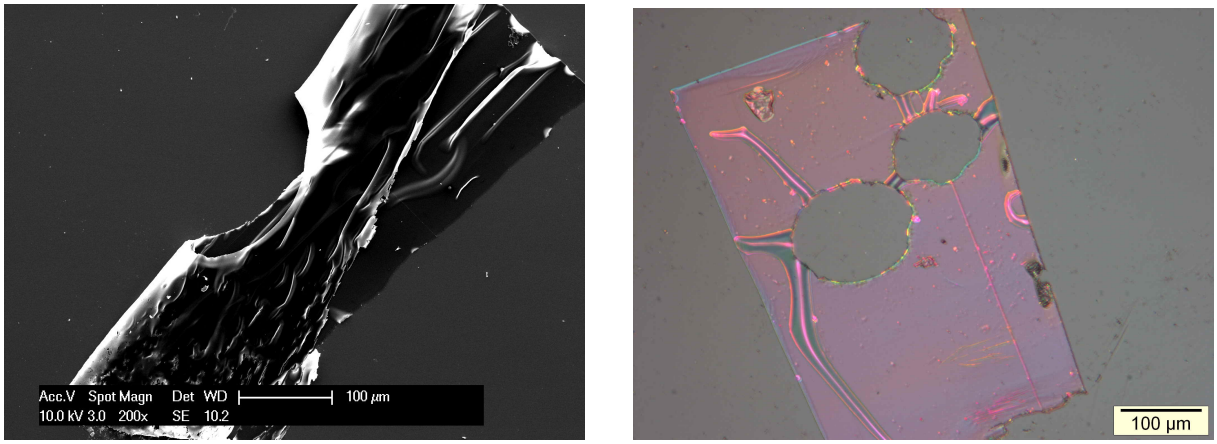

Figure 3.4: SEM (left) and OM (right) of 300 nm thick slices, used for further AFM imaging.

3.4.5 Single capsule compression

The study of the mechanical properties of UF and PU/UF capsule shells was accomplished using single capsule compression. For single capsule compression, a motor driven indenter (1.5 µm/s displacement rate) compresses a single microcapsule with known diameter, placed on the sample holder. Force-displacement data were acquired using a Futek LMP200 load cell (0-100 mN). An analytical model was then used to extract the Young's modulus of the shell material by fitting the modeled response to the experimental data, as detailed in [14] and briefly described as follows.

The model used was based on the work by Feng *et al.* [142] and Lardner *et al.* [143], concerning the compression of spherical not inflated membranes containing incompressible fluids when compressed between two plates. Figure 3.5 shows a schematic of the geometrical deformation of a capsules with the corresponding parameters.

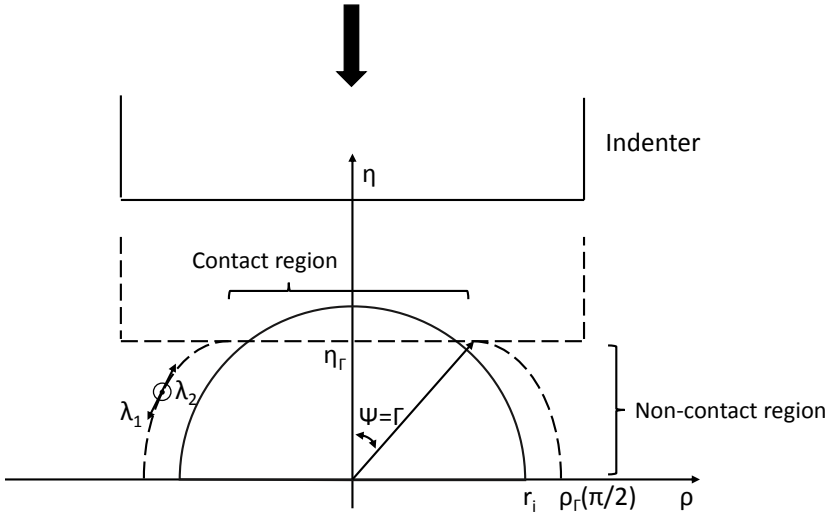

Figure 3.5: Schematic showing the single capsule compression geometry (based on [144]). The solid and dashed lines indicate the initial and deformed capsule geometries, respectively.

Using expressions for the stretch ratios λ_1 and λ_2 along the meridian and circumferential directions respectively, Feng *et al.* derived two systems of ordinary differential equations (ODE): one for the flat membrane area in contact with the plate and one for the free (stretched) membrane not in contact with the plate. The initial radius is indicated as r_i and the contact angle as Γ. The deformed shell has a height η_Γ for a given Γ and a circumference of $\rho_\Gamma(\pi/2)$. For membranes filled with incompressible fluids, the solution of ODEs needs to satisfy an additional constant volume boundary condition. Other assumptions are: (i) isotropic, linear elastic and time-independent ODEs, (ii) negligible membrane bending resistance, (iii) air surrounding the membrane, (iv) constant thickness before deformation and (v) absence of friction between the rigid plates and the membrane. The expression of the ODEs system for the contact and non-contact region are found in Equation 3.1 to Equation 3.5, with further definitions in Equation 3.6 to Equation 3.11 and the boundary conditions in Equation 3.12 to Equation 3.17. All variables are function of the contact angle ψ, giving the position of the membrane. P, E, h_0 and ν are the pressure inside the membrane, the Young's modulus, the membrane thickness and the Poisson ratio, respectively. From the calculated stretch ratios λ_1 and λ_2, the Cartesian coordinates of the deformed membrane ϱ and η can be derived.

Contact region

$$\lambda_1^{'} = -\frac{\lambda_1}{\lambda_2 \sin\psi}\left(\frac{f_3}{f_1}\right) - \frac{\lambda_1 - \lambda_2\cos\psi}{\sin\psi}\left(\frac{f_2}{f_1}\right) \tag{3.1}$$

$$\lambda_2^{'} = \frac{\lambda_1 - \lambda_2\cos\psi}{\sin\psi} \tag{3.2}$$

Non-contact region

$$\lambda_1^{'} = \frac{\delta\cos\psi - \omega\sin\psi}{\sin^2\psi}\left(\frac{f_2}{f_1}\right) - \frac{\omega}{\delta}\left(\frac{f_3}{f_1}\right) \tag{3.3}$$

$$\delta^{'} = \omega \tag{3.4}$$

$$\omega^{'} = \frac{\lambda_1^{'}\omega}{\lambda_1} + \frac{\lambda_1^2 - \omega^2}{\delta}\left(\frac{T_2}{T_1}\right) - \frac{\lambda_1(\lambda_1^2 - \omega^2)^{1/2}Pr_0}{T_1} \tag{3.5}$$

where

$$\delta = \lambda_2 \sin\psi \tag{3.6}$$

$$f_1 = \frac{\partial T_1}{\partial \lambda_1} \tag{3.7}$$

$$f_2 = \frac{\partial T_1}{\partial \lambda_2} \tag{3.8}$$

$$f_3 = T_1 - T_2 \tag{3.9}$$

$$T_i = \frac{1}{\lambda_1\lambda_2}\frac{\partial W}{\partial \lambda_i}\lambda_i^2 \tag{3.10}$$

$$W = \frac{Eh_0}{2\left(1-\nu^2\right)}\left[\left(\lambda_1 - 1\right)^2 + \left(\lambda_2 - 1\right)^2 + 2\nu\left(\lambda_1 - 1\right)\left(\lambda_2 - 1\right)\right] \tag{3.11}$$

with the following boundary conditions

$$\psi = 0 : \lambda_1 = \lambda_2 = \lambda_s \tag{3.12}$$

$$\psi = \Gamma : \lambda_{1,non-contact} = \lambda_{1,contact} \tag{3.13}$$

$$\psi = \Gamma : \delta = \lambda_{2,contact} \sin \Gamma \tag{3.14}$$

$$\psi = \Gamma : \omega = \lambda_{1,contact} \tag{3.15}$$

$$\psi = \pi/2 : \omega = 0 \tag{3.16}$$

$$\Delta V = V_{compressed} - V_{initial} = 0 \tag{3.17}$$

The two ODE systems were numerically solved with the Runge-Kutta method using MATLAB. The algorithm is detailed in [14]. Figure 3.6 shows the computed shell geometry and the resulting force-displacement relation. The geometry of the compressed capsules shows the flat contact surface which increases with contact angle as well as the free non-contact region which widens to compensate the volume reduction at the poles. The force vs. displacement plot shows the increasing force at the flat top, generated by the increased area of contact and increasing pressure inside the membrane. In what follows, these results of the standard model were used for fitting experimental data as obtained with the single capsule compression experiments. Namely, the Young's modulus was then extracted and associated to a certain type of capsule.

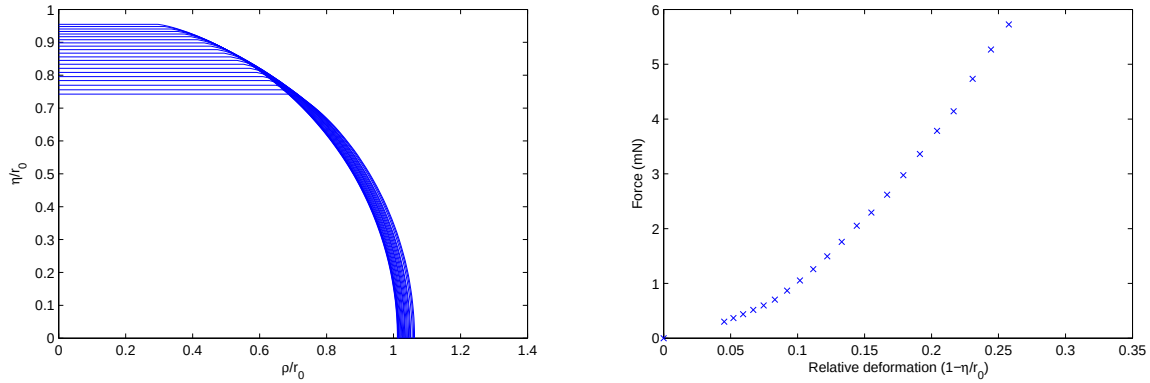

Figure 3.6: Deformed shape of the capsule for increasing contact angles (left) and computed force vs. deformation of the capsule (right).

3.5 Capsule integration

Manual sieving was selected as technique to integrate the capsule within the composite prior to processing. In order to validate this technique as suitable for achieving a satisfactory degree of capsule distribution, a simple visual test was performed with the

following procedure. Determined amounts of *healing* capsules (corresponding to 10, 20 and 30 vol% over a fictitious matrix fraction) were manually dispersed (using a 250 µm sieve by Cole Parmer) onto 50 × 50 mm fabric squares and a photo of the functionalised fabric was taken. Obtained images were visually compared with a model image obtained with Mathematica that simply visualises a random dispersion of circles -with diameters corresponding to the capsule diameter range- on a 50 × 50 mm area. This was intended to be a simple visual comparison to qualitatively quantify the degree of capsule distribution, thus the effectiveness of the manual sieving as functionalisation technique. It is underlined that the Mathematica simulation allows the capsule superposition and takes into account a flat surface.

3.6 Samples for CAI tests

3.6.1 VARIM and sample preparation

Manufacturing of composite panels was performed by Vacuum-assisted resin infusion molding. For this, the consumables as indicated hereinafter were used:

- ▷ peel ply: A100 PS (Cytec);
- ▷ flow mesh: PE <90°C (Suter-Kunststoffe AG);
- ▷ vacuum bag: VACFILM 400Y272, yellow, <150°C (Cytec);
- ▷ mould release agent: Xtend 832 Release (Axel);
- ▷ resin inlet and vent spirals: No. 77009.0912, PE 9 × 12 mmø;
- ▷ resin inlet and vent pipes: No. 77008.0810, PE 8 × 10 mmø (Suter-Kunststoffe AG);
- ▷ flow mesh of resin inlet and vent spirals: No. 61040.0460, <125°C, 6/12 mmø (Suter-Kunststoffe AG);
- ▷ sealant tape: BT100, brown, <100°C (Cytec).

For further thickness measurements and CAI testing, three types of composite plates were processed by VARIM, containing no capsules (referred to as *plain*), healing capsules (*healing*) and control capsules (*control*). Different overall capsule volume fractions were used, namely 0, 1.25 and 6.5 vol%, corresponding to volume fractions of capsules in the matrix of 0, 2.5 and 13 vol% respectively. Capsules were sieved onto all plies, the targeted fibre volume fraction V_f was 50 vol% and the final plate thickness 5 mm. A stacking sequence of [(+45/-45)/(0/90)]4s was used, according to the ASTM standards [123, 124].

A representation of the VARIM assembly used (cross section schematic and top view photo) is reported in Figure 3.7. Note that the VARIM processing was performed with 0.09 MPa pressure difference Δ_{vac} and using EPON 862 as infusing resin more suitable for VARIM compared to EPON 828EL, thanks to the lower viscosity enabling processing at ambient temperature. Unless otherwise defined, in all cases, inlet and vent valves were closed as far as the infusion was concluded. After processing and curing, the plate thickness was measured in 15 points and averaged. The same panels were used the to obtain samples for CAI tests.

3.6.2 CAI test and healing assessment

The CAI test was used in order to assess the compression properties of the panels containing different capsule concentrations, namely $V_c = 0$, 1.25 and 6.5 vol%, and to evaluate their healing efficiency. The specimens for these tests were cut from the infused panels using a Maïco machine equipped with a diamond saw. Final dimensions were of 100 × 150 mm. According to the ASTM standards [123, 124], care was taken to to avoid notches, undercuts, rough or uneven surfaces or delaminations due to inappropriate machining methods. The final dimensions were obtained by water-lubricated precision sawing (Kugel Muller, available at the Laboratory of Construction Materials of EPFL), which also enabled to make the sample edges flat and parallel, which is extremely important for the compression test. Impact tests were performed following the procedure as indicated in the standard indicated above. The impact energies were calculated considering the impactor mass of 3 kg. In particular, samples were impacted with 5 J energy, known from previous tests as enough to induce microcracking. The specimens were impacted once without any rebound impact, in the center. All impacted *healing* samples were given 20 days to heal before further compression tests. This resting period was at room temperatures and without any additional pressure applied to the samples. The compression test was carried out using a support fixture as indicated by the standard and the hydraulic machine (Walter and Bai, max. load 330 kN) also available at the Laboratory of Construction Materials of EPFL. The compression test was performed with a loading speed of 0.6 kN/s and the compressive strength (load at failure) was recorded. Care was taken for the specimens installation and alignment, since they significantly influence the results; specifically, any lack of alignment can cause sample buckling (thus no pure compressive load). The presence of healing was estimated by simply comparing the residual compressive strength of *healing* samples with that of *plain* and *control* samples.

3.6.3 Optical microscopy (OM)

Optical microscopy was used for evaluating the quality of the impregnation and the capsule distribution. The images were taken with the optical microscope Olympus BX61 and

processed, when needed, with a multiple image alignment software.

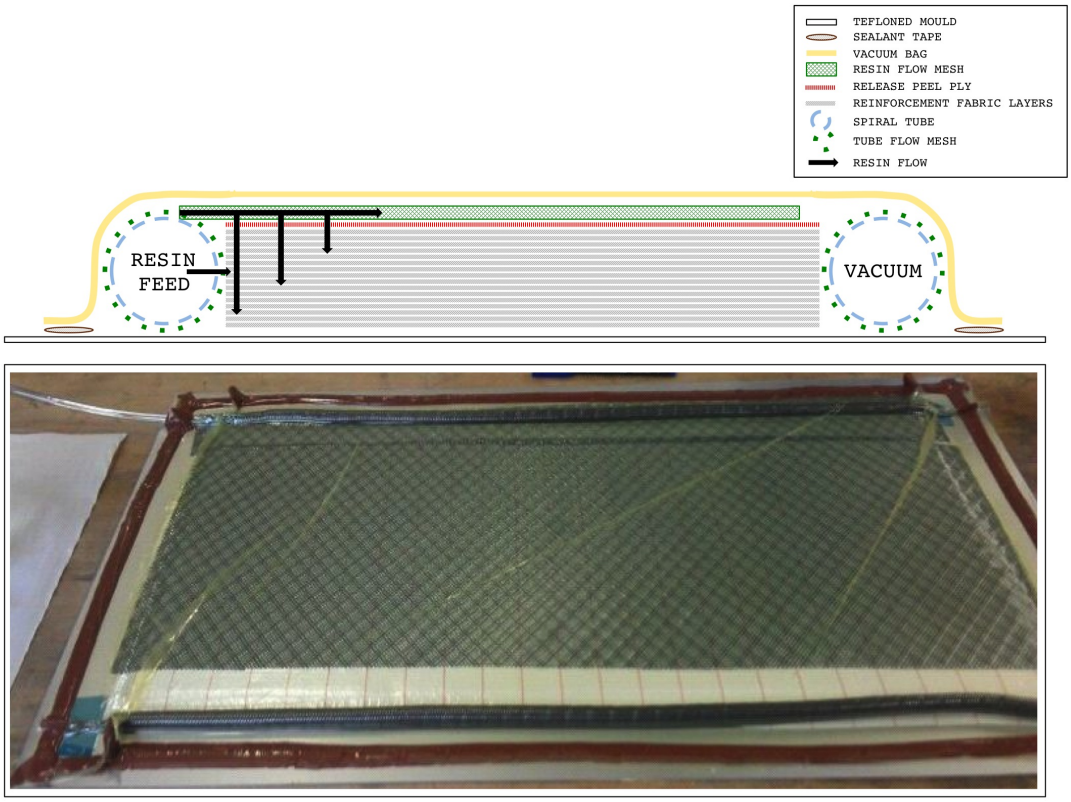

Figure 3.7: Representation of the VARIM lay-out cross-section (schematic) and top view (photo).

3.7 Study of packing and permeability properties of fibre stacks

3.7.1 Compaction test on dry fabrics

The packing properties of plain and capsule-functionalised fabrics were analysed. 100 × 100 mm squares of fabric reinforcement were carefully cut and weighed; consequently, for plain samples, they were simply stacked following the sequence as indicated herein-before, whereas for functionalised samples, different amounts of capsules were manually sieved (250 μm sieve by Cole Parmer) onto each layer while stacking. Overall capsule volume fractions (V_c) of 1.25, 2.5 or 3.75 vol% were used, corresponding to volume fractions of capsules in the matrix (V_c^*) of 2.5, 5 and 7.5 vol% respectively. Samples were analysed in a Universal Testing System (Walter & Bai AG, Switzerland), equipped with a 100 KN loading cell and an inductive displacement sensor (W20, HBM). A displacement

controlled compression test was performed on the samples, between two metal plates, at a constant speed of 2 μm/s, with a pressure cycle ranging from 0 to 1 bar. This pressure range was here chosen since it corresponds to the effect of the pressure difference during VARIM, which is a possible processing technique for further manufacturing. As soon as the maximum pressure was reached, samples were unloaded at the same speed to achieve a zero-stress position. Load-displacement data were recorded both while loading and unloading. An illustration of the apparatus is given in Figure 3.8.

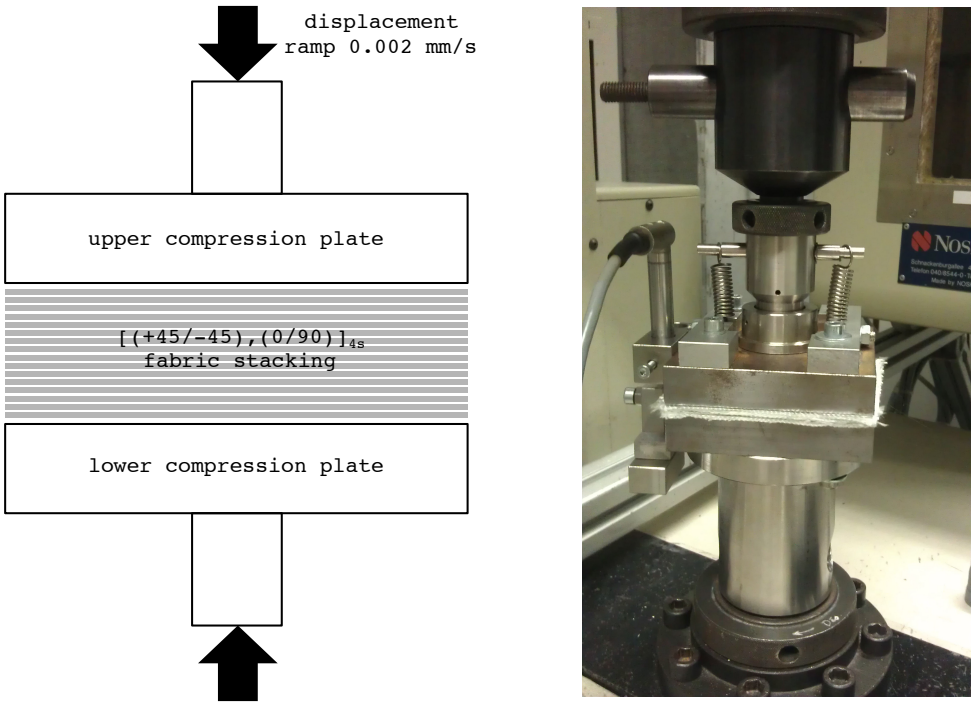

Figure 3.8: Schematic and picture of the apparatus for the compaction of dry fabrics.

3.7.2 Longitudinal unsaturated permeability test

Longitudinal unsaturated permeability was studied for plain and capsule-functionalised fabrics. As impregnating fluid, a commercial silicone oil (polydimethylsiloxane trimethylsiloxy terminated, ABCR), with a kinematic viscosity of 100 cSt as given by the manufacturer, was used; the viscosity at different temperatures was measured with an AR 2000 ex (TA instruments) rheometer with a standard Smart SwapTM Peltier plate for the temperature control in a range of -40-200°C. The test procedure consisted in a continuous flow-mode temperature ramp at 0.5°C/min between 15°C and 25°C, at a constant shear stress of 60 Pa. Tests were performed following recommended test procedures [145], with the apparatus shown in Figure 3.9. As for compaction tests, 16 layers of fabric reinforcement were carefully cut (without inducing any deformation in the fabric and by cutting straight and smooth edges) in 60 × 260 mm rectangles, weighed and stacked. For capsule-functionalised samples, different amounts of capsules were manually sieved, as for

compaction tests. The samples were then placed onto the lower part of an 320 × 320 mm steel mold; around the fabric a 6 mm thick silicone joint and a 5 mm thick steel frame were placed, in order to create the sealed cavity for the impregnation. A 5 mm thick steel frame was chosen in order to reach a fibre volume fraction V_f of 47 vol% with the use of the selected fabric, thus simulating conditions of a further VARIM process. The upper mold (steel and transparent tempered glass) was placed above and screwed at the corners with four steel pillars and at two edges with two stop screws. A pressure of 2 bar was applied to close the mold through the air bags lifting the mould on its sliding pillars, at a temperature of 20°C. The pressurised pot (Hypajet, Plastech, UK) was connected to the mould inlet with polyethylene tubes and a pressure/temperature sensor (Keller, mod. S30X) was placed at the inlet of the mould to measure the injection pressure over the time of the impregnation. The impregnating fluid was injected, after degassing, with a targeted pressure close to 1 bar, which was recorded through the sensor acquisition. A rule was drawn on the glass of the upper mold and a camera was installed above to record the flow front position. Permeability was calculated using the Squared Flow Front Approach [145]. Note that the longitudinal permeability in one fabric direction only was here investigated, in order to focus more on the capsule influence and also because in the VARIM processing one direction is predominant.

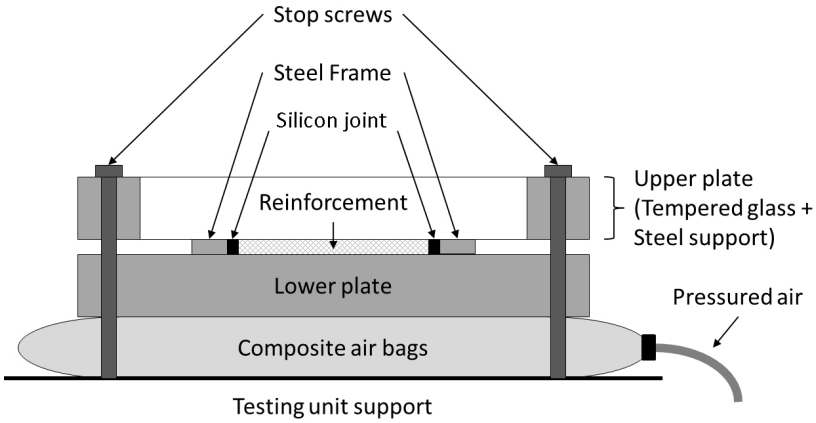

Figure 3.9: Longitudinal permeability set-up and mold components.

3.7.3 Transverse saturated permeability test

The impregnating fluid was in this case a solution of polyethylene glycol (PEG, Sigma Aldrich, M_n = 35000 g/mol) in distilled water; this was chosen for reasons of easy handling and non-toxicity, since no specific standards exist in literature for through-thickness permeability tests indicating the fluid to be used. As for the silicone oil, the Newtonian behavior of the solutions was checked. The viscosity of the solution was easily adjustable by varying the PEG molar concentration and measured with a rheometer as indicated

in § 3.7.2. As showed in Figure 3.10, the experimental setup, very similar to the one used by Merhi *et al.* [146], consisted of a pressurised pot (Hypajet, Plastech, UK) for degassing and injecting the fluid, which was connected to a transparent cylinder cavity to host the fibre stack, held between two aluminum honeycomb; the cylinder was then connected to a balance (Mettler Toledo PG8001) to measure the flow rate by the use of a camera (Canon PowerShot SX 100 IS) and a chronometer. A sensor (Keller, mod. S30X) was placed between the pressurised pot and the cylinder cavity in order to measure the injection pressure and temperature. For the preparation of the experiments, 16 layers of fabric reinforcement were carefully cut in circles of 50 mm diameters, weighed and stacked with the orientations as explained above for the longitudinal permeability tests. The samples were then placed in between the honeycombs with a distance h of 4.7 mm, which correspond to fibre volume fraction V_f of 50 vol%, which was in the same range as of longitudinal permeability samples; in between all the elements which constitute the cylinder, circular rubber joints were placed in order to prevent lateral leakages on the cylinder walls and let the flow to be guided across the fabrics only. The cylinder was closed with lower and upper lids, compacting the fibre stack to fit into the 4.7 mm spaced impregnation cavity. The pressure pot was connected to the pressure/temperature sensor and further to the cylinder inlet with polyethylene tubes. Analogously to longitudinal tests, the impregnating fluid was injected, after degassing and once the flow was stable, with a pressure difference of 1 bar, which simulates full vacuum-VARIM conditions and was recorded through the sensor acquisition. The measurement of the flow rate was performed in order to calculate the saturated permeability. Assumptions for the calculation were: (i) the outlet pressure is equal to the atmospheric pressure; (ii) the cylinder and the tubes do not significantly influence the pressure drop; (iii) the fluid velocity in the in-plane direction, thus the in-plane permeability, are negligible; (iv) the race tracking is minimal. Assumptions (i) and (ii) were justified by measuring the outlet pressure and by performing tests with no samples, respectively; assumptions (iii) and (iv) were only visually verified during the experiments.

3.8 Samples for DCB and ENF tests

3.8.1 Vacuum compaction test of the preform

Prior to the production of FRP panels through VARIM for producing DCB and ENF tests, an initial test was performed in order to assess the highest degree of vacuum which could be applied during processing without rupturing the shell of the capsules embedded in the composite. Indeed, according to results reported in § 4.4 and 6.1, the capsule bursting force is low and capsule bursting can occur when capsules are present on each ply and high compaction pressures are applied. However, the capsule configuration and

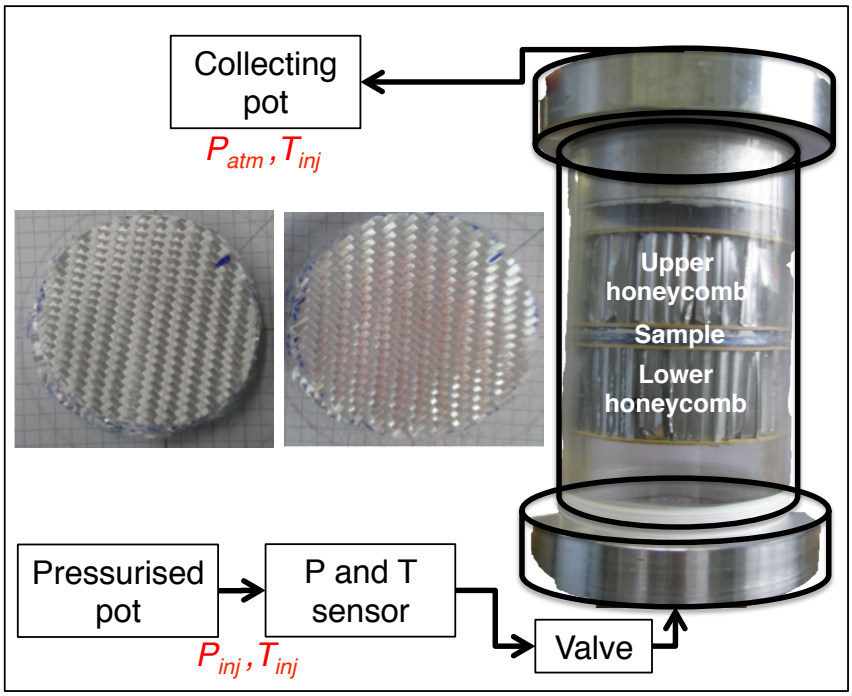

Figure 3.10: Schematic of the transverse permeability set-up. Plain and a capsule-functionalised samples are also shown.

the loading mode are different herein as capsules are sieved only onto the central ply of the stack (rather than onto all) and the pressure is applied by vacuum (rather than with a compression plate). Thus, it was not possible to rely on the results obtained in § 4.4 in order to assess the maximum degree of vacuum to prevent capsule breakage, and a more adapted test was performed. 16 layers of fibre reinforcement were then cut in 100 × 100 mm squares and stacked with the same sequence of [(+45/-45)/(0/90)]4s. Between the two central plies, an amount of capsules corresponding to a surface density of 2.56 mg/cm^2 was manually sieved by using a 250 μm mesh sieve (Cole Parmer). The specimen was placed under a vacuum bag and subject to a gradual increase in vacuum of 0.1 bar from 0 to 1 bar pressure difference. Optical images (Olympus BH-2) were taken after each step of 0.1 bar to observe the amount of capsule damaged/broken as a function of the applied pressure (ΔP_{vac}). This test is based on the most critical step of the VARIM process, during which the fabrics are subject to the vacuum before impregnation, which translates into a mostly uniaxial compression on the capsules. As soon as the matrix starts to impregnate the capsule-functionalised fabrics, capsules become subject to the hydrostatic pressure of the surrounding fluid, representing a less critical condition.

3.8.2 Preliminary tests for resin selection

In order to quantify the swelling of neat EPON 862 compared to EPON 828EL in EPA solvent, a swelling test was accomplished. Three small cylinders of 9.7 mm diameter and 4.9 mm height were cast using EPON 862 and DETA. Different curing and post-curing

scenarios were studied. The samples were immersed into EPA solvent and their weight uptake was recorded after 1, 3, 5 and 7 days using a high-resolution precision balance (Mettler Toledo, AT261 DeltaRange, 0.01 mg reading, repeatability 0.015 mg). Prior to recording the weight, excess solvent was removed from the sample surface using Kimtech Precision Wipes (Kimberley Clark, ref. 7552). The procedure followed that used by Neuser *et al.* [9], to which we refer for the swelling data of neat EPON 828EL samples, for comparison.

This swelling test was of a great importance in order to select an epoxy system and cure schedule suitable for solvent healing.

Together with swelling, the degree of polymerisation was also calculated for both EPON 862 and EPON 828EL after being subjected to the same thermal treatment (curing of 24 h at 25°C and post-curing of 24 h at 35°C). DSC analysis (TA Q100) was used in order to quantify the degree of polymerisation after 24 h curing (referred to as "-1 day"), after 24 h post-curing (referred to as "0 day"), and after 1 and 5 days ageing in dry conditions (22°C, 20% relative humidity). Samples originated from samples cast in a silicone mould and cut in pieces of 5-10 mg. Sets of three samples underwent a temperature ramp from -50 to 300°C at 10°C/min.

Moreover, rheological measurements were also carried out in this phase in order to measure the viscosity values of EPON 828EL mixed with the viscosity modifier Heloxy 61 or heated at approximately 30°C. The measurements were carried out with an AR 2000 ex (TA instruments) rheometer with a standard Smart SwapTM Peltier plate for the temperature control (temperature ramp at 0.5°C/min) or at constant temperature.

3.8.3 VARIM and sample preparation

Vacuum-assisted resin infusion molding was performed here with the same manufacturing consumables as indicated in § 3.6.1.

In order to produce DCB and ENF samples for healing assessment, three types of composite plates were processed by VARIM, containing no capsules (referred to as *plain*), healing capsules (*healing*) and control capsules (*control*). The targeted fibre volume fraction V_f was 50 vol% and the final plate thickness 5 mm. The preforms to be infused were prepared following the lay-out as depicted in Figure 3.11. A release film (A600BNP15, Cytec, 15 µm, non perforated, <230°C) was placed between the two central plies to form the notch which acts as the starting point for the delamination in Mode I DCB and Mode II end-notched flexure (ENF) samples. Several preliminary infusions were performed in order to determine the optimal position and geometry of the notch, taking into account that the release film is resin proof and strongly hinders the impregnation of the eight fabric layers underneath. *Healing* or *control* capsules corresponding to a surface density of 2.56 mg/cm^2 were introduced in the respective plates, sieved onto a surface of 40 ×

300 mm on the same ply where the release film was laid and next to it. The chosen capsule surface density is equivalent to a "local" capsule weight fraction of 15 wt% (16.94 vol%), based on previous studies for solvent-based self-healing of neat resins [7, 10, 12]; this corresponds to an overall capsule volume fraction of 0.085 vol%. According to the results indicated in § 5.1, it is known that the functionalisation of the fabrics with capsules by manual sieving prior to infusion ensures an acceptable capsule dispersion for flat shapes, thus it was deemed a suitable technique for the present investigation. Moreover, it is also known that a stack of capsule-functionalised fabrics presents a different behavior in terms of the packing response over loading and the longitudinal permeability towards the impregnating fluid, but not on the transverse permeability. Herein, the presence of capsules only on the confined space of the middle ply will not considerably modify the infusion behavior. According to the results of the preliminary swelling test for the selection of the matrix to use, EPON 828EL was used for VARIM in this case. Prior and during processing, both the matrix and the preform were heated to 35-40°C in order to decrease the viscosity of the matrix (dropping from 20 to 2 Pa s by heating from 20 to 35-40°C, as reported in § 7.2) and improve the quality of impregnation. In such a temperature range, the pot-life of EPON 828EL/DETA is approximately 30 minutes. In order to overcome this time restriction, three pots of matrix were prepared and degassed in succession with approximately 10 minutes gap in between. This enabled the constant infusion of the preform throughout one hour. The vacuum pressure difference was consistently kept between 0.3 and 0.4 bar during the entire processing time, following the results of the compaction test under vacuum (§ 7.1). The plates underwent a curing treatment of 24 h at 25°C and post-curing of 24 h at 35°C. According to previous studies for the neat EPON 828EL [10], this was supposed to obtain an incomplete degree of cure; since in this case a fibre reinforcement was also present, degrees of polymerisation were checked (§ 7.6.1). DCB and ENF samples were cut out of the plates (dimensions are indicated in Figure 3.11) using a Maïco machine equipped with a diamond saw. For each sample, the weight was recorded, the thickness measured in 3 points and averaged and the fibre volume fraction calculated. Moreover, optical images were taken of plain and capsule-containing composite cross-sections, in order to verify the quality of the panels (no significant porosity) and the state of adhesion and dispersion of the capsules.

Several additional samples were then prepared for comparison. First, DCB samples of pure resin (referred to as *neat*) were manufactured with the same geometry and thermal treatment as for composite ones, by casting EPON 828EL into silicone moulds. Second, joint specimens (referred to as *joint*) were prepared. For these, two composite plates of approximately 2 mm (containing 8 glass fabric layers) were joined with a 15 wt% *healing* capsule-loaded thick layer of matrix (1 mm) containing the usual notch. These specimens were intended to simulate a composite beam with a central layer of matrix (containing capsules) thicker than that of the previous composite beams as processed by VARIM. It

was expected that this would eliminate all influences of the fibre reinforcement on healing capability.

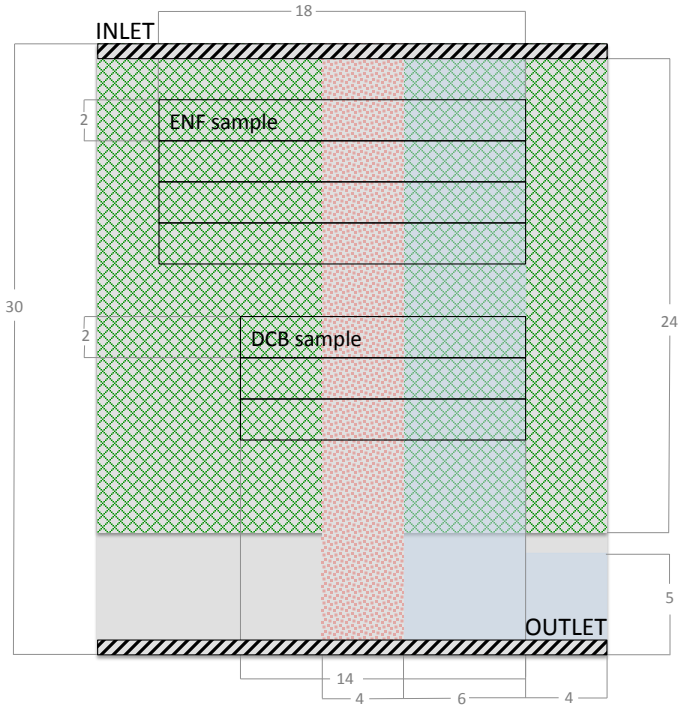

Figure 3.11: Schematic top view of the VARIM lay-out, including the fibre preform (grey), the flow medium (green), the release film (blue), the sieved capsules location (red), the inlet and outlet lines. Note that the release film and the sieved capsules lie on the eighth ply, but are shown at the top for clarity. The geometries of DCB and ENF samples are also showed.

3.8.4 DCB and ENF testing and healing assessment

The fracture behavior of the prepared samples was assessed in Mode I DCB and Mode II ENF tests. DCB tests followed the ASTM standard D5528 [147], whereas ENF tests followed the JIS standard K7086 [148], both using Universal Testing Machine (Walter & Bai AG, Switzerland), equipped with a 1000 N loading cell and using a test speed of 4 mm/min. The load was introduced into DCB samples via the adhesion of aluminum blocks on each side of the samples using Spabond resin cured (5 minutes curing at room temperature) with Spabond adhesive non-pigmented hardener purchased from Gurit. Each sample underwent four loading-unloading cycles. The first three correspond to the test of the virgin specimen, whereas the fourth was applied to the healed specimen after a given rest time. In the first cycle, loading was performed to create a pre-crack and a fast unloading speed used until the load reached zero. In the second cycle, loading was

performed until displacement reached 7.5 mm for ENF and 25-30 mm for DCB followed by an unloading at the same speed of 4 mm/min until the load reached zero. In the third cycle, a small loading-unloading cycle was performed immediately after testing until 3 mm displacement was attained, in order to quantify appearance of possible "stiffening" (see below). Finally, after 1 or 5 days, a loading-unloading cycle was performed on the same specimens to assess the healing efficiency and the crack was further propagated by 5 mm. At least 5 tests were performed for each condition (1 or 5 days healing time, *plain*, *healing* or *control* specimens) and each test (DCB or ENF). The samples were stored at 22°C with 20% relative humidity during healing, as recommended from a previous ageing study [10]. DCB samples were left unloaded during healing, with only the crack faces imposed to be in contact at the location of the loading blocks (this induced a reduction in the crack thickness, but no clamping at the crack location was applied). Some tests were also performed with an actual clamping pressure at the crack location in order to verify whether this could increase the healing efficiency by reducing the damage volume. A typical load-displacement curve showing the main loading-unloading cycle of the *virgin* specimen and the loading-unloading cycle to monitor the "stiffening" behavior is shown in Figure 3.12(left) for DCB tests and in 3.12(right) for ENF test. The importance of this "stiffening" cycle immediately following the main test is highlighted. Particularly, this subsequent loading slope is slightly higher than the unloading slope of the main cycle, especially for Mode II testing. This phenomenon is not related to any healing process but is rather attributed to artifacts of the testing procedure. For ENF, it is believed that friction phenomena between the crack faces affect the fracture behavior, and this is enhanced by the debris present on the crack faces when capsules are present [149–151].

Healing efficiency is usually estimated by comparing the virgin and healed fracture toughness, which implies monitoring of the crack length during testing. In the present study, while it was possible to measure the crack length for the virgin specimens, this was not feasible for the healed specimens, as the sides of the specimens still showed the presence of the previous crack. As a consequence, the healing efficiency was calculated by comparing the slope during loading of the *healed* specimen ($slope_{load,healed}$, after 1 or 5 days healing) to the slope during loading ($slope_{load,virgin}$, 100% efficiency) and unloading (0% efficiency) of the virgin specimen. We view this simple method as a preliminary quantitative indication of the healing occurrence. Moreover, in order to take the explained "stiffening" phenomenon into account, healing efficiencies were assessed by considering as 0% the loading slope of the small "stiffening" cycle ($slope_{load,stiffening}$) instead of the initial one. The efficiency is therefore defined as in Equation 3.18

$$\eta = \frac{slope_{load,healed} - slope_{load,stiffening}}{slope_{load,virgin} - slope_{load,stiffening}} \cdot 100 \tag{3.18}$$

Furthermore, in order to quantify the effect of the presence of capsules on the mechanical properties of the samples tested in propagation Modes I and II, the maximum load values were extracted from the load-displacement curve of each sample, normalised over the fibre volume fraction of the sample, and averaged for *plain*, *healing* and *control* batches. Finally, the interlaminar fracture toughness was calculated for plain and capsule-loaded composites, based on crack length measurements for Mode I tests (Modified Beam Theory) [147] and based on calculations for Mode II tests (Compliance-Based Beam Method) [152, 153].

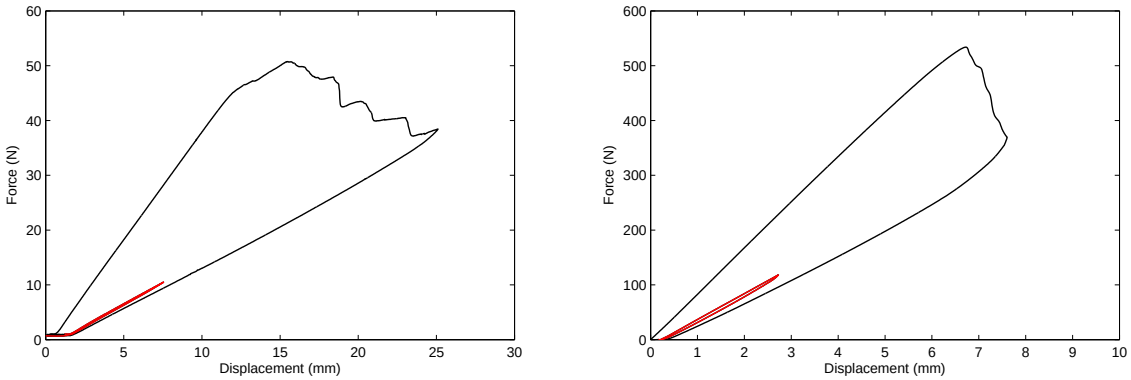

Figure 3.12: Typical loading-unloading cycles for (left) DCB test and (right) ENF tests. The "stiffening" cycle is also shown (in red).

3.8.5 Post-testing characterisation

3.8.5.1 Swelling test in EPA

In order to quantify the swelling of the composite in EPA solvent, a swelling test was performed, equivalent to that explained in § 3.8.2. Three small cylinders of 9.7 mm diameter and 4.9 mm height were cut from each processed composite plate and immersed into EPA solvent. Their weight uptake was recorded after 1, 3, 5 and 7 days using a high-resolution precision balance (Mettler Toledo, AT261 DeltaRange, 0.01 mg reading, repeatability 0.015 mg). Prior to recording the weight, excess solvent was removed from the sample surface using Kimtech Precision Wipes (Kimberley Clark, ref. 7552). The procedure followed that used by Neuser *et al.* [9], to which we refer for the swelling data of neat EPON 828EL samples, for comparison.

3.8.5.2 Differential scanning calorimetry (DSC)

DSC analysis (TA Q100) was used in order to quantify the degree of polymerisation of the resin in the composite samples, after 24 h curing ("-1 day"), after 24 h post-curing ("0 day"), and after 1 and 5 days ageing in dry conditions (22°C, 20% relative humidity). Samples originated from the same portion of fibre-reinforced resin cast in a silicone mould

and cut in pieces of 5-10 mg. Sets of three samples underwent a temperature ramp from -50 to 300°C at 10°C/min. The samples were subsequently taken out of the DSC hermetic aluminum pan and subject to TGA measurements (Mettler Toledo sDTA851e, heating ramp 30-600°C, 10°C/min, under nitrogen) in order to extract the matrix volume fraction for each sample, which corresponds to the mass loss over the temperature interval. For comparison, neat resin data were also taken from Neuser *et al.* [10].

3.8.5.3 SEM

Fracture surfaces were observed by SEM (XLF-30 FEG, FEI, available at CIME, EPFL) and the chemical components present on these surfaces quantified by energy-dispersive X-ray spectroscopy (EDX) using the same apparatus.

Chapter 4

Characterisation of solvent-filled PU/UF core-shell capsules

In the context of capsule-based self-healing materials, the encapsulation of liquid phases is a crucial step. The healing agent has to be protected during handling and processing and then released during a damage event. For incorporation of microcapsules into fibre-reinforced materials, the requirements for the mechanical stability become even higher, since manufacturing conditions in terms of stresses can be harsher. Thus, the thermal and mechanical properties of the healing capsule membrane, or shell, are of great importance. First, the shell material needs to survive to processing and service temperatures. Secondly, the mechanical requirements are such that the membranes survive processing stresses but in the same time should rupture by a matrix crack. Additionally, their adhesion to the matrix material needs to be sufficient in order for cracks not to detach the embedded microcapsules, but pass through, thereby releasing the healing agent.

In this chapter, the morphological and thermal characterisation of pure-UF and PU/UF shells is first presented.

Concerning the mechanical properties of the shell, Keller *et al.* [101] characterised the properties of monomer-filled UF microcapsules by single capsule compression and using an analytical model, the Young's modulus of the shell membrane was extracted. Unfortunately, the pure-UF encapsulation protocol does not allow straightforward tuning of the shell thickness (which was reported to be in the 160-220 nm range [94]) and consequently mechanical properties cannot be changed. Later, Caruso *et al.* [83] described a method to reinforce the UF shells by adding an aromatic diisocyanate to the core fluid which forms a PU layer at the emulsion interface. These hybrid PU/UF shells were shown to increase the bursting force as well as thermal stability but the shells were not characterized using the aforementioned analytical model. The goal of this work was then to complete this analysis and study how the mechanical properties of PU/UF composite shells change as a function of the shell thickness, composition and the capsule diameter. Therefore, polyurethane-reinforced PU/UF microcapsules filled with a solvent were produced fol-

lowing the protocol explained in § 3.3 and analysed in detail. An analytical model was adapted to extract the Young's modulus of the hybrid shell and evaluate the mechanical properties' dependency on capsule diameter. This was accomplished using single capsule compression, then by fitting these results to the shell model, which allows an accurate description of the Young's modulus of the PU/UF composite shell.

4.1 Capsule aspect and average diameter

Typical micrographies showing the 125-250 μm fraction of different type of produced capsules are presented in Figure 4.2. Any significant difference is noticed under optical microscope between different capsule cores or between pure-UF and PU/UF capsules (different shell). Moreover, Figure 4.1 can suggest some of the following observations:

- ▷ some capsules totally or partially released their content after they damaged during the encapsulation process or handling (the color loss might be a good indication of the released content);
- ▷ junk particles were observed (not formed microcapsules, debris of broken shells, agglomerates of not reacted components);
- ▷ the fracture behavior of the outer shell is visible: the shell starts to break creating two hemispheres tearing apart and the content is released [88]; the sharp fracture plane indicates a brittle behavior related to the UF shell.

All microcapsule batches were characterised in terms of size. Table 4.1 summarises the number-length average diameters values obtained for the batches used in the different studies.

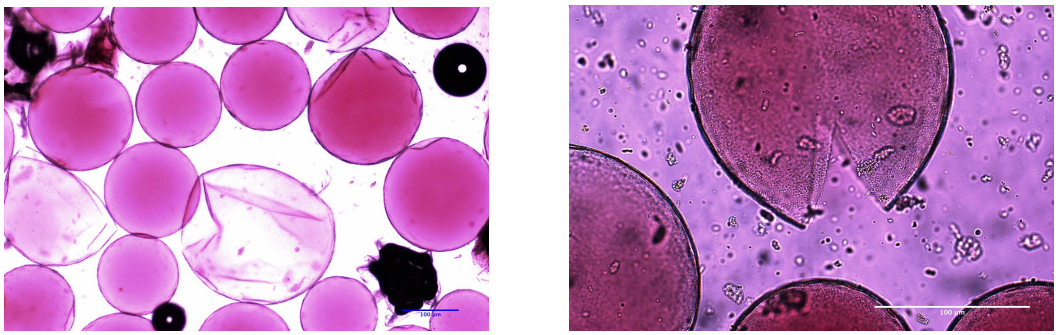

Figure 4.1: Some evidences of damaged/empty capsules, debris and capsule tearing. 90-125 μm of pure-UF capsules is shown.

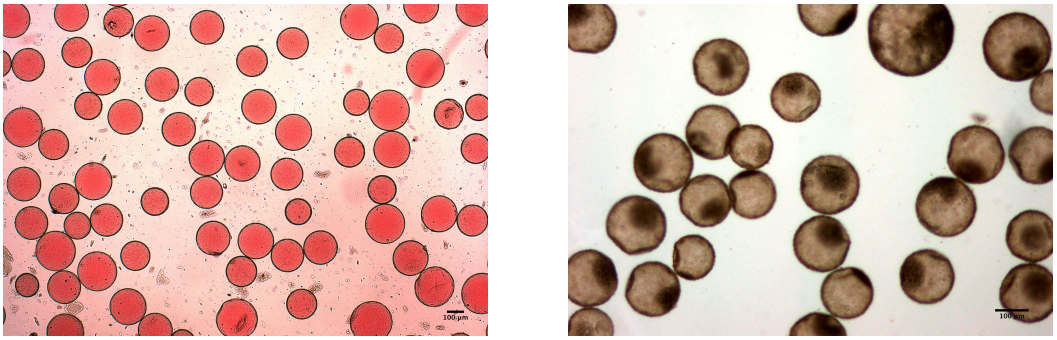

Figure 4.2: OM images for pure-UF (left) and PU/UF capsules with 7.5 g PU prepolymer (right). 125-250 μm fractions are visualised.

Capsule compression tests (125-355 μm fraction) - § 4.4	
Pure-UF, *healing*	224 ± 51
2.5 g PU/UF, *healing*	166 ± 25
5 g PU/UF, *healing*	215 ± 29
7.5 g PU/UF, *healing*	183 ± 33
Functionalised fabric tests (125-250 μm fraction) - § 6	
Pure-UF, *healing*	201 ± 22
CAI tests (125-250 μm fraction) - § 5	
Pure-UF, *healing*	185 ± 29
Pure-UF, *control*	191 ± 30
DCB/ENF tests (125-250 μm fraction) - § 7	
Pure-UF, *healing*	191 ± 33
Pure-UF, *control*	183 ± 33

Table 4.1: Number-length average diameters (μm) for the microcapsule batches used for different studies.

4.2 Capsule thermal properties

The thermal properties of microcapsules were investigated through TGA measurements.

Firstly, the comparison between pure-UF and PU/UF microcapsules, *i.e.* presenting different shells but the same *healing* core, was performed. Figure 4.3 shows the mass loss of UF and PU-reinforced microcapsules as a function of temperature. In UF microcapsules, a small evaporation of moisture occurred between 70 and 100°C, followed by a mass loss at a gradually increasing rate, peaking at approximately 280°C. Beyond, only the shell material remained. Concerning PU-reinforced capsules, the results suggest a very low moisture content in all three batches with different PU precursor amounts. As opposed to pure-UF shells, PU/UF shells offer very high thermal stability, with no significant mass

loss until 240°C, well above the boiling point of core solvent EPA (229°C). Beyond 240°C, the capsules release the solvent and at 275°C, almost all the solvent had evaporated for all three types of PU/UF capsules. Note that for higher PU contents, the residual weights after solvent evaporation are also higher. At 290°C, the residual weight is 1.9, 2.6, 6.0 and 7.8% for pure-UF, 2.5, 5.0 and 7.5 g PU/UF microcapsules, respectively.

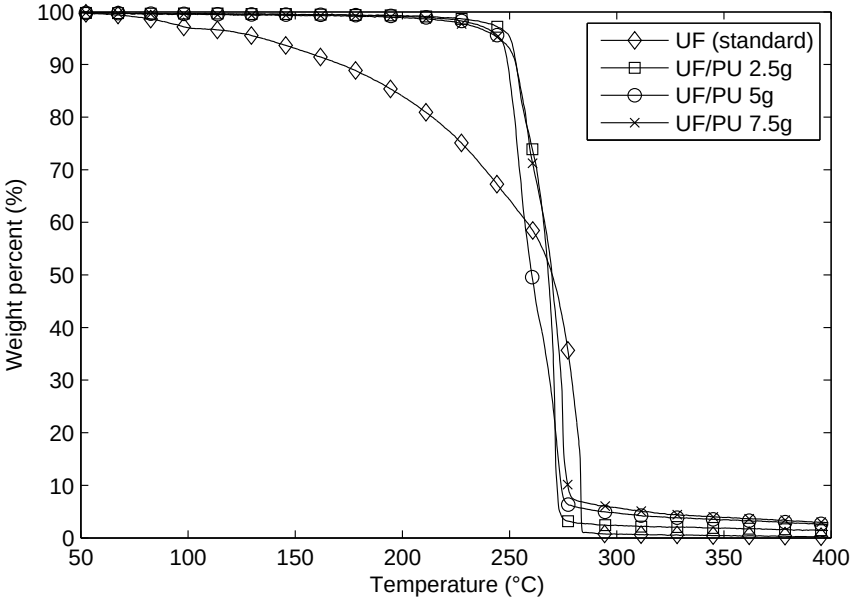

Figure 4.3: Mass loss of pure-UF *and* PU-reinforced microcapsules as a function of temperature.

Secondly, thermal properties are compared for *healing* and *control* capsules, *i.e.* presenting different core material, as reported in Figure 4.4. No significant difference in behavior was noticed between healing and control capsules, except for a shift of the main weight drop due to the different boiling temperatures of EPA (229°C) and HA (171.5°C).

In summary, we can conclude that

- ▷ for UF shell capsules, the capsule core does not influence the thermal behavior, however it relates to the temperature at which the mass loss is located, which is associated to the boiling point of the core material;

- ▷ the double-wall provides to the capsules an undoubted higher thermal stability, independently of their shell, that makes them suitable for higher temperature applications. In our case, since the maximum temperature which is attained during curing and post-curing is 35°C, there is no specific need of double-wall capsules. It is important to notice that over manufacturing the local temperature inside the composite can raise (compared to the process temperature) due to the high exothermicity of the matrix polymerisation (specific heat and experimental total heat of reaction of the EPON 828EL cured with DETA are 2.09 J/g °C and 558 J/g respec-

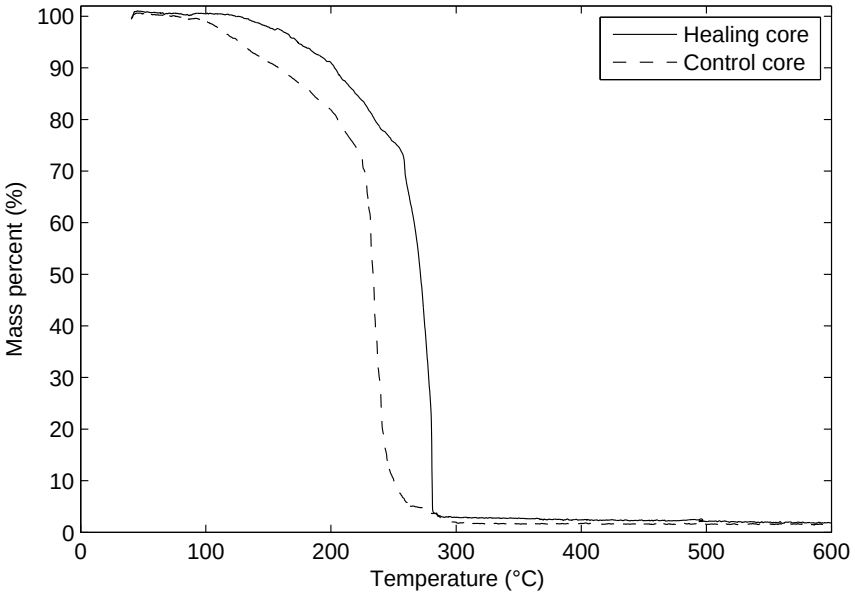

Figure 4.4: Mass loss of *healing* and *control* microcapsules as a function of temperature.

tively); however, thanks to the presence of many heat dissipation media, this does not have significant effect.

4.3 Capsule shell thickness and morphology

The shell thickness of pure-UF and PU/UF microcapsules was investigated by SEM analysis. Example images of microcapsules shells are shown in Figure 4.5.

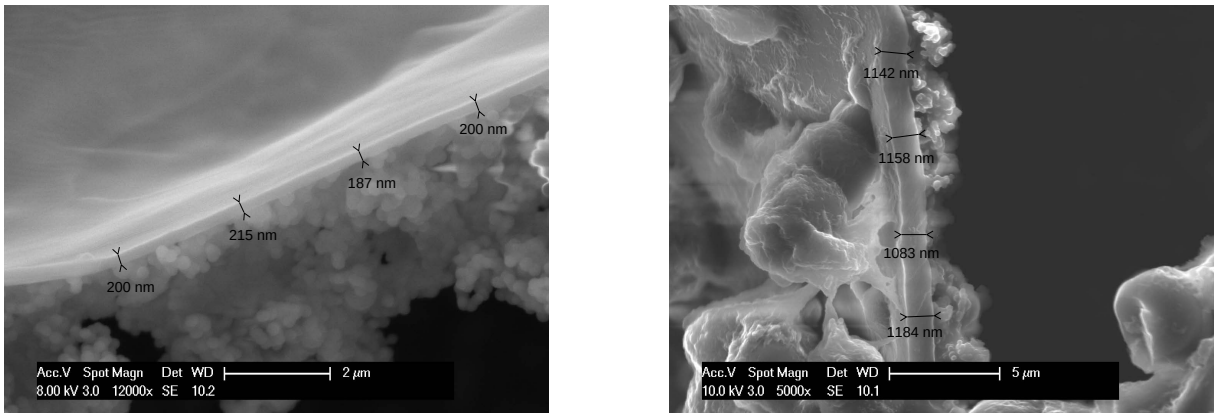

Figure 4.5: SEM images of shell of (left) pure-UF capsules (180-250 μm fraction) and (right) 7.5 g PU/UF capsules (180-250 μm fraction). Note that the measured thickness refers only to the smooth layer and does not include the inner and outer agglomerates.

For pure-UF shells, Figure 4.5(a) shows a capsule of the fraction comprised between 180 and 250 μm. This type of capsule had an average shell thickness of 189 nm and in general was characterised by a very smooth interior as opposed to the rough surface. Urea

and formaldehyde react in the water phase, they condense at the oil-water interface and as the reaction proceeds, larger agglomerates form in the water phase which then stick to the already formed, smooth shell, as was also reported by Brown *et al.* [94]. For the 7.5 g PU/UF shell, in Figure 4.5(b), the average thickness was almost sixfold higher, at 1134 nm, and large agglomerates of PU were visible in the interior of the shell.

In Figure 4.6, the shell thicknesses are summarised for the four types of microcapsules (pure-UF, 2.5, 5.0 and 7.5 g PU/UF) as well as 5 different size fractions (<90, 90-125, 128-180, 180-250, 250-355 nm). One can observe that, for pure-UF capsules, the shell thickness is around 200 nm, independently of the capsule diameter, whereas for PU-reinforced capsules, the shell thickness is higher overall and additionally increases with increasing capsule diameters. While for 2.5 g PU/UF shells, the thickness increases gradually from approximately 400 to 800 nm for increasing capsules diameters, a plateau is reached for higher PU contents. For instance, for 7.5 g PU/UF shells, the thickness increases from 800 to 1200 nm already for capsules with <90 μm and 90-125 μm, respectively, and is roughly constant thereafter even for very large capsules. The reason for the different trends is due to the dissimilar shell forming principles: for pure-UF shells, the polymerisation takes place in the water phase and the UF polymer available per droplet surface is constant and independent of the droplet diameter. In contrast, the PU is formed through the reaction of the isocyanates dissolved in the core droplet. Therefore the total mass of PU is proportional to the cube of the droplet diameter whereas the droplet surface only scales with the square of the diameter. For the case of 2.5 g PU/UF shells, if one subtracts the thickness of the UF shell, the PU shell thickness is increased approximately threefold, from approximately 200 to 600 nm for the smallest to the largest fraction, in line with the increasing average diameter. For higher PU contents, a saturation value is reached: at 7.5 g added PU, the maximal thickness of approximately 1200 nm is already reached for the capsules in the 90-125 μm diameter range while for 5 g, the saturation is only reached for the largest fraction analysed in this work.

Atomic force microscopy allowed us to better visualise the difference in shell morphology between pure-UF and PU/UF capsules, thereby verifying the supposed mechanisms of the shell formation. Figure 4.7 shows two phase-contrast AFM images of a pure-UF capsule air-shell interface and that of a PU/UF capsule. For pure-UF capsules, the shell is composed of only one phase, with a smooth inner and a rough outer layer. For PU/UF capsules, instead, three different morphologies, composed of two different material phases, were observed: the inner part corresponds to the PU phase and is rough with PU agglomerates; the central part consists of a PU and UF mixture and is smooth with constant diameter; finally, the outer layer is rough again and consists of UF agglomerates.

In conclusion, a change of morphology between pure-UF and PU/UF capsules was demonstrated by AFM. Moreover, it was found that while pure-UF capsules have a shell thickness which is independent of the capsule diameter, the thickness of PU-reinforced

shells scales with the capsule diameter until a saturation value. In addition, the presence of an additional PU layer increases the thickness of approximately 4 to 6 times. This is extremely important for the consequences on the capsule mechanical properties, as it will be explained hereinafter.

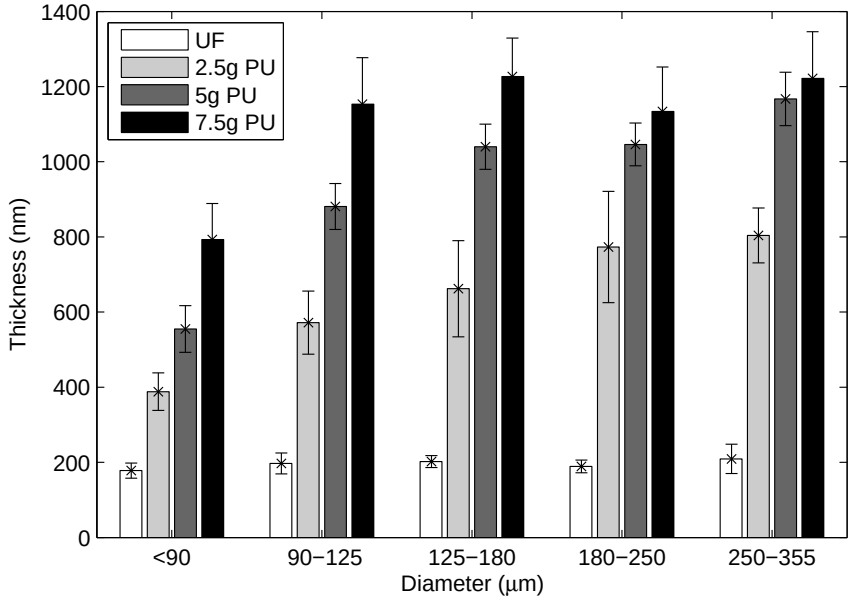

Figure 4.6: Shell thickness as a function of PU content and average diameter of capsules.

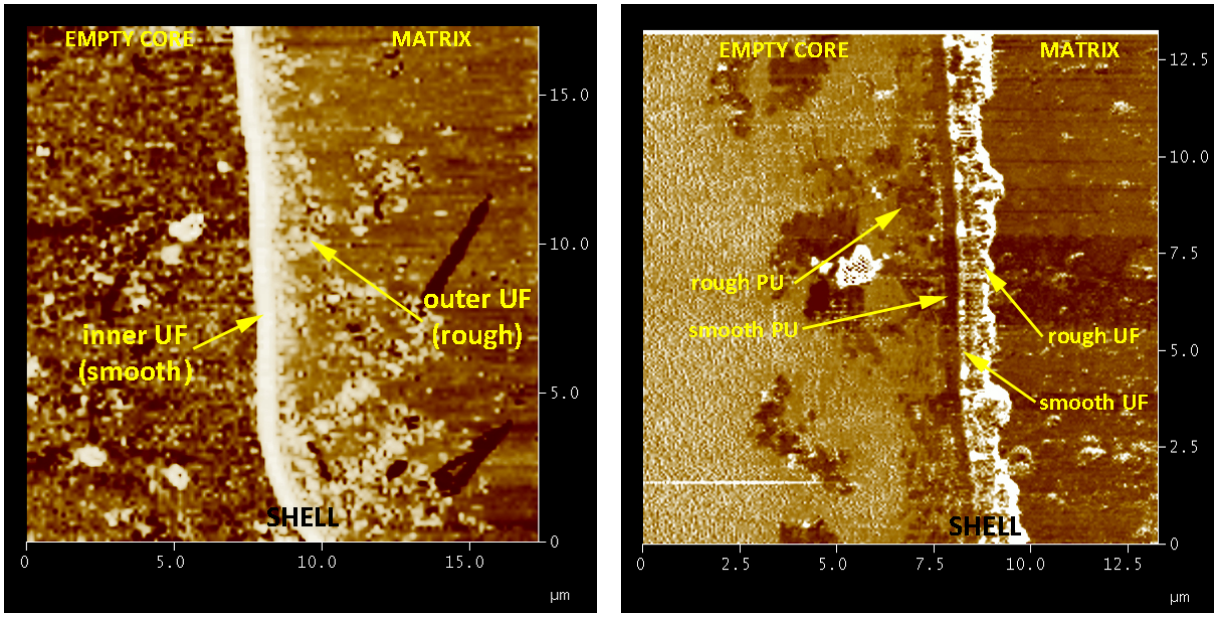

Figure 4.7: Phase-contrast AFM images of the shell of pure-UF (left) and 7.5 g PU/UF (right) capsules.

4.4 Capsule compression properties

The mechanical behavior of the different types of microcapsules was experimentally tested in single capsule compression test.

The microcapsules generally presented a constantly rising resistance for relative displacements up to 20-30%, followed by slight yielding of the membrane polymer just before shell bursting, characterised by a sharp drop in force due to liquid leakage and associated pressure drop inside of the capsule. Figure 4.8 shows two typical results of capsule compression for a pure-UF shell, as well as a 7.5 g PU/UF shell where the Young's modulus based on the capsule diameter and the shell thickness was computed by using the model fit [13], as detailed in § 3.4.5. For the present pure-UF capsule, the diameter was 142 μm and therefore the shell thickness was 202 nm, based on Figure 4.6. The resulting Young's modulus was 2.34 GPa. The 7.5 g PU/UF capsule was 187 mm in diameter with a corresponding shell thickness of 1134 nm. The resulting Young's modulus for the PU/UF composite shell was 0.62 GPa. Although the 7.5 g PU/UF capsules showed higher force readings at a given deformation as compared to the pure-UF shell, the modulus is much lower due to the almost sixfold higher shell thickness and higher capsule diameter.

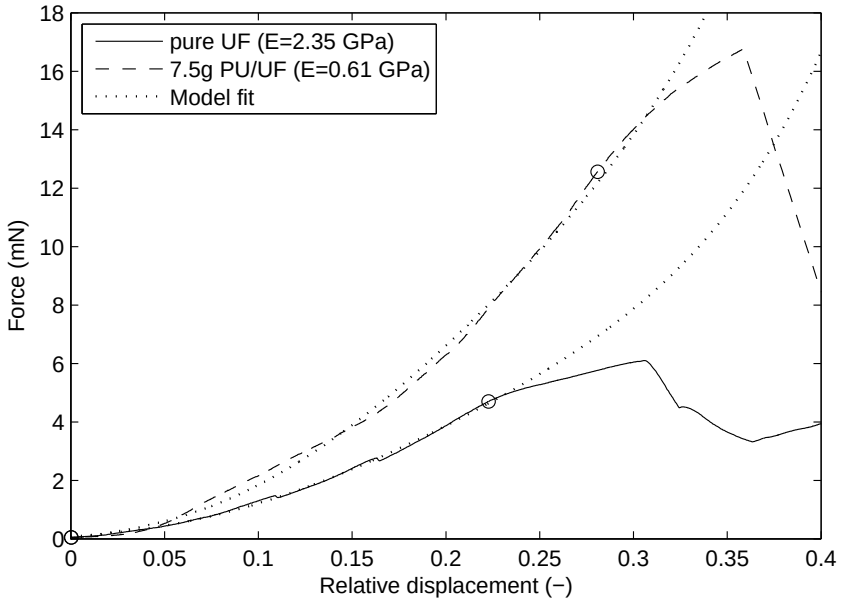

Figure 4.8: Typical results of a pure-UF and 7.5 g PU/UF shell single capsule compression experiment. Yielding is marked by a circle and the dotted line represents the fitted model.

Figure 4.9 summarises the Young's moduli for pure-UF, 2.5, 5.0 and 7.5 g PU/UF shells, as computed using the model described in § 3.4.5. The results for the UF shells are quite variable but in average presented a modulus of 3.54 GPa, as also reported by Keller *et al.* [101]. For PU-reinforced shells, the Young's moduli were much lower: 1.15 GPa for 2.5 g, 0.83 GPa for 5.0 g and 0.71 GPa for 7.5 g PU/UF shells. Using a simple rule of mixture

based on the shell thicknesses, the average modulus of the PU is computed as 0.20 ± 0.05 GPa. Additional compression tests on pure-UF and 7.5 g PU/UF microcapsules batches which were stored for at least 8 months at ambient conditions showed very similar values as compared to freshly prepared microcapsules as the computed Young's moduli were found to be 3.46 ± 0.24 and 0.58 ± 0.13 GPa, respectively. Furthermore, the bursting forces as a function of capsule diameter and shell composition are shown in Figure 4.10. Trend lines show the linear fit using a least squares method. While the modulus of PU-reinforced microcapsules was much lower than that of UF capsules, their bursting force is higher and also scales more with capsule diameter as compared to pure-UF capsules. We attribute this behavior to two different properties of PU/UF membranes: (i) the shell thicknesses of PU/UF shells scale with capsule diameter whereas they are almost constant for pure-UF shells and (ii) PU/UF shells exhibit slightly higher strains at bursting as shown in Table 4.2, meaning higher ductility in terms of elongation at break. Therefore, for small capsule diameters, pure-UF and 2.5 g PU/UF shells have similar bursting forces. For higher capsule diameters, the trend lines of PU/UF shell bursting forces converge because the higher capsule diameters lead to a higher PU mass to shell surface ratio and ultimately lead to a saturation thickness of the shell, confirming the observation above.

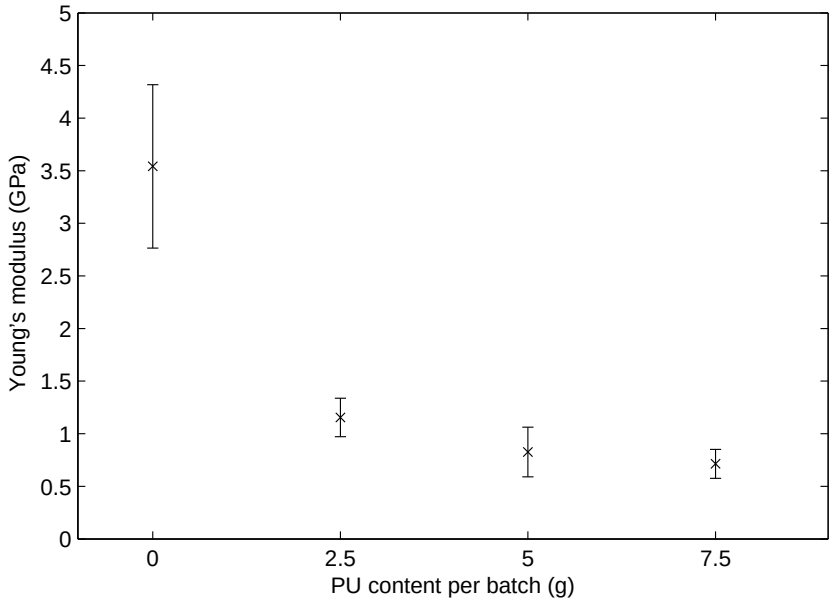

Figure 4.9: Average Young's modulus of the shell as a function of PU content.

In summary, it was shown that the modulus of PU-reinforced shells is much lower than that of pure-UF capsules, but that burst forces and elongation at break are higher in PU/UF shells due to the higher shell thickness and ductility in terms of elongation at break. For applications of these microcapsules in new self-healing composites, the present findings suggest that PU/UF capsules are more appropriate as compared to UF capsules, as they show both higher strains and forces at bursting, making them more resistant to

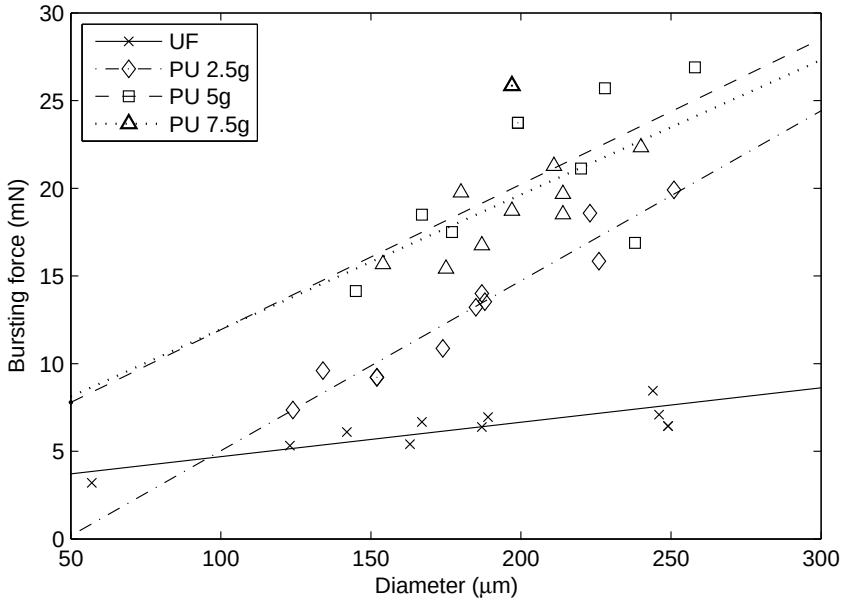

Figure 4.10: Burst force as a function of PU content and capsule diameter.

Shell type	**Deformation at yield**	**Deformation at rupture**
Pure-UF	0.25 ± 0.03	0.35 ± 0.08
2.5 g PU/UF	0.26 ± 0.02	0.46 ± 0.04
5 g PU/UF	0.30 ± 0.05	0.50 ± 0.08
7.5 g PU/UF	0.26 ± 0.03	0.42 ± 0.06

Table 4.2: Deformation at capsule yielding and rupture.

harsh processing conditions. Furthermore, if very small capsules are desired (diameter in the low μm range), our results indicate that high concentrations of PU will have to be added to the core fluid in order to form thicker shells; concentrations which might influence the effectiveness of the core phase's healing ability. On the other hand, for larger capsules, the shell thickness converges to a maximal value dictated by the curing kinetics rather than available monomer and the PU prepolymer concentration can be reduced.

4.5 Summary

An oil-in-water emulsion technique enabled the successful production of solvent-filled capsules with diameters in the range 90-250 μm. Setting the stirring rate of the emulsion enabled to tune the capsule diameter. The 125-250 μm was considered as the most suitable size fraction of capsules in the majority of the case studies. As will explained hereinafter, capsules with such a size can fit the interbundle volumes that the selected woven fabric reinforcement presents, by keeping protected and safe. We note that the emulsion protocol could have allowed us to produce smaller size capsules (using a lower stirring rate): smaller capsules could have been promising for interfering less with the fabric reinforce-

ment (especially in terms of packing and permeability properties) and fit better within the fabric interstices, however they would present a lower bursting force, provide less healing agent at equal content and might be filtrated through the fabric plies during impregnation due to a significant through-thickness flow. As a result, the largest capsule size still able to fut within the tow spacing of the reinforcement fabric was selected for the rest of the study.

It was possible to produce capsules with different core materials (EPA, HA) and different shells (pure-UF, UF-PU) by using the same technique. In terms of thermal properties, it was found that the capsule core does not influence the thermal behavior; however, it relates to the temperature at which the mass loss is located, which is associated to the boiling point of the core material. Moreover, the double-wall provides an undoubted higher thermal stability, independently of their shell, that makes these capsules suitable for higher temperature applications. For our purposes, mono-wall capsules were selected as suitable, since the maximum temperature which is attained during curing and post-curing does not go above 35-40°C. The morphology of the shell was also analysed and a change between pure-UF and PU/UF capsules was demonstrated. Moreover, it was found that pure-UF capsules have a shell thickness which is independent of the capsule diameter, while the thickness of PU-reinforced shells is 4-6 times higher and scales with the capsule diameter until a saturation value. Single capsule compression testing, with the help of an analytical model, demonstrated that the modulus of PU-reinforced shells is much lower than that of pure-UF capsules, but burst forces and elongation at break are higher in PU/UF shells due to the higher shell thickness and ductility in terms of elongation at break. Thus, for harsh processing conditions, PU/UF capsules are more appropriate as compared to UF capsules, although they are less fragile. Again, for our purposes, pure-UF capsules were considered as more suitable in order to privilege fragility rather than bursting force. Indeed, fragility is the a necessary condition for the capsule breakage thus the solvent release.

Chapter 5

Preliminary assessment of solvent healing through CAI tests

As mentioned previously, introduction and survival of the healing system is one of the major issues in the manufacturing of self-healing composites. Concerning microcapsule-based self-healing composites, two techniques for incorporating the healing agent have been proposed so far. Kessler *et al.* [1, 2] and Patel *et al.* [125] simply mixed capsules with the epoxy resin prior to hand lay-up; this solution leads to two side issues, typically the increase of the matrix viscosity, with consequent risk of poor impregnation, and the possible retention of capsules through the fabrics. Sanada *et al.* [134] slightly modified this methodology performing a dip-coating of the reinforcement (carbon fibre strands) in a strongly capsule-loaded resin, followed by partial curing and further impregnation with the same resin. A second strategy consisted instead in functionalising the fibre reinforcement rather than the matrix. Blaiszik *et al.* [137], although dealing with single glass fibres, used a dip-coating technique in order to couple catalyst particles first and then 1.5 μm diameter healing capsules; the dipping medium was in this case a liquid destined to evaporate. This procedure is undoubtedly elegant but might become significantly time-consuming. Jones *et al.* [11] also functionalised single fibres by dipping them in an aqueous solution of capsules, with the aim of further embedding them in epoxy droplets and testing the healing mechanism of the epoxy-fibre interface through a microbond test.

An alternative method of fabric functionalisation consists in the manual dispersion of capsules by sieving, which ensures an acceptable degree of capsule distribution, although is not indicated for non-flat shapes. In literature, such a technique can be found for the functionalisation of preforms with binders or tackifiers [138], and it lends itself to scale-up using the same automatized methods as for binder deposition on fabrics directly following the weaving process. This technique was chosen for the present work and is presented in this chapter.

Following to the preparation of capsule-functionalised fabrics, a preliminary assessment of healing was carried out by using CAI test and is presented in the second part of

this chapter. CAI test is a standardised test in aerospace industry [123, 124], which has been developed to characterise the damage tolerance for composite materials. This test provides the quantification of the residual compressive strength after an impact with a specific energy. The impact largely involves a Mode II high shear rate crack propagation leading to multiple delamination, while the compression loading causes further growth of the delamination cracks by macrobuckling in a dominant opening Mode I fracture [154]. The healing evaluation of interlaminar cracks is thus possible by simply comparing the residual compressive strength of impacted samples with and without healing. Difficulties of the test consist in (i) the perfect alignment conditions required for the compression test, meaning the need of very accurate sample edges grinding and compression frame alignment procedures and (ii) the need of thick samples (*e.g.* 5 mm) so the adaptation of the liquid manufacturing techniques. As yet, only a few papers have been published which presented the evaluation of healing of impact cracks. Using hollow fibre extrinsic approach (§ 2.2.2), Bond *et al.* studied the healing of damage created through quasi-static indentation (similar to impact damage) and the recovery of damage was assessed with four-point bending tests [43, 44, 46]. Williams *et al.* used CAI test with 3 J impacts and demonstrated recovery of CAI strength with healing at 125°C [47]. Using another healing system, namely epoxy capsules with latent hardener, Yin *et al.* also performed CAI test on woven fibre-glass epoxy composites and showed healing of low-impact cracks with the application of lateral pressure and 140°C heating [136]. Alternatively, with the use of the pioneering healing approach, Patel *et al.* [125] investigated low-velocity (up to 45 J) impact damages again using CAI test. Results indicated that healed specimens exhibited a decreased crack length and partial recovery of residual compressive strength; a greater recovery was shown when samples were subject to a 1077 kPa lateral pressure during the healing time, which induced a damage volume reduction. No studies are present so far which used CAI test combined with a solvent capsule-based healing system.

5.1 Fabric characterisation and functionalisation with capsules

The chosen method for the introduction of the healing capsules was the fabric functionalisation, consisting in the manual dispersion of capsules by hand sieving. Before functionalisation, the adapted size range of capsules was selected for use, depending on the fabric interbundle (or interstitial) dimensions). "Interstice" refers to the volume contained between the fabric tows, which is related to the type of weaving. Optical imaging of a plain fabric (not functionalised), as showed in Figure 5.1(left), demonstrated interbundle interstices in the range 150-200 μm (width), in which particles with 125-250 μm diameter can thus fit, as observed in Figure 5.1(right). Since optical imaging does not

provide any information about the interstitial dimension along the z-coordinate, X-ray micro-computed tomography was also performed. Figure 5.2 shows a reconstructed and thresholded slice of one layer of the selected glass fabric; the yellow area gives a visual indication of the volume –in scale– occupied by capsules with a size range of 125-250 μm if laid within the interstices and/or onto the fibre bundles. Indeed, by visually analysing the functionalised fabrics after the sieving process, it was observed that capsules partially fall down within the interstices and stay there, and partially fall down on the surface of warp/weft tows and stay there or roll down to an interstice, as Figure 5.3 shows. It was supposed that capsules fitting in the interstices remain more protected and safe and do not significantly increase the overall thickness of the stack, whereas those onto the yarns are responsible for a thickness increase and more susceptible to rupture while the fabric is compressed during processing. In order to have most of the capsules within the interstices of the selected fabric (with a specific dimension), it was thus fundamental to select appropriate capsule dimensions for a certain fabric type with a specific interstice volume. As explained above, the 125-250 μm fraction was found herein as suitable from a geometric standpoint.

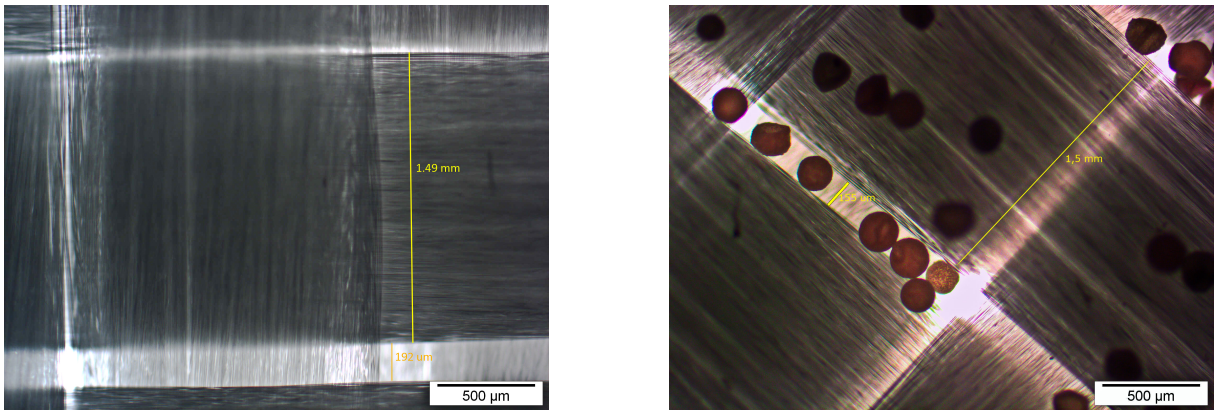

Figure 5.1: Optical image of the plain fabric, showing the bundle and interstices dimensions (left), and of the fabric with microcapsules (125-250 μm fraction) sieved onto the surface and fallen mainly within the interstices (right).

Figure 5.2: X-ray micro-computed tomography image of one plain fabric ply. The yellow area indicates the volume –in scale– that would be occupied by capsules with a size range of 125-250 μm laying within the interstices and/or onto the fibre bundles.

Furthermore, in order to validate this method and verify the degree of distribution of the capsules onto the fabric surface, a "visual test" was performed. The procedure is reported in § 3.5. Figure 5.4 shows the results, compared with the Mathematica model of

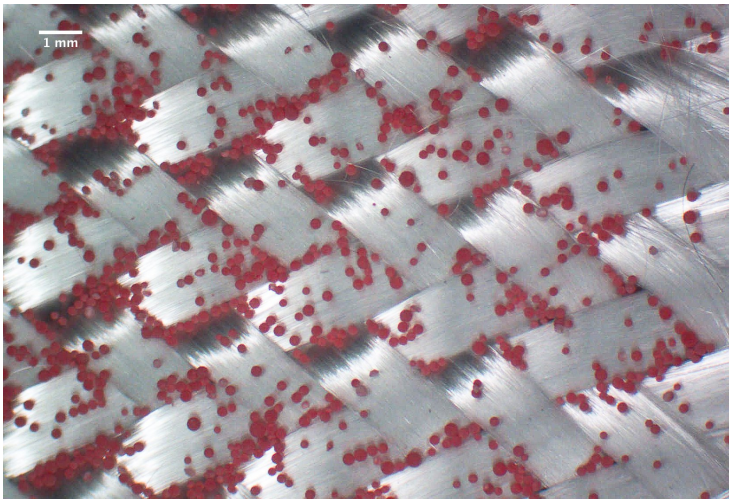

Figure 5.3: Optical image of the fabric with sieved 125-250 μm capsules.

surface coverage described in § 3.5, for the three different capsule volume fractions in the matrix V_c^*, namely 10, 20 and 30 vol%. Qualitatively, the degree of distribution was found satisfactory. Since it is a manual process, the quality of the results obviously depends on the accuracy taken by the operator while sieving. We notice that, especially in the presence of higher capsule amounts, presence of capsule "heaps" are visible and more uneven distributions are found. However, at a laboratory scale and for smaller capsule loadings, this technique can be considered sufficiently effective. Higher distribution accuracy and reproducibility could be obtained with an automatisation of the same technique, using vibrating tables for instance, which might be suggested for an industrial process.

As a conclusion, manual sieving was chosen as an effective method for functionalising the fabrics prior to processing. Indeed, it was qualitatively verified that an acceptable degree of capsule distribution is achievable with such a method. Moreover, it was observed that 125-250 μm diameter capsules can geometrically fit the interstices of the chosen fabric, thus revealing as the appropriate capsule size fraction for manufacturing a capsule-based self-healing FRP. However, a certain fraction of capsules, depending on V_c^*, will lay onto the yarns: as a consequence, an increase of the stack thickness and a change in the compressibility and permeability properties are expected.

5.2 Influence of capsules on fracture properties

Once the panels were produced through VARIM as described in § 3.6.1, samples for CAI test were prepared and tested. Prior to any healing evaluation, the influence of the capsule presence on the compression properties was first evaluated. As Figure 5.5 shows and Table 5.1 summarises hereinafter, the compressive strength was calculated for unimpacted samples containing no capsules (*plain*) and containing control capsule volume fractions of V_c of 1.25 vol% and 6.5 vol%. Herein, for studying the capsule influence

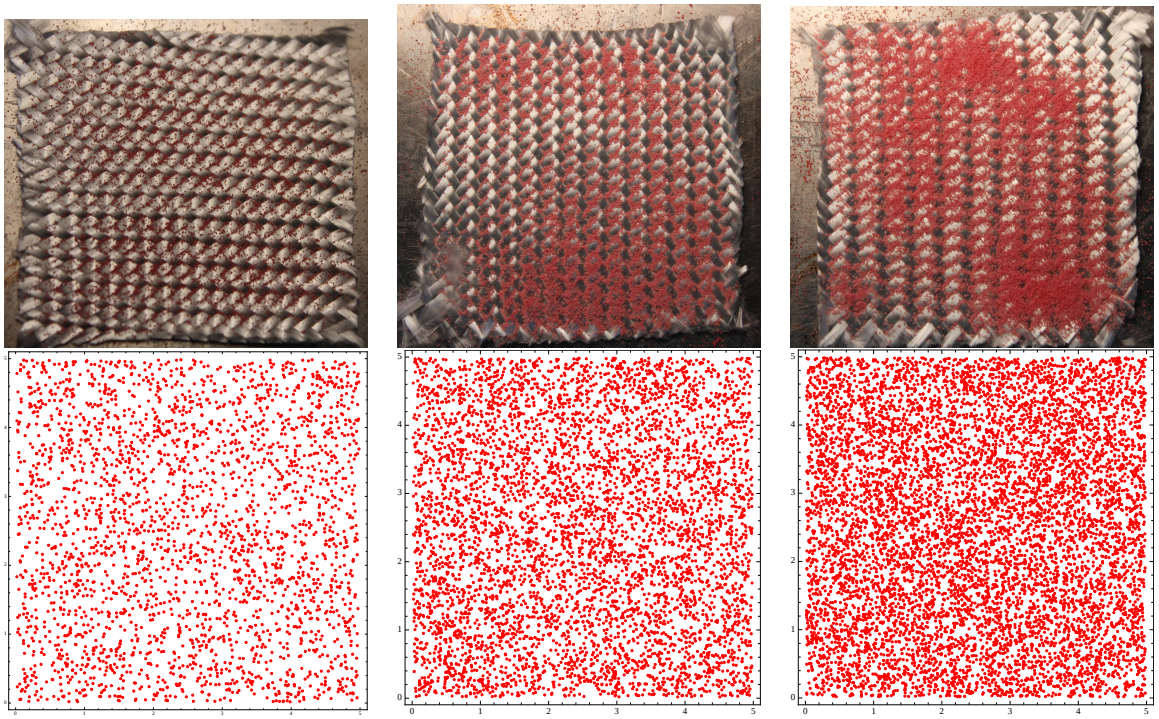

Figure 5.4: Dispersion test on 50 × 50 mm functionalised fabrics with V_c^* of 10, 20 and 30 vol%.

on the fracture properties (independently on the impact), unimpacted *control* samples were considered since they do not provide any healing thus any recovery of compressive strength. The results showed that the capsule presence results in a drastic decrease of compressive strength up to 53% for $V_c = 6.5$ vol%. In the case of $V_c = 1.25$ vol%, the obtained value is difficult to interpret, as it seems that the presence of capsules leads to a slight increase of compressive strength (+1.2%); the presence of $V_c = 1.25$ vol% can thus be considered as having a negligible effect on the compressive strength. Moreover, two additional pieces of information could be obtained. First, the compressive strength of the plain composite ($V_c = 0$ vol%), despite the incomplete polymerisation, showed quite high values up to approximately 265 MPa; these values were higher than what was obtained for other capsule-based self-healing composites [125]. Second, impacts of 5 J energy were found to not significantly affect the compressive strength. Indeed, as summarised in Table 5.1, the decrease of compressive strength due to 5 J-impacts corresponds to approximately 4.5% for $V_c = 1.25$ vol%. For $V_c = 6.5$ vol%, instead, the slight increase of compressive strength after impact must be considered as negligible.

In summary, we could conclude that, in general, the capsule presence negatively influences the compressive properties, especially for high loadings. This was also confirmed with images taken on the sample surface perpendicular to the compressive failure propagation plane (Figure 5.6), showing propagating microcracks attracted by the dispersed capsules, which acted as inclusions. Such inclusions surely represent weakening points for the material where cracks can be attracted, thus explaining the decrease of compressive

strength; however, concurrently, this is a necessary condition for the healing mechanism to occur. Nevertheless, some results concerning the effect of the capsule presence and the 5 J-impacts on the compressive strength could still not be explained and further investigations would be needed to assess the fracture mechanisms in these heterogeneous materials.

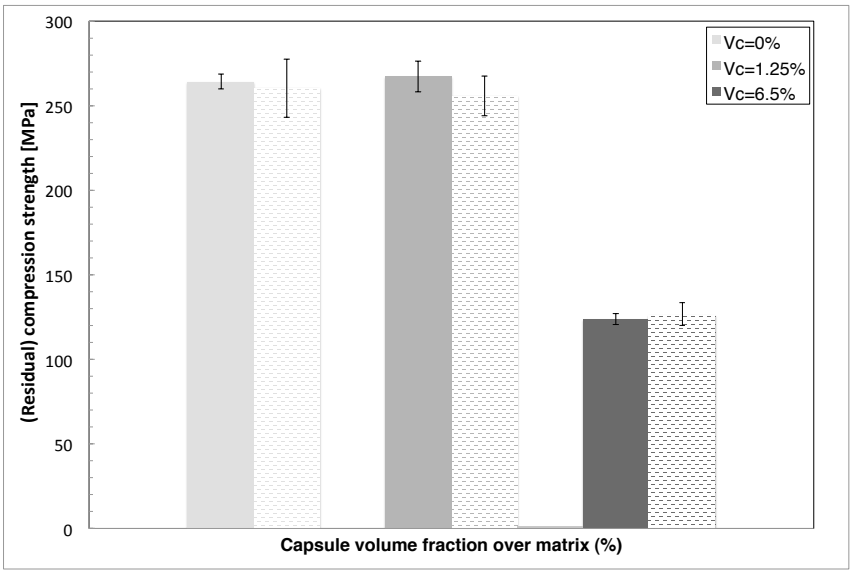

Figure 5.5: (Residual) compression strength measured by CAI test for samples with different *control* capsule concentrations. Bars with plain and dashed background indicate unimpacted and impacted (5 J) samples, respectively.

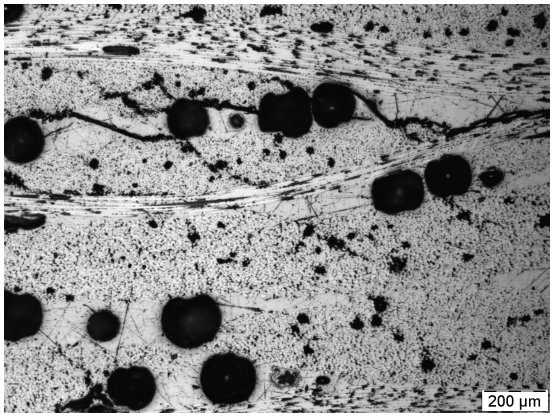

Figure 5.6: Crack propagating through dispersed capsules. The image was taken on a plane perpendicular to that of the compressive failure propagation.

5.3 Healing efficiency assessment

A preliminary assessment of the healing capability of such samples was carried out and the results are herein presented. The presence of healing could be detected by comparing the change of residual compressive strength (RCS) between *control* and *healing* samples:

if healing occurred, the cracks due to impact would have repaired at a certain extent and the residual compressive strength would present higher values (possibly equivalent those of the compressive strength of unimpacted samples in case of 100% healing). Results are presented in Figure 5.7 and summarised in Table 5.1. Only in the case of $V_c = 1.25$ vol% a little healing could be observed, since the drop of compressive strength due to the impact damage was slightly lower for *healing* samples as compared with *control* ones. Unfortunately, this could not be detected for samples with $V_c = 6.5$ vol%, for which it is not possible to validate the results. Several reasons could be suspected for explaining the lack of healing and the surprising values of residual compressive strength of certain samples:

1. capsule breakage during processing, probably due to a vacuum pressure difference applied during VARIM which was too high and led to bursting of a certain amount of capsules sieved on each ply, thus lack of healing agent;

2. damage extent and crack thickness induced by impact, which was probably too large;

3. lack of effectiveness of the solvent healing mechanism for this type of resin system (EPON 862) and composite.

The first potential reason could be verified by analysing the optical images of the sample cross-sections. Indeed, as visible in Figure 5.8, although good quality of impregnation (low porosity content) and capsule dispersion were observed for all panels, damaging of some capsules occurred. This was believed to be due to a vacuum pressure difference that was too high and could be one explanation for justifying the lack of healing. However, the two other reasons remained at this point only uncertain suppositions which could not be verified. The next chapters of the manuscript will address these issues in depth, by analysing compression properties of capsule-functionalised fibrous stacks, resin swelling, processing and healing with controlled crack propagation and location.

Sample	**Capsule influence**	**Δ(RCS) (%)**
Plain ($V_c = 0$ vol%)		-1.5%
Control ($V_c = 1.25$ vol%)	+1.2%	-4.4%
Control ($V_c = 6.5$ vol%)	-53.2%	+2%
Healing ($V_c = 1.25$ vol%)	-	-3.5%
Healing ($V_c = 6.5$ vol%)	-	+5.3%

Table 5.1: Summary of CAI test results: influence of capsules and percentage decrease/increase of residual compressive strength.

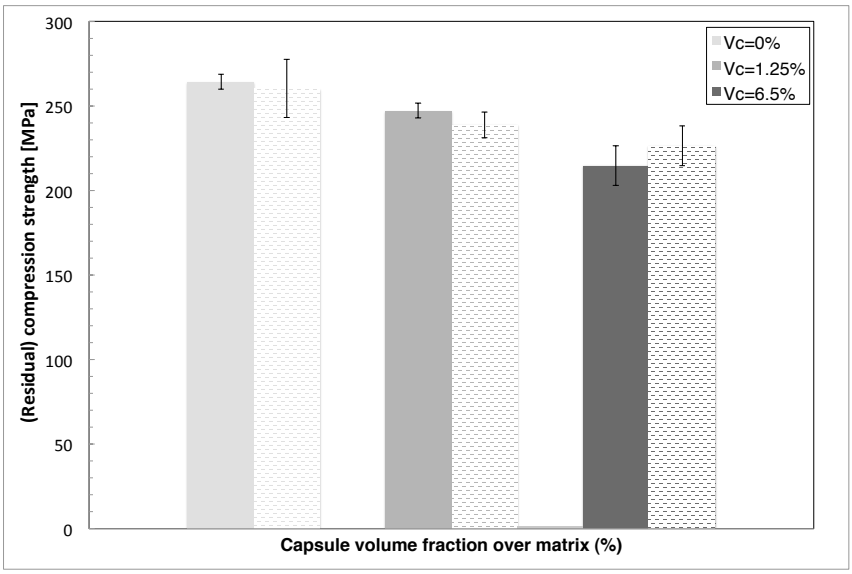

Figure 5.7: (Residual) compression strength measured by CAI test for samples with different *healing* capsule concentrations. Bars with plain and dashed background indicate unimpacted and impacted (5 J) samples, respectively.

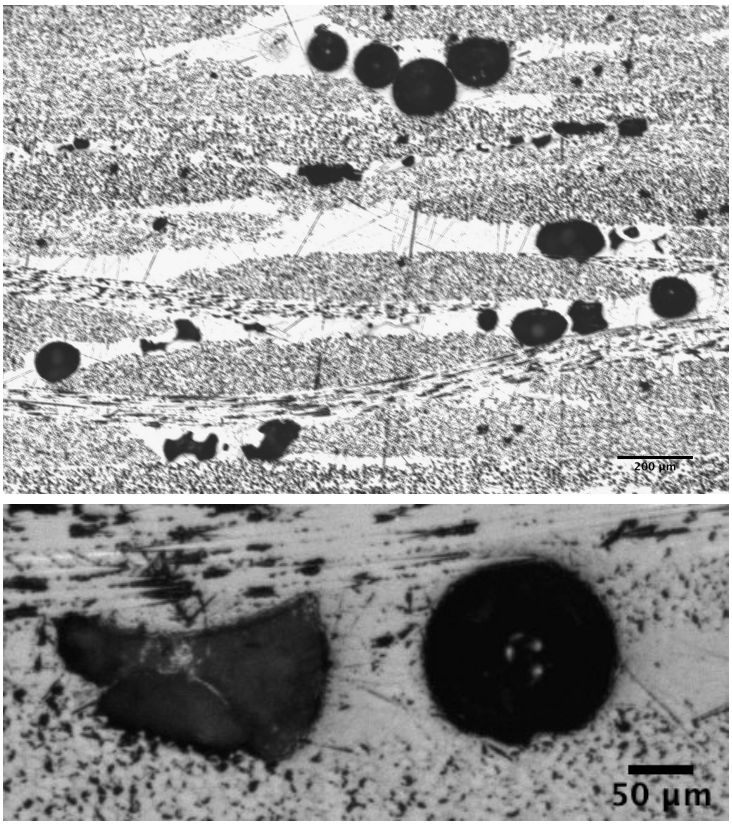

Figure 5.8: Examples of damaged capsules contained in a panel with $V_c = 6.5$ vol% and processed at 0.09 MPa pressure difference.

5.4 Summary

In this chapter, the approach to introduce the healing system within the composite was first presented. Manual sieving was validated as a laboratory-scale technique suitable for obtaining satisfactory degrees of capsule distribution onto the fabrics prior to processing. Concurrently, an adapted capsule size was selected depending on the interbundle dimensions of the woven selected fabric. Following to the fabric functionalisation with capsules, VARIM allowed us to obtain samples for further CAI experiments. Sample quality was overall good, capsules were well distributed but some ruptured during the process. CAI testing mainly showed (i) a drastic decrease of compressive strength due to the presence of capsules, especially at higher loadings, and (ii) lack of healing. Several causes were namely the loss of the healing agent proposed in the capsule due to breakage during processing and the lack of effectiveness of the healing mechanism. In parallel, CAI testing did not enable an effective healing evaluation. Indeed, it does not provide a precise locationand thickness control of the cracks appearing under the impact location thus a suitable spot where to study the healing mechanism; moreover, the healing efficiency expressed as recovery of residual compressive strength seems a too macroscopical parameter compared to the microscopical scale of the healing phenomenon.

Chapter 6

Packing and permeability properties of capsule-functionalised fabrics

Prior to processing, the reinforcement stack is usually characterised in terms of packing properties in dry conditions. The fabric stress–strain curve in compression gives an indication of the degree of fabric compaction for a given load (enabled by phenomena such as nesting depending on the fabric architecture), which is important for all techniques of composite manufacturing where pressure is applied (mechanical pressure or vacuum) and an infiltrating fluid is present. The degree of compaction is directly linked to the permeability of the reinforcement during infiltration, the achievable thickness of the part and consequent fibre volume fraction [155, 156]. Many studies are present in literature about the compressibility of various plain fibre reinforcements [146, 157–164]; however, only a few concern particle-functionalised ones, although it has been found that polymer binders distributed on a reinforcement surface affect the compressibility of the preform, may dissolve in the resin and change its viscosity and, not least, alter the overall composite mechanical properties [165]. Besides the compressibility, the fibre reinforcement is also usually analysed in terms of permeability (longitudinal and transverse). For a certain type of reinforcement, with a particular architecture, the permeability values are known to change depending on the fibre volume fraction and the degree of nesting (thus compression) of the stack [166, 167]; moreover they show scatter due to injection pressure variations and race tracking, as well as intrinsic variability of the textile. It is here believed that the presence of capsules may also affect the permeability, as they modify the porosity of the dry reinforcement available for the impregnation. Their presence can thereby induce an interference with the resin flow during processing, leading to possible variation of the flow rate depending on the capsule concentration. Both for compaction and permeability properties, capsule size distribution needs also to be taken into account and correlated to the interstice volume available between the tows of industrially relevant fabrics.

In this chapter, the functionalisation of glass reinforcements with healing capsules is

performed with manual sieving and, mainly, the effect of the presence of capsules on the packing and permeability properties of a stack of woven glass fabrics is investigated.

6.1 Packing behavior

The results concerning the packing behavior of dry plain and capsule-functionalised fabrics are here reported. Figure 6.1 shows the result of compression tests for plain ($V_c^* = 0\%$) and capsule-functionalised ($V_c^* = 2.5$, 5 and 7.5%) fabrics. For all curves, *i.e.* all capsule concentrations, the usual behavior of an overall thickness decreasing over loading till reaching a plateau was found, together with an hysteretic behavior while unloading (not shown here for clarity). However, the presence of capsules causes an increase of the overall stack thickness at equivalent applied pressure. Capsules, mainly those laying onto the fabric yarns (i) increase the thickness of the stack already in unloaded conditions and (ii) constitute an interference for fabric nesting over loading. This phenomenon becomes more marked as the amount of capsules increases, since the probability of capsules laying onto yarns rather than within interstices increases. Therefore, a shift of the compression curves related to the functionalised fabrics was observed as compared to the plain fabric. This result confirmed what obtained for samples used for CAI testing, which presented an increasing composite thickness with increasing capsule loads. Indeed, as shown in Figure 6.2, the cured plate thickness is plotted as a function of the capsule volume fraction of the panels. The values are scattered, but they confirm the tendency of an increasing thickness with increasing capsule loading. As comparison, compressibility data obtained on the dry fabrics are also reported (extracted from the graph in Figure 6.1), indicating the thickness values which are achievable at an applied pressure of 0.09 MPa.

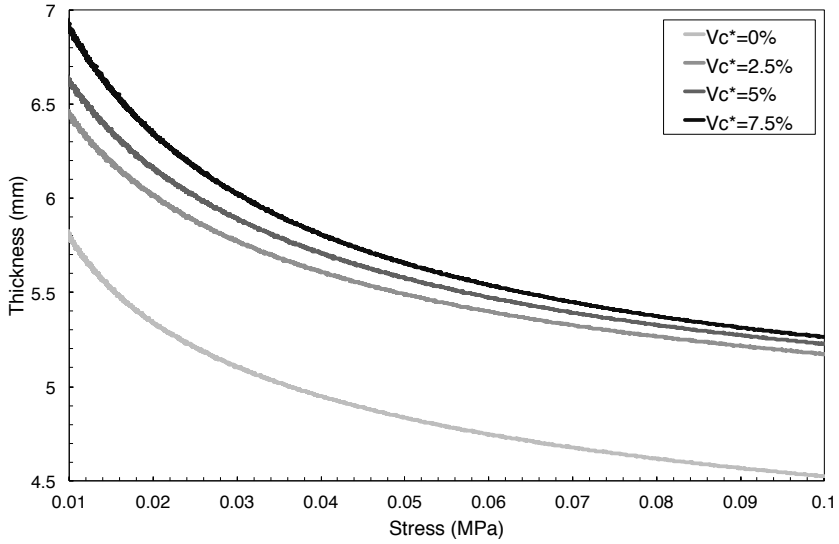

Figure 6.1: Compressibility of plain and capsule-functionalised fabrics in terms of thickness over loading (zoom 0.01-0.1 MPa).

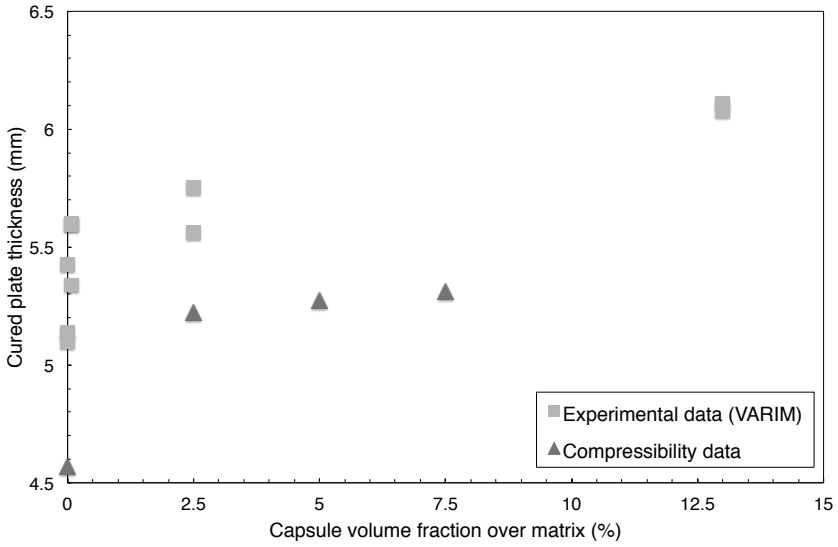

Figure 6.2: Thickness of the fibre stack (from compressibility data) and of the experimentally infused plates, as a function of capsule volume concentration over matrix.

The pressure-thickness data can be used to calculate the respective curves that represent the maximal achievable fibre volume fraction as a function of pressure. Equation 6.1

$$V_f = \frac{gsm}{\rho_f t} \tag{6.1}$$

was used, where V_f is the fibre volume fraction, gsm the fabric areal weight, ρ_f the density of the fibre material and t the total thickness of the stack.

Figure 6.3 reports the plots of applied stress in log scale versus V_f. For a given applied pressure, for example in a vacuum-assisted infusion process with 0.09 MPa pressure difference, lower fibre volume fractions are achievable with capsule-functionalised instead of plain fabrics. One can expect to reach V_f of 51.0% for the plain composite, whereas the same applied pressure leads to V_f of 43.8, 43.0 and 42.2% for capsule-containing composites with V_c^* of 2.5, 5 and 7.5 vol% respectively. For such a three-phase material (matrix, fibres and capsules), the curve of applied stress in log scale versus the pore volume fraction, that is calculated as 1-V_f-V_c, is reported in Figure 6.4. One can notice that the presence of capsules, compared to the plain fabric, increases the porosity at all applied pressures, denoting that capsules constitute an hindrance for fabric nesting and packing, thus explaining the lower achievable fibre volume fractions. By carefully analysing the portion of the curves at high applied pressures, a decrease of slope is observed, mainly for $V_c^* = 7.5\%$. This is attributed to capsule rupture, which occurs more frequently for higher capsule concentrations, since more capsules are on the yarns and directly exposed to the effect of pressure.

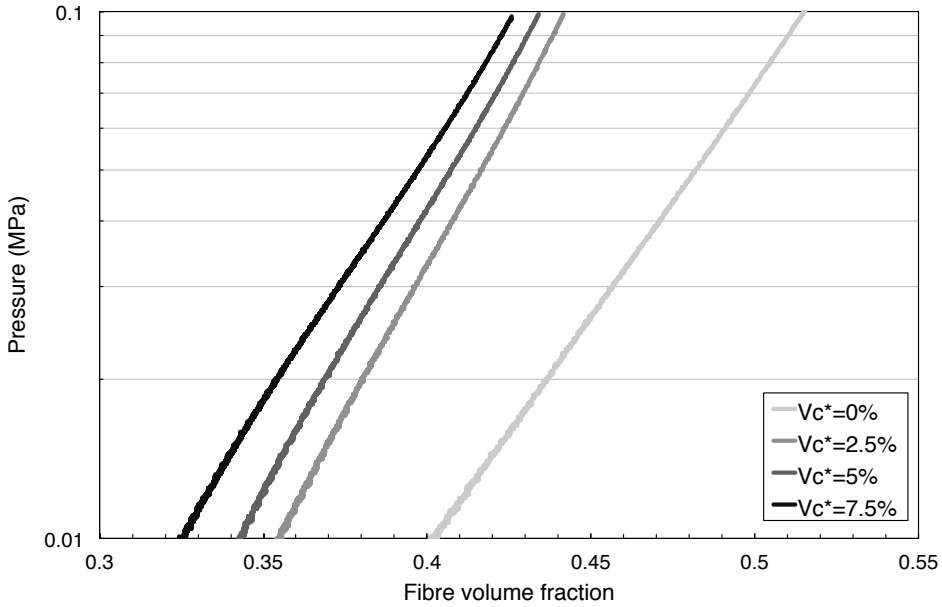

Figure 6.3: Compressibility of plain and capsule-functionalised fabrics in terms of fibre volume fraction over loading (zoom 0.01-0.1 MPa).

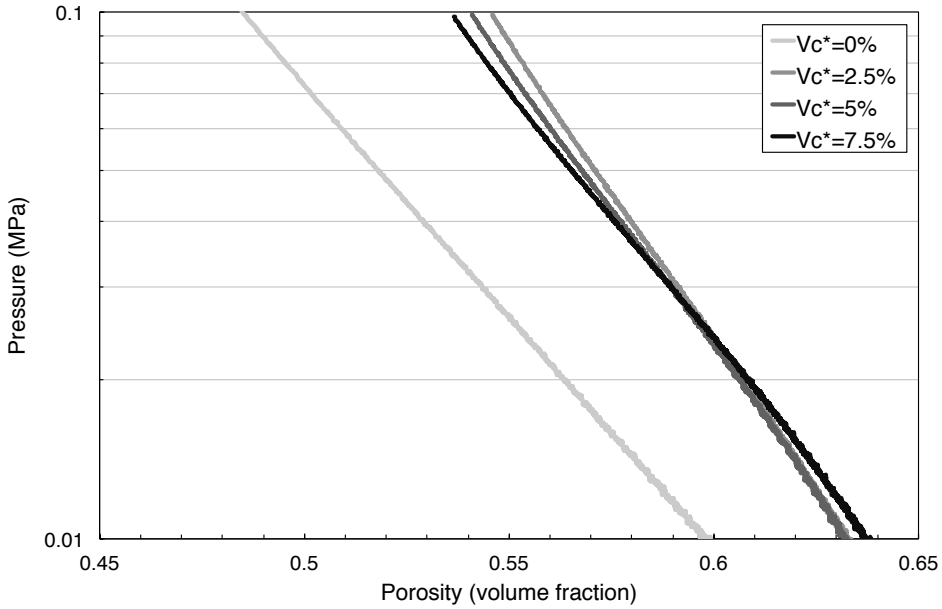

Figure 6.4: Compressibility of plain and capsule-functionalised fabrics in terms of porosity (calculated as 1-V_f-V_c) over loading (zoom 0.01-0.1 MPa).

Compression curves for textile preforms have been shown to follow a simple power law, Equation 6.2

$$P = a(V_f - V_{f0})^n \tag{6.2}$$

where P is the applied pressure, V_f is the fibre volume fraction, V_{f0} the initial (unpacked) fibre volume fraction, a and n are the coefficient and the exponent of the power law

respectively [155,156]. Results are shown in Figure 6.5 in log-log plot. We remark that in such a log-log plot, a standard plain fabric is usually characterised by a linear compaction behavior, that is a linear logarithmic pressure increase with the logarithmic fibre volume fraction.

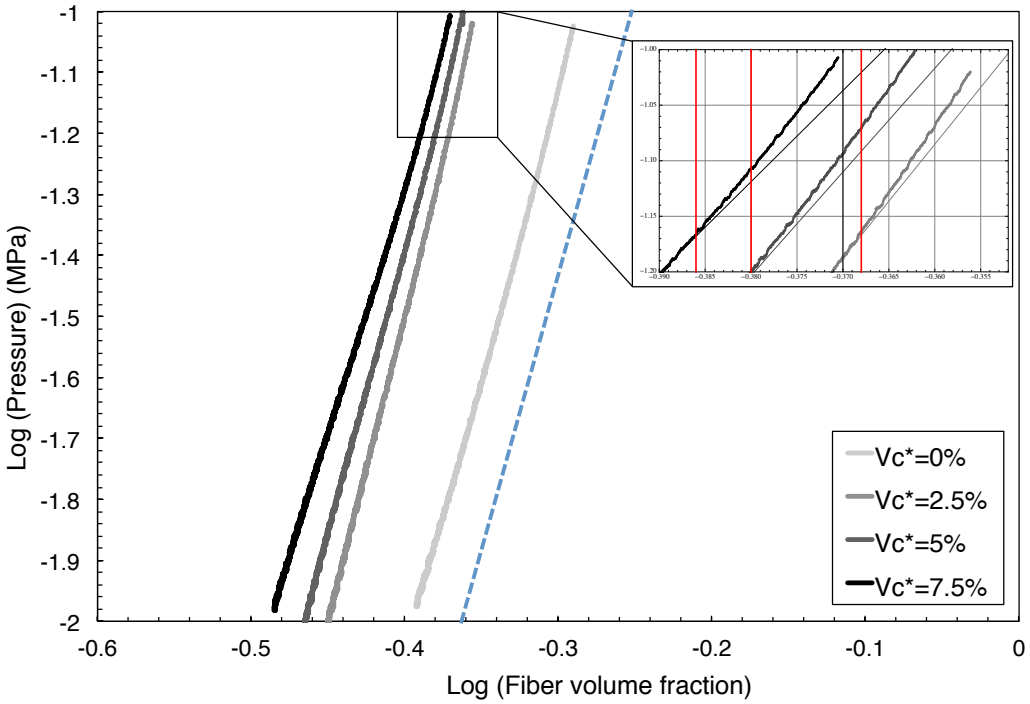

Figure 6.5: Log-log compressibility curves of plain and capsule-functionalised fabrics. The dashed line indicates a power law index of 9.3, which corresponds to the average index for all curves. The zoomed area shows the deviation from linearity occurring for capsule-functionalised samples at pressures between 0.01 and 0.06 MPa.

The presence of capsules, although decreasing the maximum achievable fibre volume fraction (at 0.1 MPa), does not significantly influence the power law exponent n, which presents a value of 9.35 for the stack without capsules and an average value of 9.25 $\pm$ 1.02 for the capsule-functionalised samples. Moreover, values of n found in literature for plain woven twill fabrics [155] agree with the ones here obtained. However, a deviation from the usual linear behavior was observed at low pressures, more remarkable along the curves of capsule-functionalised fabrics. This is interpreted as an effect of the presence of the capsules that is relevant when the pressure applied is low, thus when the capsules are still intact; this effect vanishes as soon as the pressure becomes higher (above 0.06 MPa) and induces capsule rupture: the remaining capsules' debris do not modify anymore the usual packing behavior of a plain stack of fabrics. Unfortunately, a correlation between compression testing of a single capsule [13] and a capsule-functionalised fabric was attempted but the result is not straightforward, as the capsule diameter is not constant and the position of the capsules within the fabric also changes. We conclude that the packing behavior is affected by the presence of the capsules at low pressures mainly, indicating

that capsules do modify the way fabrics nest and compress. At higher pressures, this phenomenon disappears and the behavior follows that of the plain fabric, with a lower V_f, probably denoting some capsule bursting under the effect of the applied pressure and remaining as debris on the tows, whereas capsules nested in the interstices do not interfere much with packing. During manufacturing of capsule-functionalised fabrics, it is thus fundamental to avoid high degrees of vacuum that can cause premature rupture of the capsules. These results demonstrated that the pressure difference (0.9 bar) used for processing panels for CAI testing (§ 5), being above the found threshold of 0.6 bar, was enough to cause capsule breakage, as was observed. This was also confirmed with the optical evaluation of the cross-sections of the panels used for CAI experiments, as presented in § 5.3.

In conclusion, it was demonstrated that the presence of capsules modifies the linear packing behavior of the glass reinforcements tested in dry conditions, especially in the first packing steps when lower pressures are applied and the capsules are still intact; at higher pressures, the probable capsule bursting corresponds to the elimination of the effect of capsules and the packing behavior follows again a power law as for plain samples. The change in compressibility properties also means that lower fibre volume fractions and higher overall stack thicknesses are achievable at equal applied pressure if capsules are present. The phenomenon is enhanced as the capsule loading increases. These results specifically applies to capsules with diameters in the range of 125-250 μm which functionalise woven fabrics with the same order of inter-tow spacing dimensions. Lower size capsules are expected to have a potentially different effect, as compaction will be less impacted. Namely, a different capsule size may translate in a different value of pressure threshold below which capsules remain intact. The results suggest the general necessity to adapt further manufacturing parameters (*i.e.* degree of vacuum and matrix content) in order to get comparable plain and capsule-containing samples as well as to avoid capsule rupture thus the loss of the healing properties, as it occurred for samples used for CAI testing. The results also suggest that for a given type of fabric architecture, only a limited amount of capsules can be introduced and nest within the interstices, depending on their size, thereby being protected during compression. Additional capsules will remain on the fabric and most probably break during compaction of the preform.

6.2 Permeability behavior

The results concerning the permeability measurements of plain and capsule-functionalised fabrics are reported hereinafter. Permeability was studied both in the longitudinal and transverse directions using two different apparati.

The rheology of the fluids used for testing was first investigated. Figure 6.6 illustrates the results of the rheological measurements as performed for the commercial silicone oil

and the PEG/water solutions with concentrations varying between 2.8 mmol/l and 8.6 mmol/l. It was found that the solution PEG/water with a concentration of 5.7 mmol/l presents viscosity values comparable to those of the commercial oil, thus it was selected for the transverse permeability tests. Note that for each permeability test, the fluid temperature was recorded at the injection point and the corresponding viscosity value was taken from the graph for the permeability calculation.

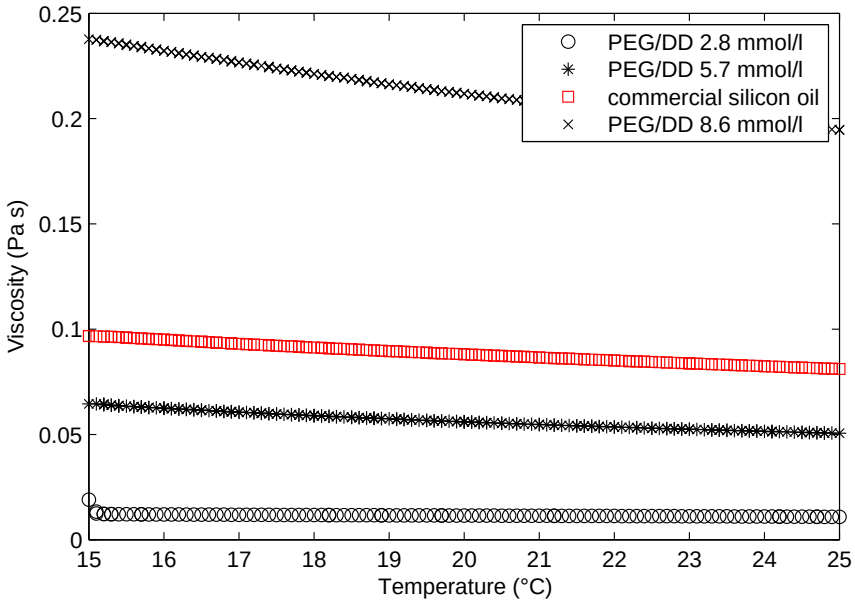

Figure 6.6: Viscosity as a function of temperature for the commercial silicone oil (in red) and the PEG/water solutions with various concentrations.

6.2.1 Longitudinal unsaturated permeability of plain and capsule-functionalised fabrics

The unsaturated permeability was calculated performing three tests for each type of sample (*i.e.* capsule concentration) and using the Squared Flow Front Approach [145]. Typical plots of squared flow front position L versus time t follow a straight line with a slope m that is determined for the calculation of the permeability. Based on Darcy's law, Equation 6.3 was used

$$K_{uns,SFFA} = \frac{\mu\varphi}{2P_{inj}}m \tag{6.3}$$

where $K_{uns,SFFA}$ is the unsaturated longitudinal permeability, μ is the viscosity of the impregnating fluid, P_{inj} the injection pressure at the inlet of the impregnation cavity and ϕ the porosity of the fabric, given by Equation 6.4 that contains the fibre and capsule contents V_f and V_c

$$\varphi = 1 - V_f - V_c \tag{6.4}$$

Equation 6.3 is valid assuming one-dimensional constant injection pressure and constant permeability along the flow direction. Before calculating the permeability values, the curves of squared flow front position versus time were analysed. For plain samples, it was found that, as expected, the curve is fairly straight, the slope m is constant and an average value of 165 mm^2/s is computed; examples are given in Figure 6.7. However, this was not found for capsule-functionalised samples ($V_c^* = 2.5$, 5 and 7.5%): for all these concentrations, the curves show two stages, with two different slopes m_1 and m_2 (Figure 6.8).

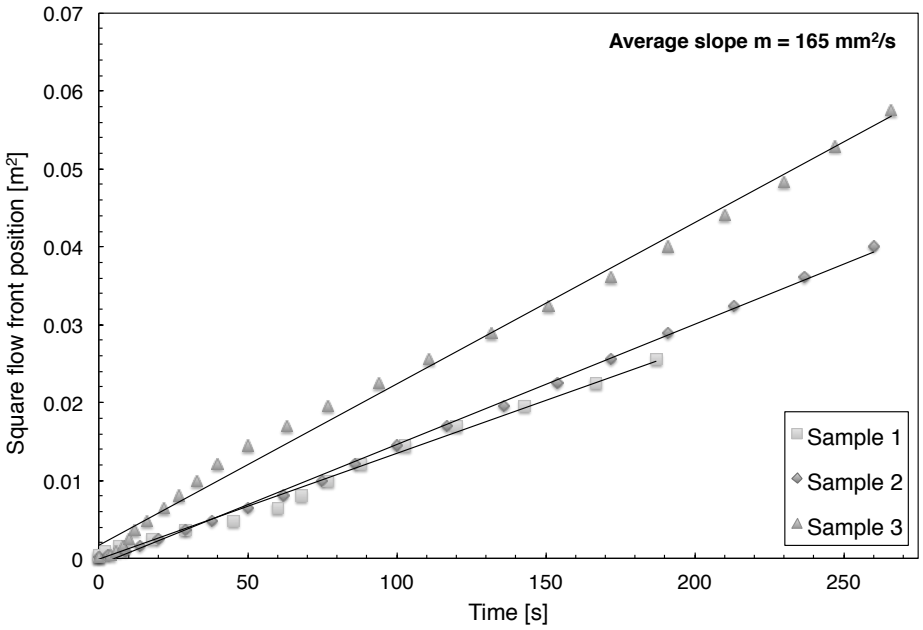

Figure 6.7: Squared flow front position versus time for plain samples. Average slope m is computed.

This is rather unusual in permeability measurement of textiles. A bilinear behavior was a first estimation step to split these two different stages that have been noticed. The first stage (up to approximately 40 mm infiltration length) was attributed to the presence of a boundary area with a smaller concentration of capsules close to the edge, possibly also escaping through manipulation of the stack. The second zone shows an increased infiltration speed, which corresponds to an increased pore space and/or most probably to increased capillary effects driving the flow in the presence of capsules. This second stage, corresponding to the largest part of the curve, was considered for the evaluation of the permeability. Particularly, under constant applied inlet pressure, it can be analytically shown that L^2/t increases if the flow reaches a higher permeability zone, since $\frac{L}{K} = \sum_i \left(\frac{L_i}{K_i}\right)$ [168]. Moreover, the capillary effects could be related to capsule presence and also rupture; indeed, as one can observe in Figure 6.1, for all capsule concentrations,

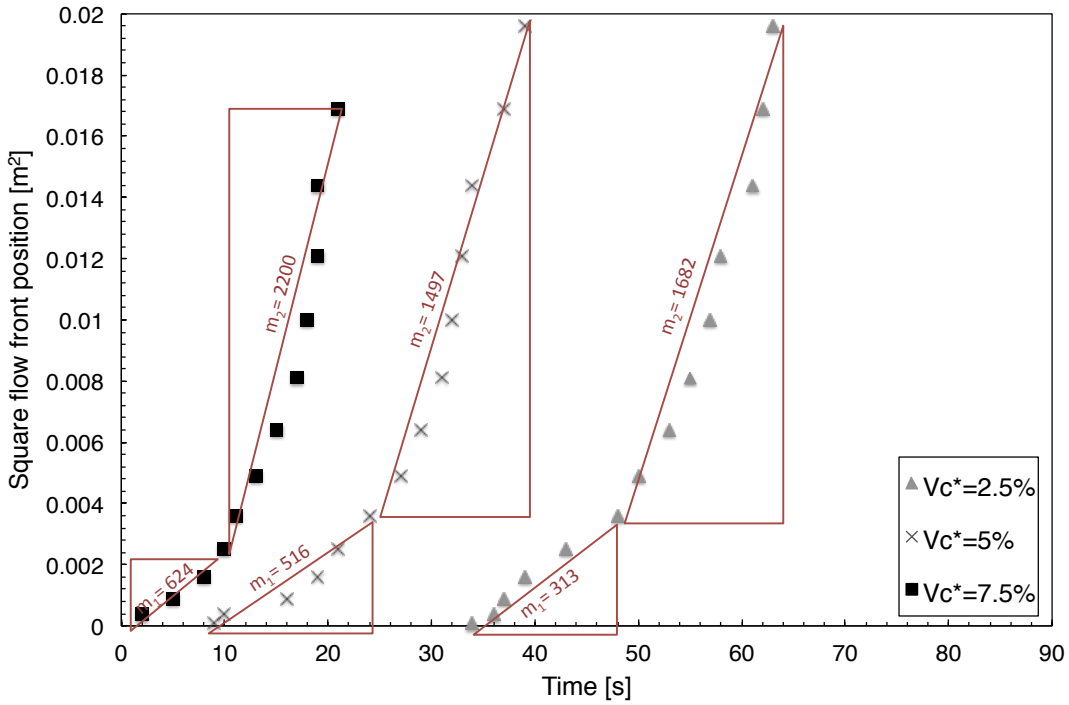

Figure 6.8: Examples of squared flow front position versus time for capsule-functionalised samples. Different slopes m_1 and m_2 are indicated (unit is mm^2/s). Curves are shifted for clarity.

with the stack constrained in a 5 mm thick frame at 2 bar closure pressure during the permeability measurement, the pressure applied to the stack corresponds to a pressure above 1 bar, and capsules may break if not properly nested in the interstices of the fabric. Consequently, debris may form, and some capsule content (EPA solvent) may be released to the impregnating fluid. The viscosity of the fluid after testing was checked and found to slightly decrease, but only by 3%, indeed contributing but not enough to explain the large increase in infiltration speed. Moreover, no wash-out of intact capsules was noticed in the outlet fluid, confirming that they stay in their position thanks to nesting and the compaction pressure. Figure 6.9 summarises the permeability values, and a factor 6 is found between the value for the plain fabric and all of the capsule-containing fabrics. The large variability in the results is attributed to the manual sieving, combined with the intrinsically high variability of permeability measurements. The similar values found for the various capsule concentrations confirms that the pore space was similar at this packing thickness for all samples, with increased breakage of the additional capsules that did not get protected by nesting. Unfortunately, partial capsule breakage could not be evaluated during or after the experiments in terms of amount of broken capsules, but could be only visually verified.

In summary, it was found that capsules increase the permeability as compared to plain samples, without any specific trend depending on their content. This increment was related with the presence of driving capillary forces, correlated with capsule presence

(higher spacing) and possible bursting. Moreover, the phenomenon is also enhanced by the imposed V_f (given by the experiment cavity), which could result in capsule breakage and release of solvent to the impregnation fluid, with consequent viscosity decrease (3%). In terms of applications, impregnation kinetics tend to be enhanced in the longitudinal direction, making the process time shorter.

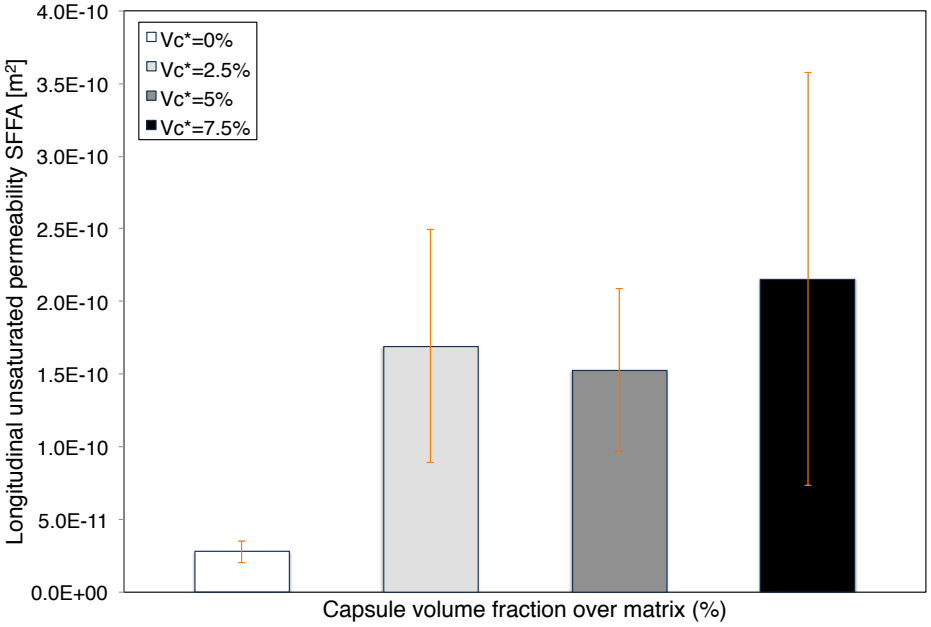

Figure 6.9: Longitudinal unsaturated permeability values as a function of the capsule content.

6.2.2 Transverse saturated permeability of plain and capsule-functionalised fabrics

The saturated permeability of plain and capsule-functionalised samples along the out-of-plane axis was investigated. The values were calculated by applying the Darcy's law as in Equation 6.5

$$K_{sat} = -\frac{QL\eta}{S\Delta P} \tag{6.5}$$

where Q is the flow rate measured at the outlet of the impregnation set-up after having saturated the sample stack, L is the impregnation length, that is the height of the sample stack, η is the viscosity of the impregnation fluid, S the sample surface (crossed by the flow) and ΔP the pressure difference measured between the injection point and the outlet. The hypotheses that Equation 6.5 requires to be applied, *i.e.* the use of a non compressible and homogeneous fluid, a laminar and steady flow (Re<1), isothermal conditions, constant pressure over the sample cross-section, are all respected. Figure 6.10 presents the obtained results, as a function of the capsule content. The absence of wash-out phenomena was

also verified with the absence of capsules in the fluid at the outlet. All values are in the range of $1 \cdot 10^{-12}$ to $3 \cdot 10^{-12}$ m^2 and the absence of large standard deviations indicates a good reproducibility of the experiment. Moreover, the results showed no remarkable variation between plain and capsule-functionalised samples and there was not significant trend that can be stated between different capsule concentrations.

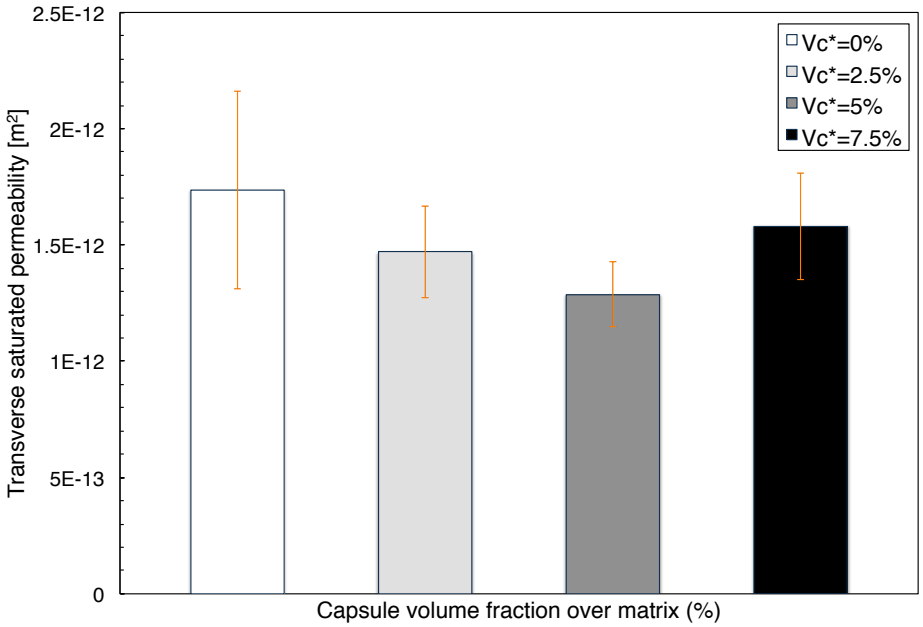

Figure 6.10: Transverse saturated permeability values as a function of the capsule content.

This leads to the conclusion that the permeability of the capsule-functionalised stack of fabrics toward the PEG/water solution as impregnating fluid is not significantly affected by the presence of the capsules sieved on each layer, for all concentrations. Since the samples are constrained to fit into a 4.7 mm spaced impregnation cavity, by closing the test cylinder, capsule bursting phenomena are here also expected. Nonetheless, the transverse permeability seems less affected by those compared to the in-plane one, possibly because it is a fully saturated measurement, not sensitive to capillary phenomena enhanced by the presence of capsules. In terms of implications for a typical VARIM processing of the same type of stack in order to obtain a good impregnation, the results bring to the conclusion that there is no need to change any processing parameters when one moulds a capsule-loaded composite compared to a plain one, at least in what concerns the out-of-plane properties.

In summary, in terms of transverse saturated permeability, the capsule presence does not present either beneficial or detrimental effects, so there are no specific implications that need to be considered during VARIM of thick panels in the presence of capsules, compared to plain conditions.

6.3 Summary

The fabric functionalisation via manual sieving was the selected method for the introduction of the healing capsules into the composite prior to processing. This methodology was validated as effective at least at a laboratory scale, since an acceptable degree of capsule distribution was achievable. Moreover, for the selected textile type, 125-250 μm was revealed as the appropriate capsule size fraction for manufacturing capsule-based self-healing FRPs: capsules could geometrically fit the interstices of the fabric, although a certain fraction of capsules, depending on V_c^*, laid onto the yarns: as a consequence, an increase of the stack thickness and a change in the compressibility and permeability properties were expected and further on confirmed. This was also in agreement with the trends of cured panel thicknesses as a function of capsule loading as obtained with samples for CAI tests.

Furthermore, it was found that the packing behavior of a fabric reinforcement stack was modified by the presence of functionalising capsules, especially in the first packing steps when lower pressures are applied and the capsules are still intact; at higher pressures, the probable capsule bursting corresponds to the elimination of the effect of capsules and the packing behavior follows again a power law as for plain samples. The phenomenon is enhanced as the capsule loading increases and also means that lower fibre volume fractions and higher overall stack thicknesses are achievable at equal applied pressure if capsules are present. These findings confirmed the existence of a threshold above which capsules rupture, as occurred for CAI samples which were processed at 0.9 vacuum pressure difference, that is well above the found threshold. An adaptation of the manufacturing parameters was thus strongly recommended in order to get comparable plain and capsule-containing samples as well as to avoid capsule rupture thus the loss of the healing properties.

In terms of permeability, the results obtained suggested that, in the presence of functionalising capsules, impregnation kinetics tend to be enhanced in the longitudinal direction, while not significantly affected through-thickness. The phenomenon seemed to be mainly related to high driving capillary forces, correlated with the capsule presence (higher spacing) and their possible bursting.

Chapter 7

Assessment of solvent healing through DCB and ENF tests

This chapter is dedicated to the critical assessment of healing a woven E-glass reinforced epoxy using the solvent system explained in § 2.2.2. Tests are performed through ENF and DCB experiments. The proposed method of integration of the healing system within the composite prior to processing, consisting in the functionalisation of the reinforcement fabrics by manual sieving, was used. Furthermore, the adaptation of the VARIM process for producing capsule-containing panels was investigated as a reproducible and industrially relevant manufacturing route, using widely used textile reinforcements and aiming at fibre volume fractions of 50 vol% in the composite plate. A preliminary study concerning the choice of an optimal vacuum pressure difference for VARIM and a suitable resin for impregnation is first presented.

7.1 Investigation of the optimal VARIM vacuum pressure difference

Figure 7.1 shows four optical images of the central capsule-functionalised ply after being subject to different vacuum pressure differences varying between 0 and 1 bar (not all shown for clarity). Capsules tend to break at the low ΔP_{vac} of 0.3 bar. The first capsules to burst were generally those laying on the tows, followed by those within the interstices which break at higher ΔP_{vac}. This suggested 0.3 bar as maximal vacuum pressure difference recommended for use during further VARIM processing.

7.2 Resin selection

Before proceeding with the panel manufacturing, the selection of a suitable resin was performed. Between the two resins available, EPON 862 (already used for producing

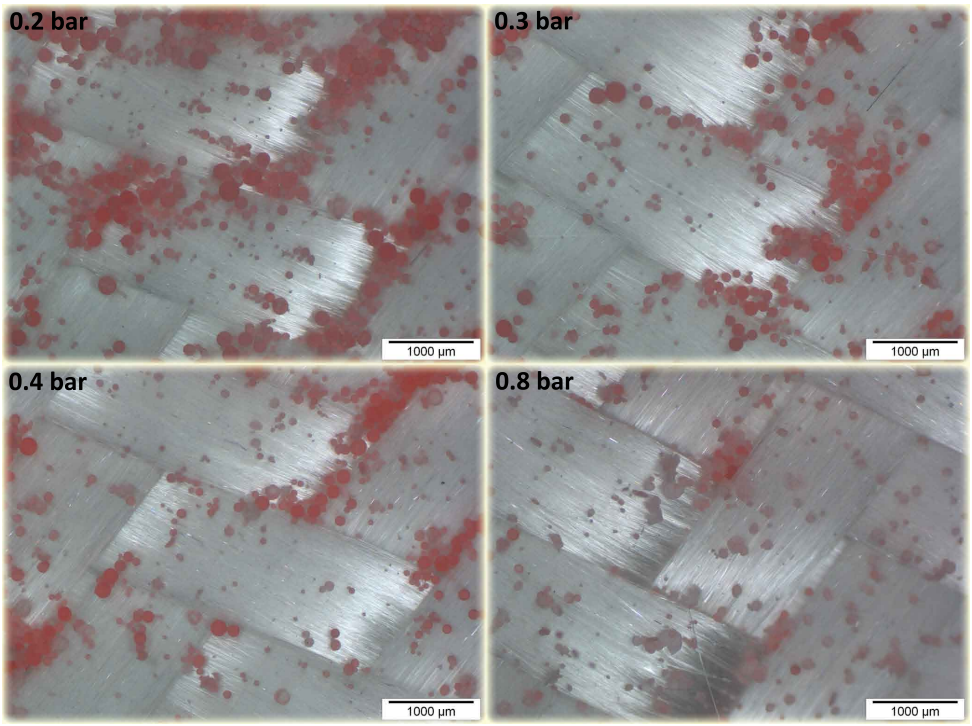

Figure 7.1: Compaction test under vacuum: optical images of the capsule-functionalised ply after undergoing different vacuum pressure differences.

CAI samples) was preferable for its lower viscosity, although its swelling properties in the presence of EPA had been not yet investigated, nor its degree of polymerisation with the cure cycle described in § 3.1.

DSC measurements of the degree of polymerisation led to find a higher conversion for EPON 862 compared to EPON 828EL, at equal thermal treatment, as shown in Figure 7.2. This translated in a lower swelling capability in the presence of EPA, as shown in Figure 7.3. The presence of fewer residual functionalities (related to a higher degree of conversion) and the consequent lack of swelling represent deleterious issues for the healing mechanism. In order to keep EPON 862 thanks to its lower viscosity more adapted to VARIM, the post-curing time of EPON 862 was reduced. However, it was found that the same swelling capability was achievable for EPON 828 and EPON 862 when post-cured at 35°C during 24 h and 0h respectively, as shown in Figure 7.4. This meant that EPON 862 should not be post-cured in order to observe a swelling comparable to that of EPON 828EL. This solution had to be rejected since the epoxy system without post-cure would be too unstable and destined to evolve (polymerise) over time at room temperature.

This result confirmed another possible reason for the lack of healing of CAI samples (§ 5), which were processed with EPON 862 and underwent a post-cure of 24 h. A too high degree of polymerisation and the subsequent lack of swelling were possible causes which could explain the failing of the healing system.

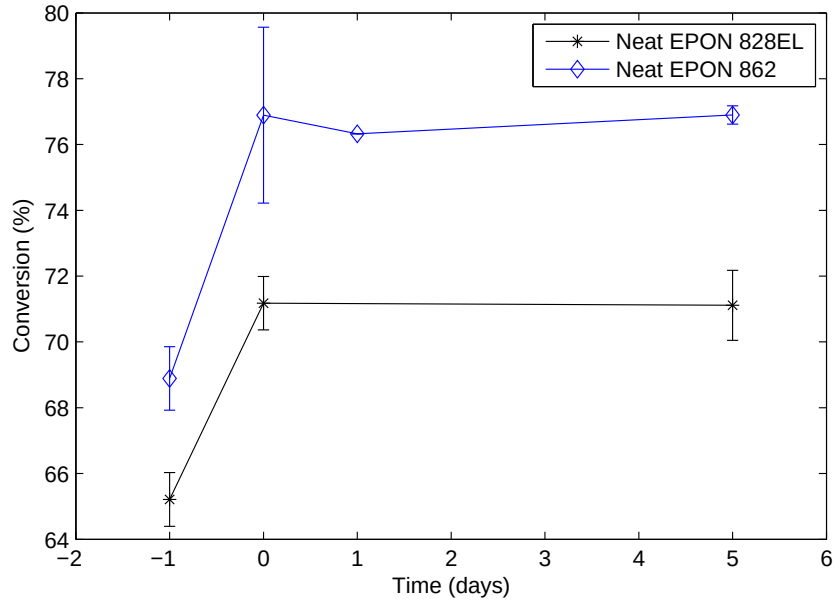

Figure 7.2: Degree of polymerisation of EPON 828EL and EPON 862 as a function of time. The conversions after 24 h curing and after 24 h post-curing are indicated with "-1 day" and "0 day", respectively. Samples were stored at 22°C with 20% relative humidity.

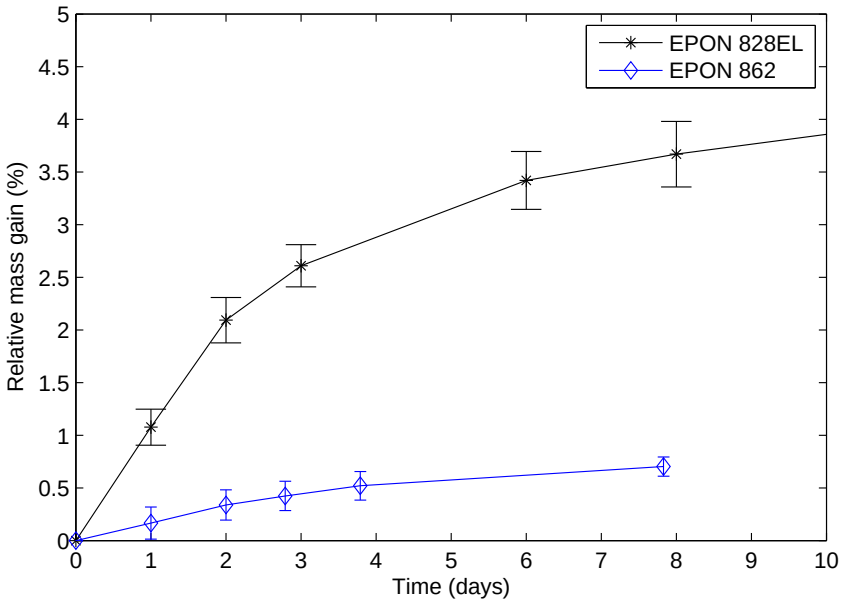

Figure 7.3: Evolution of relative mass gain of neat EPON 828EL and EPON 862 cylinders immersed in EPA over time. Samples underwent 24 h post-curing at 35°C.

EPON 828EL was finally retained for our purposes, although its viscosity needed to be tuned for use in a processing such as VARIM. Two solutions were proposed and investigated by rheology measurements: (1) the addition of 5-10 wt% of Heloxy 61 (viscosity modifier) to the resin during mixing and (2) heating up the resin to 35-40°C during degassing and molding. The results are reported in Figure 7.5. The second solution was

favored, since no additional components had to be added to the system. Heating at approximately 30°C was causing the viscosity to drop from 20 Pa (20°C) to 2 Pa, reaching a similar value compared to that of EPON 862. Moreover, it was verified that such a thermal treatment did not modify the degree of polymerization after post-cure.

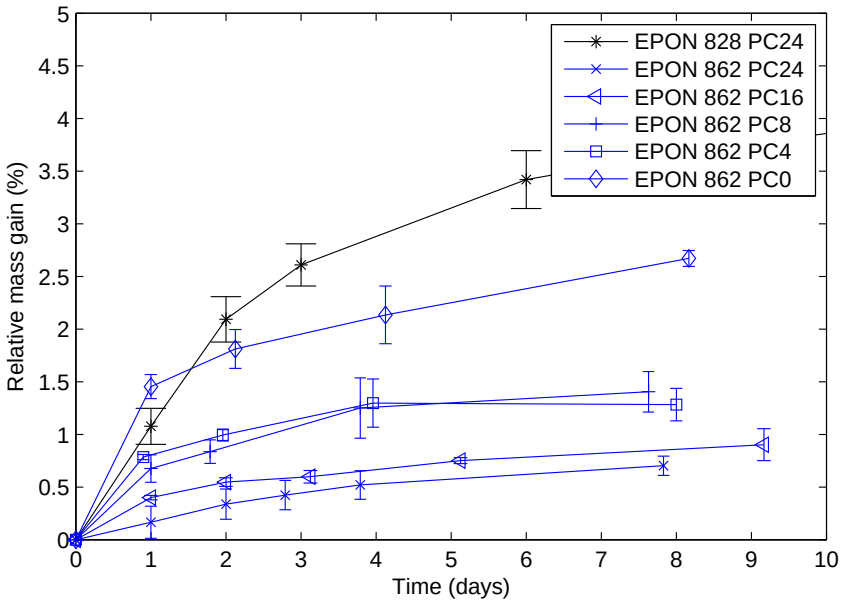

Figure 7.4: Evolution of relative mass gain over time for EPON 828EL and EPON 862 with different degrees of post-cure (referred to as "PCnumber of hours of post-cure"). Samples underwent 24 h curing at 25°C.

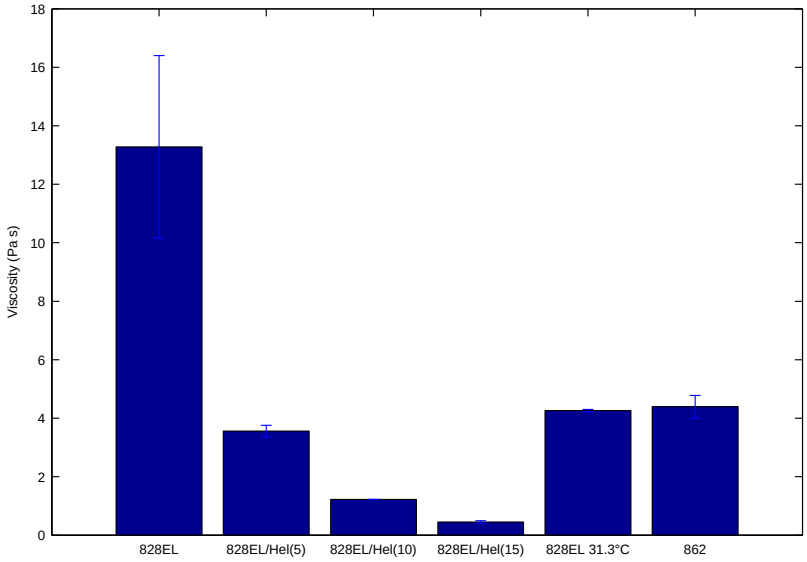

Figure 7.5: Viscosity values for EPON 828EL with Heloxy 61 (5 and 10 wt%) and heated at approximately 30°C, compared with EPON 862.

7.3 Post-processing evaluation of the panels

After processing, the quality of the panels produced by VARIM with EPON 828EL (at 35-40°C and 0.3-0.4 bar vacuum pressure difference) was evaluated by optical imaging of the composite cross-sections. Micrographs were taken on polished cross-sections cut in different positions of the panels (top, center and bottom), parallel and perpendicular to the resin flow. No significant differences in quality were noticed depending on the orientation or on the position, and all images showed a very low porosity content (0.09%, average on 5 micrographs). An example of the cross section of a plain composite is reported in Figure 7.6.

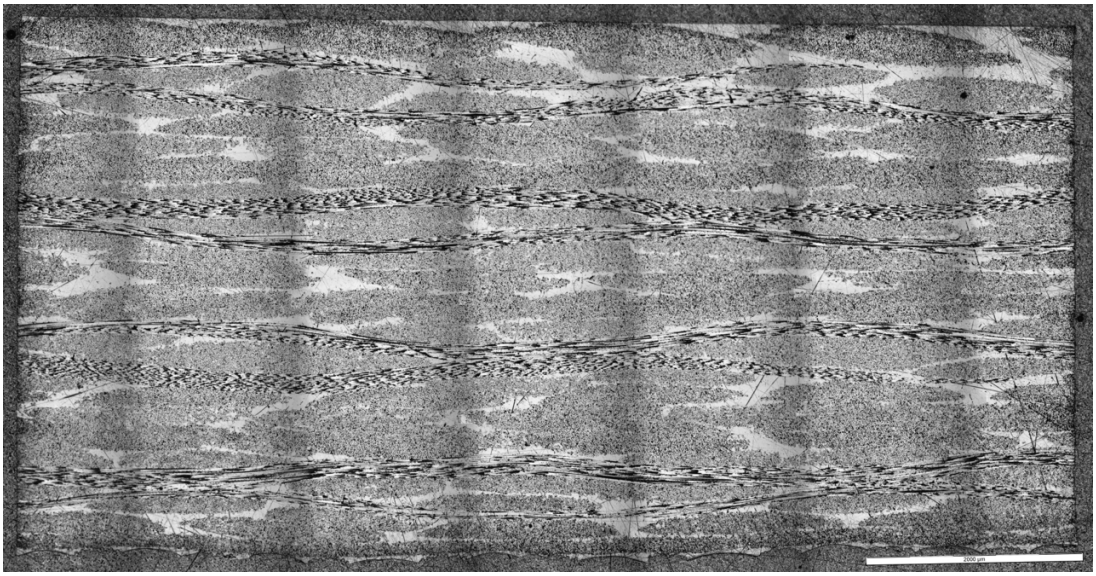

Figure 7.6: Optical image of the cross-section of a plain sample. Scale bar indicates 2 mm.

Capsule-containing panels were also analysed. Again, no significant porosity was present, with equivalent values to those obtained for plain samples. It was visually verified that capsules did not burst during processing and were still intact, and that their adhesion to the matrix was good. We noted that capsules could indeed fit the interply matrix pockets, aligning onto the ply they were sieved onto. Figure 7.7 shows a polished cross-section optically imaged at the capsule location.

7.4 Influence of capsules on fracture properties

As explained in § 2.3.1, it is important to evaluate to which extent the presence of the healing system influences the mechanical properties of the virgin material, prior to any healing test. Here, Figure 7.8 and Table 7.1 show the results for DCB and ENF tests respectively, for both plain and capsule-loaded composites. Note that the fibre volume fraction was approximately 50 vol% for all samples. For a capsule loading of 15 wt%

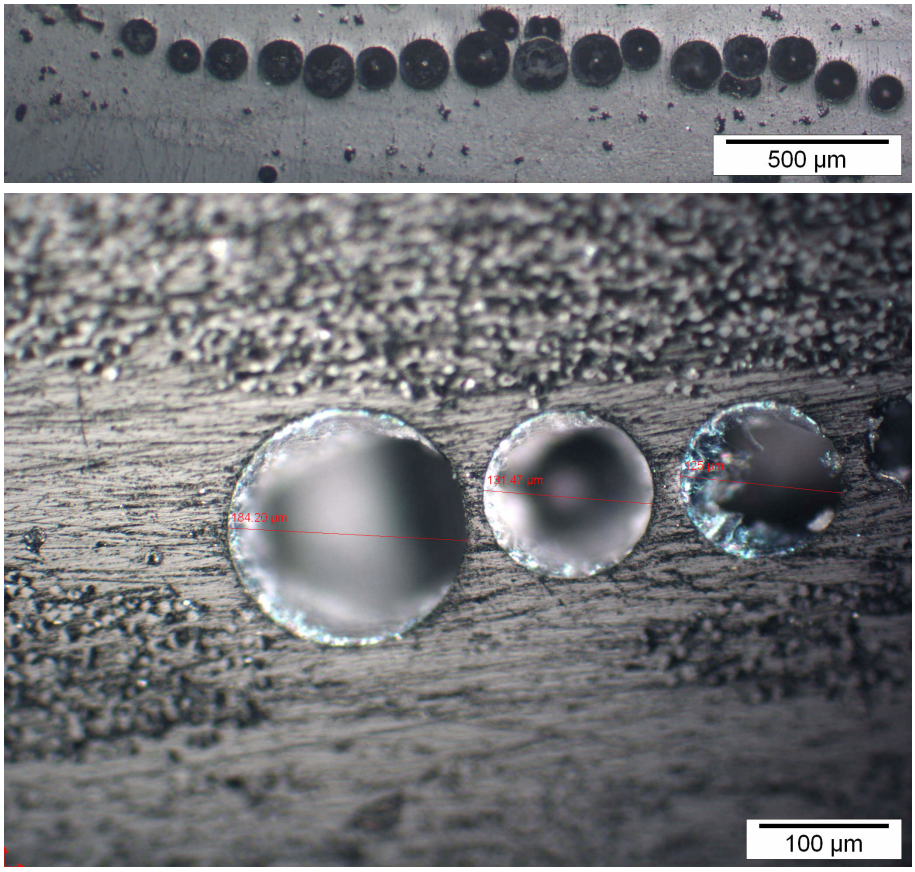

Figure 7.7: Optical images of the cross-section of a capsule-containing sample, at the capsule location.

over the "local" matrix of the ply (equivalent to an overall capsule volume fraction in the composite of 0.085 vol%), the normalised maximum load was not affected, in either Mode I or II propagation. The fracture toughness, instead, showed a decrease of 25-30% for both propagation Modes. Thus, in terms of energy release rate during the crack propagation, the mechanical behavior of the virgin capsule-loaded composite was decreased compared to that of the plain composite.

Test	V_c^* **(wt%)**	V_f **(%vol)**	**Normalised max load (N)**	**Interlaminar fracture toughness (J/m²)**
DCB	0	55.0 ± 0.010	101.1 ± 5.8	1152.0 ± 143.9
	15	54.0 ± 0.012	85.9 ± 6.8	796.8 ± 139.2
ENF	0	44.5 ± 0.010	1447.7 ± 99.0	2987.1 ± 177.9
	15	43.3 ± 0.006	1301.1 ± 102.1	2277.7 ± 294.0

Table 7.1: Normalised maximum load and interlaminar fracture toughness values of samples tested with DCB and ENF tests, containing 0 and 15 wt% capsules over the "local" ply matrix. Relative fibre volume fractions are also indicated.

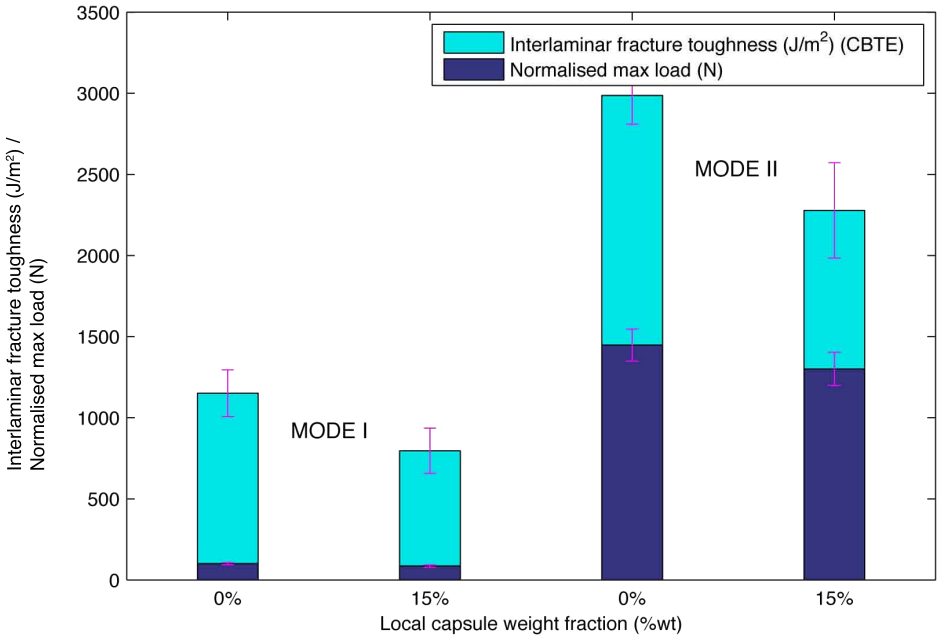

Figure 7.8: Normalised maximum load and interlaminar fracture toughness for samples tested in Mode I and Mode II as a function of the "local" capsule weight fraction.

7.5 Healing efficiency assessment

The effectiveness of the solvent healing system was investigated and results are reported hereinafter.

7.5.1 DCB testing

Healing efficiency values were calculated using Equation 3.18 and are reported in Table 7.2. As aforementioned, the efficiency was calculated as a recovery of initial stiffness. The values were found to be null after 1 or 5 days rest for *control* specimens, as expected. However, healing was also not observed for *healing* specimens and this was quite surprising, given the efficiency of the same healing system demonstrated by Neuser *et al.* for the neat resin [9]. An example of loading-unloading virgin and healed cycles for a specimen containing *healing* capsules with a healing time of 1 day is shown in Figure 7.9. No recovery of stiffness between the virgin and the healed cycle is observed. Also, the maximum load of the virgin cycle was not fully recovered during healing. A stick-slip behavior was observed during propagation in both virgin and healed cycles, consisting in several drops of load when the crack jumps ahead. Such behavior is commonly reported in literature for crack growth of woven FRP specimens [1, 169].

Several tests were then performed in order to understand the absence of healing in these FRP specimens. Towards verification that sufficient healing agent was available to fill the delamination volume, a rapid primary investigation step was performed. Given that the solvent-based system is able to heal only up to a certain crack gap size [9], this

Test	**Sample**	V_f **(vol%)**	**Healing efficiency (%)**	
			1 day	**5 days**
DCB	*Plain*	55.0 ± 0.010	-	-
	Healing	54.6 ± 0.015	-1.73 ± 1.75	1.89 ± 4.52
	Control	53.5 ± 0.013	-0.75 ± 1.70	-2.16 ± 1.04
	Neat	-	100.39 ± 10.28	-
	Joint	-	13.47 ± 13.12	11 ± 6.63
ENF	*Plain*	44.5 ± 0.010	-	-
	Healing	42.9 ± 0.008	10.70 ± 5.23	10.76 ± 1.94
	Control	43.8 ± 0.005	14.07 ± 3.08	12.79 ± 4.22

Table 7.2: Healing efficiencies (calculated as recovery of stiffness) of DCB and ENF tests, for *healing*, *control* and *neat* samples, after 1 or 5 days healing. Relative fibre volume fractions are also indicated.

consisted of a reduction in the crack size during healing by bringing the two crack faces of the *healing* specimens in closer contact thus minimising the damage volume. This was achieved by clamping two specimens at the crack locations, rather than only imposing the two faces in contact at the location of the loading blocks. However, efficiency values were calculated and no improvement was remarked.

Secondly, the healing capability of neat resin samples in the absence of reinforcing fibres was verified. The mechanical tests, only performed with 1 day healing time, showed full recovery of the initial slope (Table 7.2). This demonstrates the effectiveness of the healing system in the case of neat resin. Note that the healing agent (approximately 3 ml) was manually injected into the delamination area in order to reproduce an ideal case of full availability within the crack volume and validate the feasibility of healing. Figure 7.10 shows an example of force-displacement plot for the aforementioned sample. Although the healed peaked load was not fully recovered, the initial slope of the virgin sample was retrieved after healing. This positive result, in agreement with previous work on solvent capsule healing of neat epoxy resins [7, 9], suggested that the lack of healing could potentially result from the presence of reinforcing fibres within the material adjacent to the crack.

The *joint* specimens were then tested in Mode I. Healing efficiencies values were very scattered, from 4 to 35% after one day, and from 6 to 21% after 5 days, indicating that some healing could take place, but potential presence of porosity play a strong role. As summarised in Table 7.2, which refers only to the average healing efficiencies, the joint samples did not show healing as effectively as neat resin samples; however, they values were not null as for for *healing* and *control* samples.

In summary, the present findings demonstrate the absence of healing in the case of composite specimens. Conversely, efficiencies up to 100% were observed for neat resin and as high as 35% (in best cases) for joint composite specimens containing a resin-rich central layer. § 7.6 will investigate the causes of this behavior.

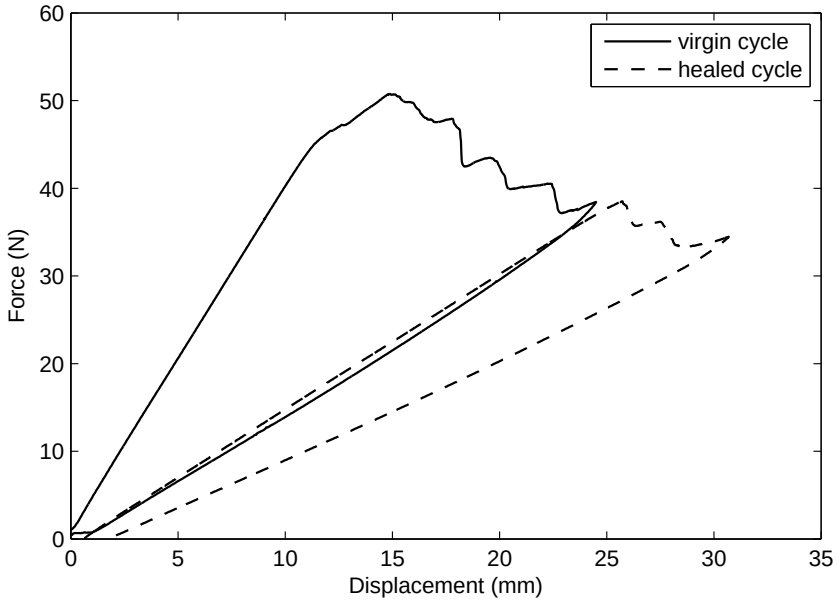

Figure 7.9: Typical DCB curves showing the loading-unloading cycles of virgin and healed composite specimens.

7.5.2 ENF testing

Healing efficiencies for samples tested in Mode II are also reported in Table 7.2. For both *healing* and *control* samples (at 1 and 5 days rest) efficiencies are higher than those obtained in DCB testing. A mechanism related to the type of testing for such samples must be responsible for the non-zero healing efficiency values. A possible explanation was found in the presence of capsules within the central ply of the specimen. After the *virgin* test, these capsules break and much debris are left on the crack plane, possibly inducing additional shear forces during the *healed* test and contributing to an increase in the energy necessary to propagate the crack. As a countercheck, it was observed that *plain* samples (without capsules) presented a null healing efficiency. In contrast with DCB testing, Mode II testing cannot be considered as an adequate technique for evaluating the intrinsic capability of samples to self-repair in the presence of embedded capsules. Indeed, the shear forces acting to propagate the crack depend on the presence of capsule debris remaining in the crack plane following the *virgin* test; thus the calculated healing efficiencies are not representative.

7.6 Post-testing investigations

7.6.1 Swelling properties of the matrix

As a result of the outcome for Mode I testing, consisting of poor healing efficiencies for the composite material but better healing properties for the neat resin, more specific

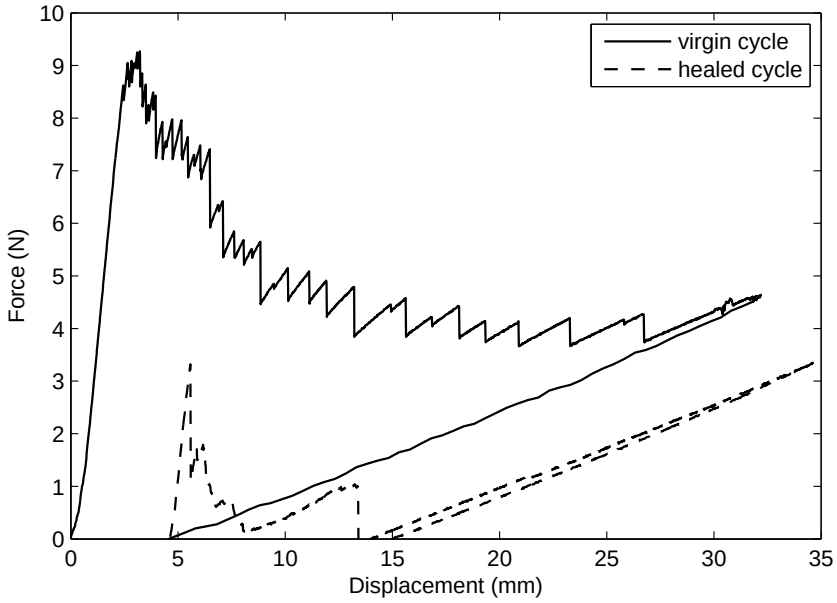

Figure 7.10: Typical DCB curves showing the loading-unloading cycles of virgin and healed neat resin specimens.

investigations were performed in order to evaluate the swelling of the material in the presence of EPA solvent. According to [9], swelling is directly related to the mass gain of the resin sample in solvent, as type II diffusion of the solvent was observed in the epoxy samples.

The results for mass gain of the composite are presented in Figure 7.11. At equal time of immersion in EPA, the fibre-reinforced samples showed a relative mass gain drastically lower, namely 5 to 20% (depending on the days of immersion) of the mass gain obtained for the neat resin samples. Similarly, low mass gains were observed by analysing the fibre-reinforced resin curve normalised to the matrix weight fraction. Thus, the presence of fibres on the sample surface significantly hinders solvent diffusion. This could be a potential explanation for the lack of healing and restoration of mechanical properties in composite materials.

As proposed by Neuser *et al.* [9], assuming a Case II diffusion with a square solvent concentration profile, the thickness of the solvated layer can be evaluated. Figure 7.12 shows the expected swelling thickness as a function of time. This is calculated by assuming the total mass gain and thus the change of volume are due to the solvent uptake, swelling is isotropic and the influence of the curvature of the cylindrical samples is negligible. From such a curve, considering a composite material, we can estimate that the maximal crack separation (double the swelling thickness indicated in the graph, assuming that both the crack faces equally swell) is equal to approximately only 6 μm after 1 day and does not increase after 5 days.

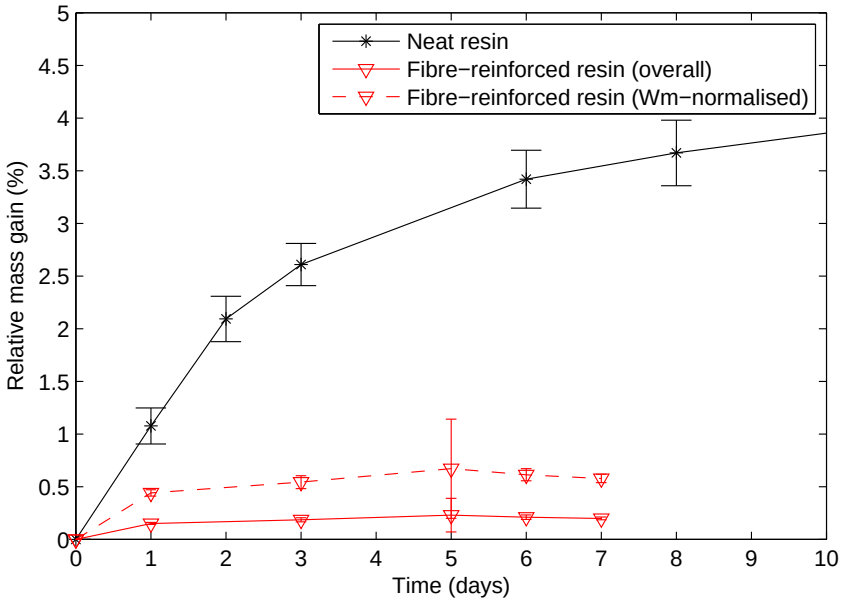

Figure 7.11: Evolution of relative mass gain of neat and reinforced epoxy cylinders immersed in EPA over time. The curve corresponding to the fibre-reinforced epoxy normalised with the matrix weight fraction is also reported.

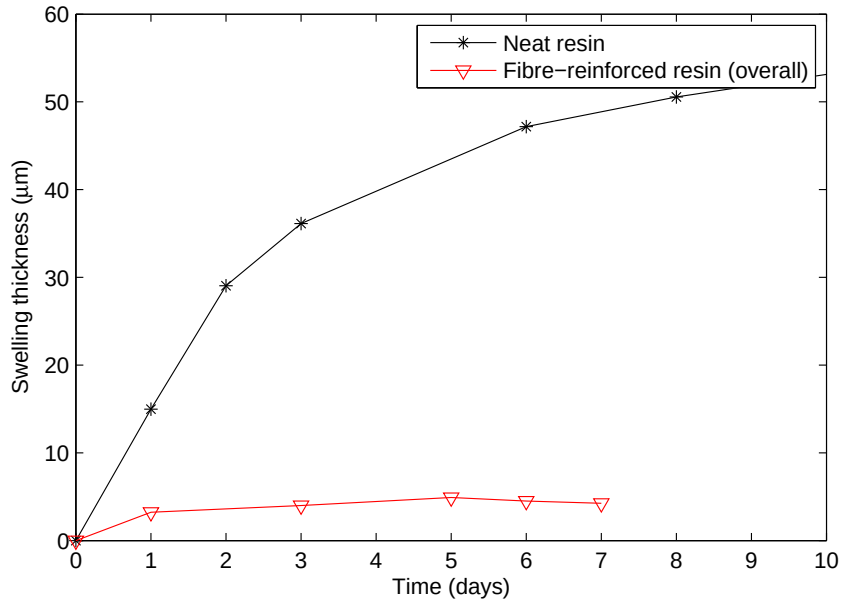

Figure 7.12: Evolution of swelling thickness of neat and reinforced epoxy cylinders immersed in EPA over time.

In order to verify that the presence of fibres was the only factor responsible for low swelling, the degree of polymerisation after curing, post-curing and 1 to 5 days dry ageing was also verified. These values were then compared with the results obtained for the neat resin [10], knowing that the matrix conversion can affect the swelling ability. As visible in Figure 7.13, it was found that the composite did not present degrees of poly-

merisation differing by more than 10% from the neat resin; consequently, varying degree of polymerisation was excluded as the cause of low swelling and healing.

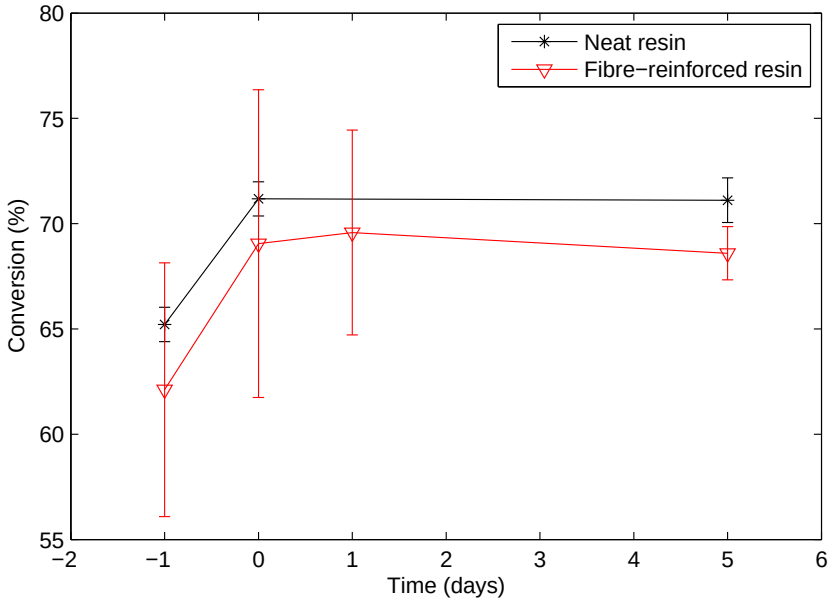

Figure 7.13: Evolution of the degree of polymerisation of neat and reinforced epoxy as a function of time. The conversions after 24 h curing and after 24 h post-curing are indicated with "-1 day" and "0 day", respectively. Samples were stored at 22°C with 20% relative humidity.

7.6.2 Fracture surface considerations

Fracture surface analysis of the tested specimens was also performed. A SEM image of the crack surface of a *plain* specimen superimposed with EDX analysis is shown in Figure 7.14.

This reveals the presence of calcium (green) and therefore allows us to distinguish the E-glass fibres (Ca-rich) from the polymer matrix. Overall, the surface ratio of matrix and fibres in the fracture plane is equal, indicating that failure is dominated by interfacial debonding between the fibres and the matrix. This mechanism of delamination between fibre bundles and their surrounding matrix has been observed previously in many cases [1, 170] for woven composites. Interfacial debonding rather than crack propagation within the intra-layer matrix is responsible for the low healing efficiencies observed, as the healing system used requires resin-rich crack faces to lead to appropriate swelling and subsequent healing.

Interfacial debonding is also observed in Figure 7.15, where the fracture surface of a *healing* specimen shows darker resin-rich zones as well as exposed fibres (brighter grey). Holes created in the resin by debonded capsules, mostly positioned within the interstices of the woven fabric, are also observed.

Observations at higher magnifications of the fracture plane (Figure 7.16) allowed the identification of four possible types of capsule rupture upon crack propagation: (1) the crack passes through the capsule breaking its shell, the healing agent is delivered and the capsule shell remains attached to the matrix; (2) the crack induces the rupture of the capsule and the delivering of the healing agent, but the capsule does not break in two parts as for case 1 (explaining the small plies observed on the fibre bundle); (3) the crack propagates at the capsule shell/matrix interface without breaking the capsules thus no healing agent is delivered. It is believed that this behavior was not the most common occurring during propagation, as visual observations during mechanical testing of the specimen showed liquid wetting the crack; (4) upon crack opening, the capsule debonds from the fibre and the matrix, and a hole is visible: Rupturing of these capsules is not certain, but can be expected based on the shear forces occurring in Mode II propagation and the crack closure when clamping the specimens.

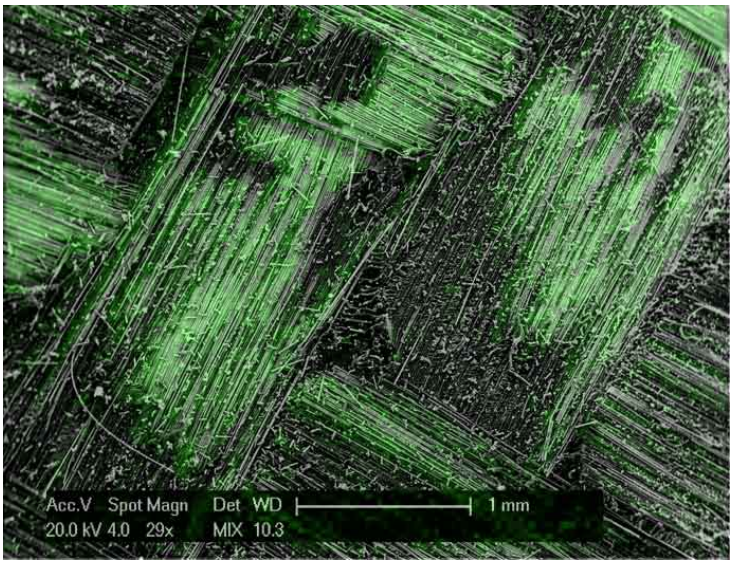

Figure 7.14: SEM image of the crack face of a *plain* specimen, superimposed with an EDX analysis which shows the presence of Calcium, *i.e.* E-glass fibres (green).

7.7 Summary

We have shown that glass fibre-reinforced epoxy plates, containing a solvent capsule-based healing system and fibre volume fractions of approximately 50 vol%, can be processed through Vacuum-assisted resin infusion molding. Particularly, the healing capsules were introduced in the composite via manual dispersion on one ply of the fabric preform prior to processing. Moreover, it was demonstrated that the vacuum pressure difference during infusion must be kept lower than 0.3 bar to avoid premature capsule breakage and that a suitable resin must be selected in terms of swelling properties and adapted viscosity. The introduction of 15 wt% of capsules within the "local" matrix of the central ply resulted

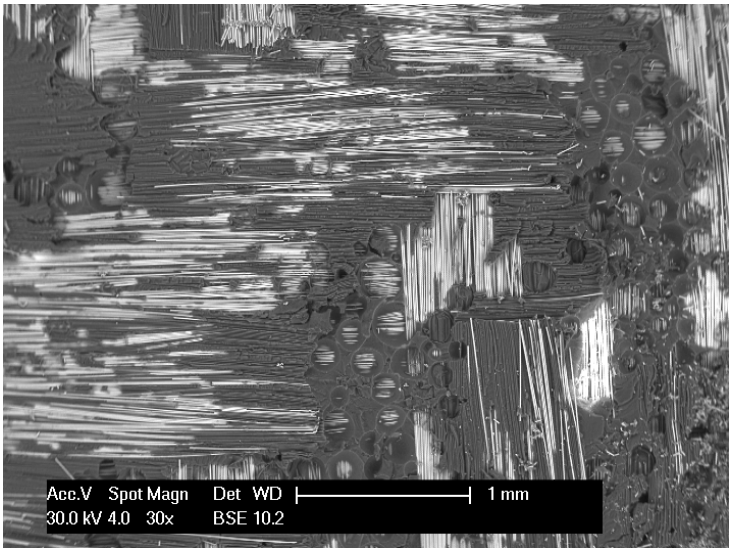

Figure 7.15: SEM image of the crack face of a *healing* specimen, showing traces of capsules and fibre bridging.

in decreased interlaminar fracture toughness in Mode I and Mode II (of approximately 25-30%) as compared to *plain* composites, but did not significantly affect the peak load. Mode II testing was shown to be inadequate for assessing the healing capability. Alternatively, Mode I testing allowed the calculation of healing efficiencies through evaluation of initial stiffness recovery. Healing was not observed for composite samples; however, efficiencies up to 100 and 35% were calculated for neat resin samples and *joint* samples, respectively. Further investigations revealed that the lack of healing could be attributed to two interdependent causes: (i) the lack of thick resin layers on the fracture surface, resulting from interfacial debonding (observed as the main fracture mechanism occurring during crack propagation), (ii) the poor swelling of the fibre-reinforced matrix in the presence of EPA, revealing a decrease of 80-95% compared to the neat resin. From the present findings, we conclude that a solvent capsule-based healing system is only suitable for repairing neat resins or fractures that occurred within the matrix rather than at the matrix/fibre interface, after static damage. Indeed, the presence of fibres hinders the main trigger of the healing phenomenon, solvent diffusion. In cases where interfacial debonding is the main failure mode and crack faces contain fibre-rich zones, other healing systems (*e.g.* DCPD/Grubbs' [1,2]) which are not based on the swelling capacity of the crack surfaces need to be selected. This may be necessary at the expense of the cost-effectiveness, toxicity and homogeneity in properties between virgin and healed material. Even in low fibre-volume fraction composites, if damage propagation occurs by interfacial failure, a solvent-based system is not appropriate. Conversely, the present solvent-based system could be applicable for self-healing of cracks presenting matrix-rich faces. Examples of this include cracks occurring within resin joints between composites and matrix microcracks in static or fatigue loading. Repair of resin-rich joints could reach that of pure resin

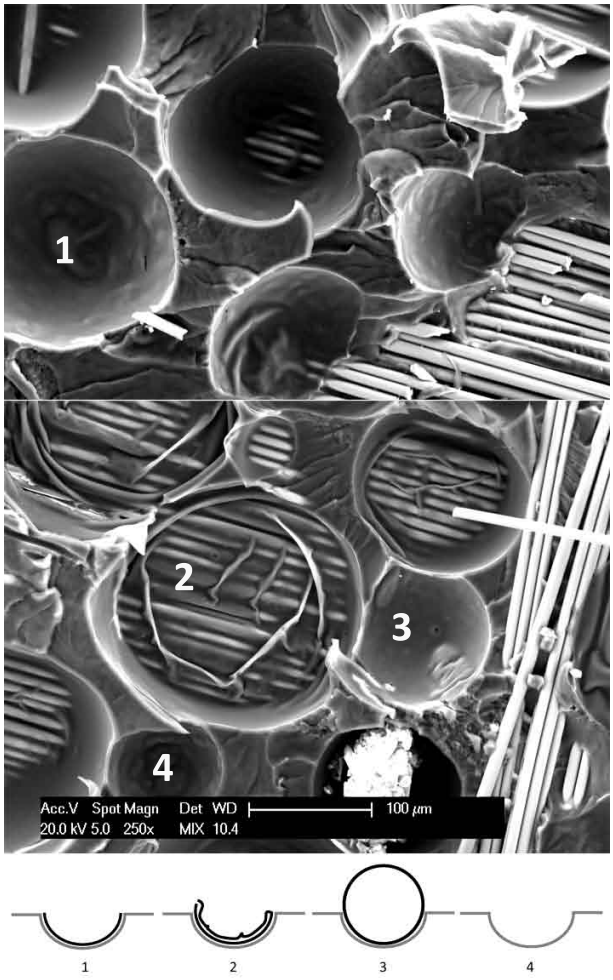

Figure 7.16: SEM image of the crack surface of a *healing* specimen, showing four different means of capsule rupture.

by tailoring microcapsule content. Alternatively, we expect that repair of matrix microcracks could occur where the crack thickness remains very low, for example in fatigue loading with resting periods under compression or in very low energy impacts, provided that interfacial failure is not the dominant damage mode.

Chapter 8

Perspectives on alternative healing routes

8.1 Critical investigation

The healing system used in this work presents two main features. First, it is capsule-based and offers several important advantages compared to tubular or vascular-based self-healing approaches, predominantly the rather reduced influence of the healing system on the V_f of the composite, as well as an easier introduction of the encapsulated agent into the material. Second, it relies on the presence of an encapsulated solvent, which diffuses through the material crack face. This is a clever concept, since it provides homogeneity between the repaired portion and the undamaged material without the need for a new, different monomer. In the case of plain epoxy specimens, the solvent is able to diffuse and swell the crack faces and cracks due to static loading can be repaired. Fatigue cracks can also be arrested owing to a reduction of the modulus at the crack tip, providing a crack blunting effect. However, we demonstrated that the presence of fibrous material (glass) on the crack plane significantly decreases the diffusion rate of the solvent molecules, prevents swelling and consequently healing cannot occur. This was confirmed for interlaminar static cracks only, although we believe that the healing phenomenon will be precluded for all other cases when interfacial failure is predominant, including fatigue cracks, although some crack blunting could still take place.

Other than demonstrating the inadequacy of this system for fibre-reinforced epoxies, this work has shown a viable route of preparation and processing which is applicable to many other capsule-based self-healing materials. Indeed, using standard textile reinforcements, a method to introduce any dispersed encapsulated material prior to processing was presented. The packing and permeability properties of such capsule-functionalised textiles were studied. Equivalent techniques can be used for other types of capsules and similar behavior could be expected. Furthermore, a reproducible processing technique

such as VARIM was adapted in order to be effective in the presence of capsules. Hence, the same manufacturing route can be proposed with other types of encapsulated (or particulate) material, with the aim of improving the healing efficiency. Some examples are indicated in what follows. An adequate selection among these solutions must also require a minimal reduction of the virgin properties due to the presence of the healing system.

Epoxy capsules The encapsulation of epoxy monomer is viable and the use of such capsules, embedded within an epoxy matrix, ensures the compatibility between the host and the repaired matrix. In the case of fibre-reinforced epoxies, such capsules can be introduced to functionalise the textiles prior to processing. Different approaches are proposed for triggering the monomer polymerisation:

- ▷ latent hardener functionalities could be present within the host matrix to react with the delivered epoxy monomer. However, these functionalities may react over time so are not suggested;

- ▷ encapsulated cross-linker can be dispersed onto textiles together with epoxy capsules prior to VARIM. This approach raises some additional issues: (i) the encapsulation of cross-linkers (such as amines) is problematic due to their reactivity and wide miscibility range, although some attempts of encapsulation were recently successful via microfluidics [171]; (ii) the epoxy/amine reaction is dictated by stoichiometry; thus, an adequate amount of capsules should be dispersed and ruptured by the propagating crack. Such a system was recently used by Neuser *et al.* [172] to restore fracture toughness in plain epoxies;

- ▷ catalyst particles can be dispersed onto textiles or within the matrix (if the matrix viscosity is not beyond the adequate range for infusion processes) prior to processing. The choice of a suitable catalyst which can initiate the polymerisation of epoxies is crucial. The recent work of Coope *et al.* [70, 71] can be referred to, with scandium(III) triflate as an available candidate. Such a catalyst, indeed, can react with epoxies such as DGEBA without any stoichiometric requirements and presents low cost and toxicity. An alternative catalyst dispersion which could also be proposed is found in the patented work of Skipor *et al.* [105]. Here, the catalyst is chemically attached to the outer shell of the monomer-filled capsule and can thus provide an in-situ polymerisation, provided the contact with the monomer is established;

- ▷ the co-encapsulation of monomer and cross-linker, provided that their reaction remains latent, could be a promising solution. Stoichiometry would be allowed and the intimate contact between the two reactants would be ensured. These two-component capsules could also be dispersed onto fabrics prior to processing.

All these solutions seem promising for the self-healing of delaminations in fibre-reinforced epoxies, including cases when the failure occurs at the fibre/matrix interface. In all cases, the amount of the epoxy monomer must be enough to fill the crack volume. Moreover, the availability of the (latent) cross-linker or catalyst on the crack plane is necessary, especially in the presence of reinforcing fibres, since the polymerisation of the epoxy monomer must occur *in situ* within the crack volume.

Other monomer capsules The incorporation of encapsulated monomers such as DCPD and ENB in the fibre-reinforced epoxy could also provide an effective healing, although the homogeneity between virgin and repaired material is not ensured. Considerations related to the epoxy capsules also apply to this approach. As yet, the choice of adequate catalysts for these monomers is required and was investigated in several studies (§ 2.2.2), trying to find solutions which were not toxic, not expensive and not stoichiometry-dependent. Single attempts using DCPD with expensive and toxic Grubbs' catalyst for fibre-reinforced matrices were performed by Kessler *et al.* [1,2]. This fully integrated system (*i.e.* both the catalyst and DCPD capsules are embedded in the matrix by pre-mixing with the epoxy matrix) led to promising efficiencies, especially in the case of "hot" healing (80°C). This can encourage new results, provided that a better and cheaper catalyst is used and a more reproducible processing (such as VARIM) is adopted.

Thermoplastic particles As mentioned in § 2, the use of low melting point thermoplastic particles embedded in thermoset matrices can be envisioned in order to provide healing. In the case of composite materials, thermoplastic particles would need to be mixed with the epoxy matrix or dispersed onto the fibre reinforcement prior to processing.The advantage of this approach is of being repeatable and latent, since the healing mechanism is inherent to the stable chemical structure of the polymer. A drawback consists however on some external activation such as heat or light required for triggering the repair [173]. The healing mechanism could be considered as belonging to the extrinsic category, since the particles are introduced as additives, but based on an intrinsic chain re-entanglement of the thermoplastic phase itself. Toughening could also be imparted if the thermoplastic particles induce crack bridging, pinning or a deflection of crack paths. Provided that the crack propagates through (or at the interface of) the thermoplastic particles, the healing mechanism upon heating would involve: (i) melting of the encapsulated thermoplastic phase, (ii) flow/reversibility of the melt and filling of the crack volume (also improved by the volume expansion of the thermoplastic upon melting, normally higher as compared to the epoxy resin), (iii) solidification of the thermoplastic phase upon cooling. Reversibility means two possible mechanisms:

1. chain re-entanglement of the thermoplastic material, based on the chain mobility which is thermically enhanced;

2. reversibility of non covalent (*e.g.* hydrogen or ionic) bonding in the thermoplastic clusters.

The use of such thermoplastic particles in thermoset resins is reported in the literature in several publications. Belonging to the second category (for which a schematic of the mechanism is given in Figure 8.1) as referred hereinabove, poly(ethylene-co-methacrylic acid) or EMAA has been widely used as the principal ionomeric copolymer for self-healing applications. This copolymer, indeed, is able to form clusters containing ionic segments that act as reversible cross-links being triggered by UV radiation or temperature.

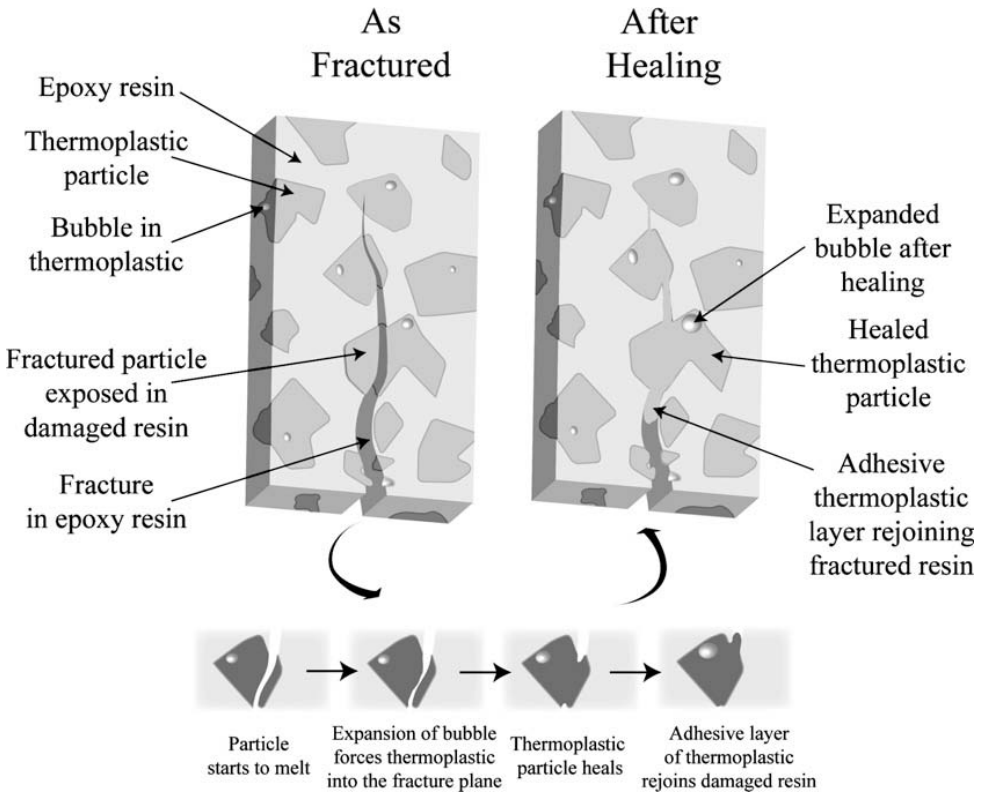

Figure 8.1: Schematic of the healing agent delivery mechanism in the presence of thermoplastic microparticles embedded in a thermoset material [174].

Meure *et al.* [174] transformed EMAA pellets into microparticles by cryogenic grinding and further mixed the particles to epoxy resin (DGEBA) heated at 70°C, prior to the addition of the hardener. The healing mechanism was assessed through testing using SENB and TDCB geometries and a recovery of fracture toughness of approximately 80% was shown. The healing cycle consisted of 30 minutes at 150°C. The same authors also showed that changes in the surface chemistry of EMAA subsequent to DGEBA and hardener adsorption revealed the likely formation of hydrogen bonds and ionic bonds respectively during the curing process. Moreover, the higher temperatures used during post-curing and healing also promoted the formation of covalent bonds as a result of acid-oxirane/acid-hydroxyl reaction that can be expected to contribute significantly to the interfacial strength [175]. EMAA under the form of microparticles were also inserted

into FRPs, namely carbon woven fabric epoxies, by Pingkarawat *et al.* [176] The composite material was manufactured by hand lay-up with 10 wt% EMAA microparticles. The healing cycle consisted of 20 minutes at 150°C and the efficiency was quantified through DCB testing. The influence of the EMAA microparticle presence on the virgin mechanical properties was also investigated and an improvement of fracture toughness of 63% was found, due to toughening mechanisms.

Besides EMAA, other thermoplastic materials such as ethyl vinyl acetate (EVA), poly(ethylene-co-glycidyl) methacrylate (PEGMA), poly(ethylene-co-methacrylic acid) (EMAA), acrylonitrile butadiene styrene (ABS), maleated styrene ethylene butadiene copolymer (SEBS) and poly(vinyl butyral) (PVB) were also explored as alternative copolymers [173].

Belonging to the first category, poly(caprolactone) or PCL is an example of thermoplastic material with a high volume expansion coefficient and able to provide chain re-entanglement upon heating, thus becoming a good candidate for healing purposes. No literature studies presented the use of PCL microparticles embedded in epoxy resin, although it is herein believed that such a morphology could also provide effective healing.

8.2 Preliminary study (thermoplastic particles)

An experimental attempt was performed during the last months of the present thesis for exploring the possibility to improve healing with the use of thermoplastic particles.

Polycaprolactone (PCL) was purchased by Sigma Aldrich, with a molecular weight of 42500 g/mol and a cost of 122 CHF per 100 g. It is presented under the form of pellets, with the characteristic temperatures as indicated in Table 8.1 and a viscosity dependence as presented in Figure 8.2.

T_g **(°C)**	-91.4 ± 0.49
T_c **(°C)**	21 ± 0.56
Crystallisation enthalpy (J/g)	66.3 ± 1.24
T_m **(°C)**	62.85 ± 1.48
Melting enthalpy (J/g)	93.7 ± 0.93

Table 8.1: Characteristic temperatures of PCL pellets as purchased, measured by DSC (cooling/heating/cooling ramp from room temperature to -150°C, then to 120°C, then to 0°C was performed at 10°C/min under nitrogen).

In order to produce self-healing FRPs based on the addition of a thermoplastic additive under the form of microparticles, intended to work similarly to the solvent microcapsules healing, PCL microparticles had to be produced. Since PCL was purchased under the form of pellets, a procedure based on [177, 178] was followed in order to transform them to particles with diameters of 125-250 μm. First, 300 mg of PCL pellets were dissolved

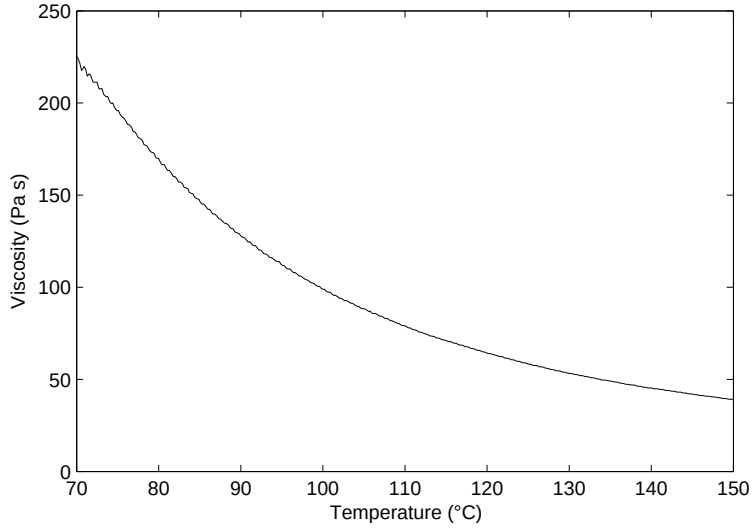

Figure 8.2: Viscosity of PCL (as purchased) as a function of the temperature. The measurement was obtained with AR 2000 ex (TA instruments) rheometer with a standard Smart SwapTM Peltier plate for the temperature control. The test procedure consisted in a continuous flow-mode temperature ramp lasting 30 min between 70 and 150°C, at a constant shear rate of 10 1/s. The Newtonian behaviour was also previously checked.

into 3 ml of dichloromethane (DCM, Sigma Aldrich) using a magnetic stirrer. The solution was then added to 40 ml of a 1% wt/v PVA aqueous solution (Sigma Aldrich) and stirred at 1300 rpm for 4 h, until the DCM is evaporated. In order to limit foaming, a few drops of octanol were added during stirring. The obtained particles were washed with distilled water and left to dry for 24 h, then sieved to retain the 125-250 μm size fraction. Figure 8.3 shows the aspect of PCL microparticles as obtained with the procedure aforementioned. The size fraction 125-250 μm was analysed. The number-length average diameter calculated for the present fraction was 206.73 ± 32 μm, which agrees with what expected by stirring at 1300 rpm and fits with our purposes.

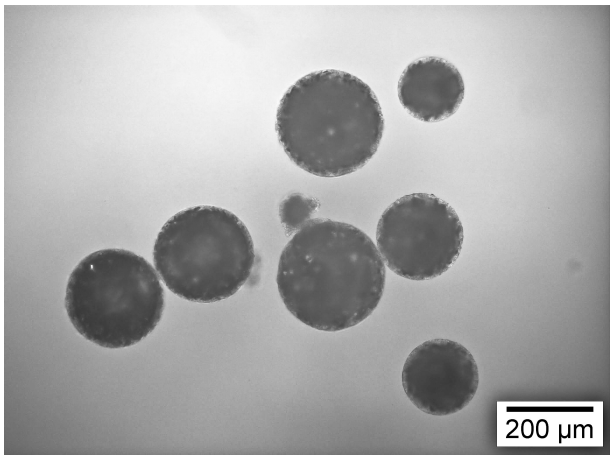

Figure 8.3: Optical microscopy image of PCL microparticles belonging to the 125-250 μm size fraction.

Moreover, it was confirmed that the procedure for transforming PCL pellets into microparticles does not significantly affect the characteristic temperatures (T_g, T_m and T_c) and the thermal behaviour, as shown in Figure 8.4.

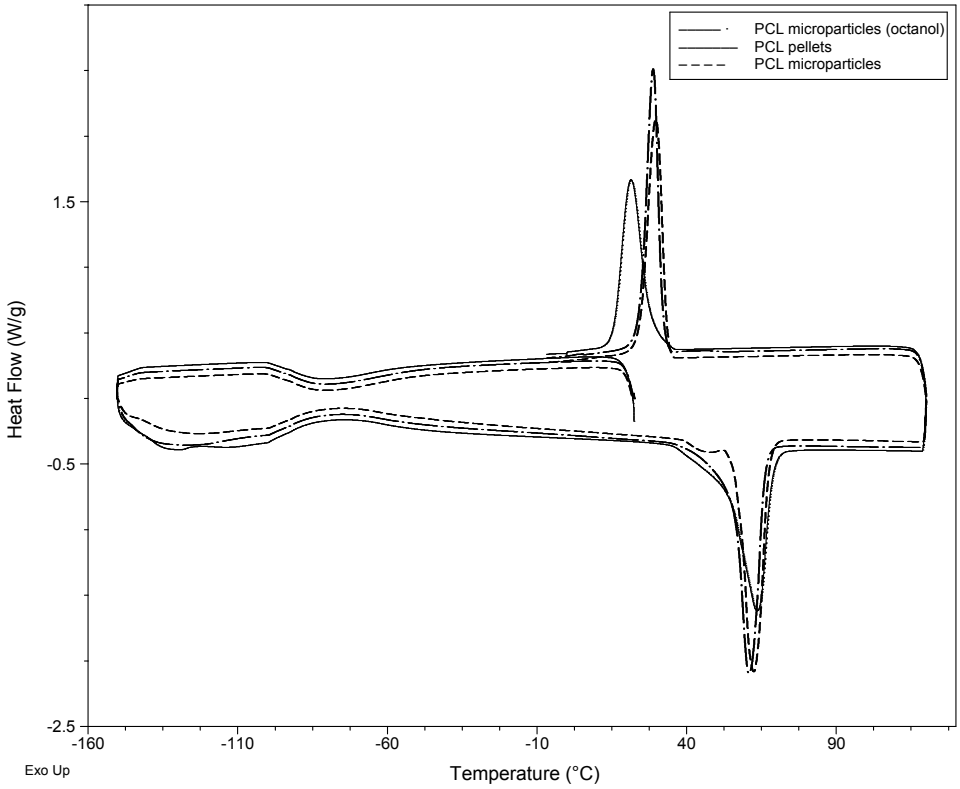

Figure 8.4: DSC curves for PCL pellets as received from the manufacturer and PCL microparticles as obtained with the indicated procedure (with and without the addition of octanol).

The procedure to introduce the thermoplastic particles into the composite followed the one developed for the introduction of solvent capsules. We refer to § 3.8.3 for detailed indication of the procedure. Namely, thermoplastic particles were dispersed by manual sieving onto fabric textiles prior to processing and then functionalised stack of textiles were impregnated with epoxy. Manufacturing of composite samples was performed by VARIM and three types of composite plates were processed, varying the loading of PCL particles, namely 0, 15 and 30 wt%, considering the ply matrix. A target fibre volume fraction V_f of 50 vol% and a final plate thickness of 5 mm were sought. The vacuum pressure difference was kept this time at 0.9-1 bar during the whole processing time, since there was no risk that the healing agent could be damaged. The plates underwent a curing treatment of 24 h at 25°C and post-curing of 24 h at 45°C, for achieving full conversion.

Testing also followed equivalent procedures (§ 3.8.4). The influence of the presence of the PCL microparticles on the mechanical properties of the virgin material was evaluated first, prior to any healing test. This was assessed through DCB tests analogously to

solvent capsule-based systems (§ 3.8.4). Figure 8.5 shows the results for plain and PCL microparticle-loaded composites, in terms of V_f-normalised maximum load and interlaminar fracture toughness in Mode I. In terms of V_f-normalised max load, the presence of PCL microparticles does not have a significant effect. However, the interlaminar fracture toughness presents a drastic decrease for 30 wt% of PCL microparticles, as compared with 0 and 15 wt%. This might indicate weak bonding between the continuous phase and PCL particulate phase, which translated in easy paths where the crack could propagate with the absence of the aforementioned toughening mechanisms.

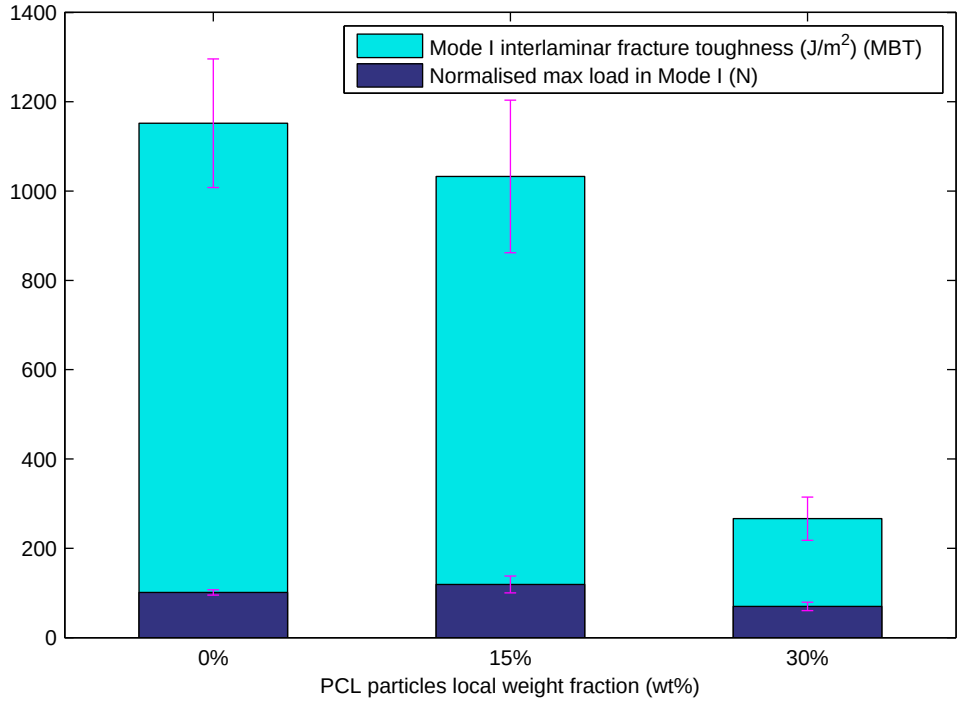

Figure 8.5: Normalised maximum load and Mode I interlaminar fracture toughness, as a function of the "local" PCL microparticle weight fraction.

Healing performance was then assessed. The healing stage consisted of a thermal treatment of 30 min at 80°C. Samples were left unloaded during healing, with only the crack faces imposed to be in contact at the location of the loading blocks (this induced a reduction in the crack thickness, but no clamping at the crack location was applied). An example of typical load-displacement curves obtained for PCL microparticles-loaded FRPs is shown in Figure 8.6, for the virgin and after healing condition.

From such curves, healing efficiencies in terms of slope and max load were calculated and are reported in Table 8.2.

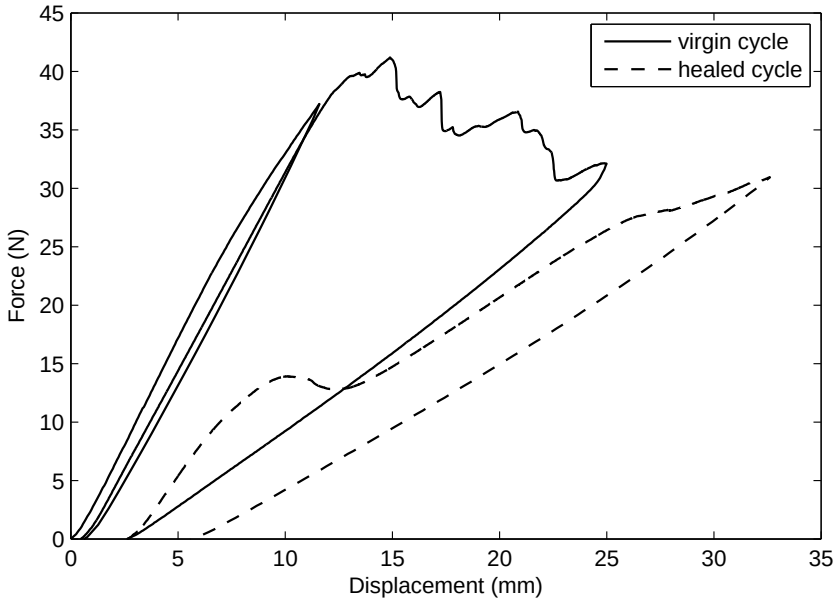

Figure 8.6: Typical load-displacement curve for PCL microparticles-loaded FRPs, tested in the virgin and healed conditions.

PCL microparticles "local" fraction (wt%)	**Healing efficiency (slope-based) (%)**	**Healing efficiency (max load-based) (%)**
15	30 ± 19	25 ± 7
30	34 ± 18	13 ± 4

Table 8.2: Healing efficiencies for 15 and 30 wt% loadings of PCL microparticles in the FRPs.

Efficiencies in terms of interlaminar fracture toughness are missing, since the crack propagation could not be determined for the healed sample. The obtained values of efficiency were low for both 15 and 30 wt% PCL microparticles, both in terms of slope and maximum load. This let us conclude that the scarce coverage of the fracture plane with PCL microparticles and/or poor interface bonding between microparticles and surrounding matrix were responsible for low healing efficiencies. SEM imaging confirmed this hypothesis, as visible in Figure 8.7, which represents a crack face after testing, healing and further testing. However, since efficiencies were not null, promising paths can be suggested for new experiments using these type of particles as repair agents. Moreover, the results can be intended as a demonstration that the same preparation and processing procedures can be successfully applied to another type of embedded particulate material and crack repair at some extent can be provided since the healing mechanism is compatible with the presence of reinforcing fibres.

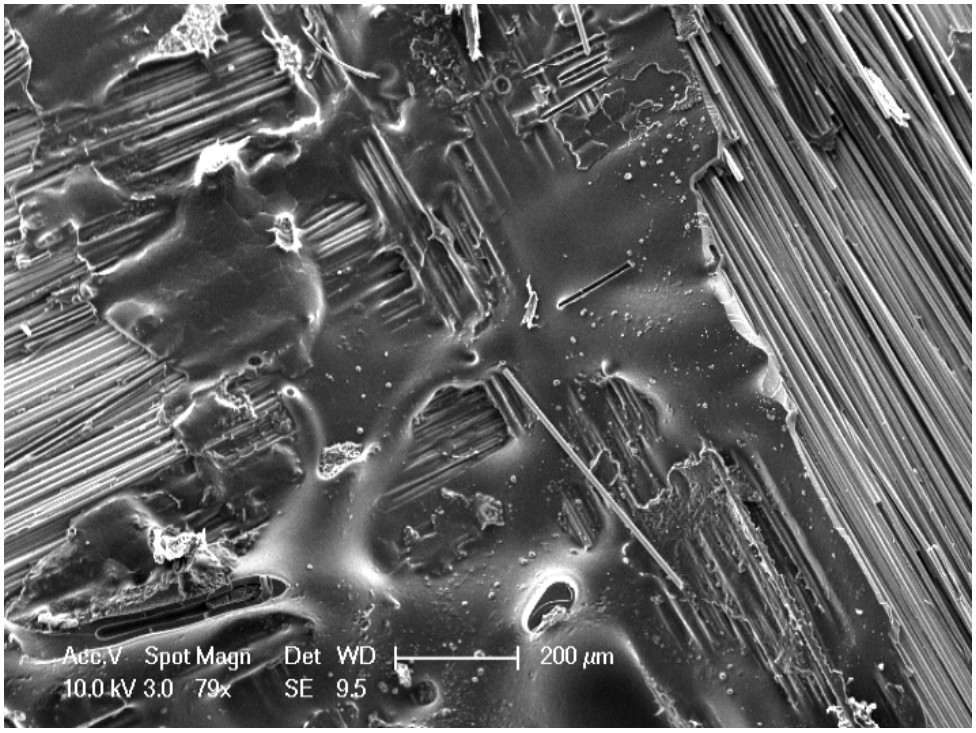

Figure 8.7: SEM image of the crack face of a sample containing 30 wt% PCL particles over the ply matrix. Prior to imaging, the sample has been tested, healed and re-tested.

8.3 Summary

This chapter summarised potential alternative healing approaches which could solve the main issue observed for the solvent capsule-based system (*i.e.* the lack of efficacy in the presence of reinforcing fibres on the crack plane). Healing solutions which could be integrated within the composite material using equivalent manufacturing routes as those developed in the present work were suggested, namely based on epoxy or other monomer capsules and thermoplastic particles. The application of one among these solutions (*i.e.* polycaprolactone particles) was also reported as a "proof of concept", although further investigations are needed and can be conceived as future work.

Chapter 9

Conclusions & outlook

The main objective of the present work consisted of the production of a woven fibre-reinforced thermoset containing an extrinsic capsule-based healing system and the subsequent study of its healing properties. Specifically, a solvent capsule healing system was selected for the repair of interlaminar damage: such a healing system was intended to serve as a model system, which is equivalent to and could be substituted with other particle-based healing approaches. Indeed, capsules or particles can be introduced in structural fibre-reinforced materials for healing or other purposes. Woven glass fabrics were chosen as standard reinforcements with a surface morphology on which capsules could be integrated. The integration of capsule-based healing system into composites, the adaptation of standard processing techniques in the presence of the healing system and the achievement of significant healing properties are still great challenges in the field of self-healing materials.

The work took place in 4 stages, namely (i) the production and characterisation of solvent-filled core/shell capsules, (ii) the integration of such capsules into the composite prior to processing and the study of packing and permeability properties, (iii) the manufacturing of the composites and the assessment of their self-healing properties using different testing approaches and (iv) a critical assessment of alternative healing routes suitable for fibre-reinforced epoxies. Several goals were achieved and the main conclusions for each of these investigations are given below.

The production of 125-250 μm solvent-filled microcapsules by the (already established) oil-in-water emulsion technique enabled tuning of the capsule diameter by setting a specific stirring rate. Capsules with different core material (EPA, HA) and mono- or double-wall shells (pure-UF, UF-PU) were obtained by using the same technique with slight variations of the procedure.

It was verified that the capsule core does not influence the capsule thermal behavior; however, it relates to the temperature at which the mass loss is located, which is associated to the boiling point of the core material.

Double-wall shells provided the capsules with an undoubtedly higher thermal stability,

independent of their core, making them suitable for higher temperature applications. Double-wall shells also presented a 4-6 times higher thickness compared to pure-UF shells, which scales with the capsule diameter until a saturation value. Double-wall shells resulted in a lower modulus, but higher burst forces and elongation at break, making them more appropriate for use in the presence of harsh processing conditions. For our purposes, mono-wall capsules were selected as suitable, since the maximum temperature which is attained during curing and post-curing did not exceed 35-40°C and mild processing conditions could be adopted.

A protocol was proposed concerning the integration of the healing system into the composite, consisting of the manual dispersion of capsules onto the reinforcement textiles by hand sieving prior to processing. This methodology was validated as effective at least at a laboratory scale, seeing as an acceptable degree of capsule distribution was achievable. Some progress can be envisioned through adaptation of this technique to more industrial scales, requiring, for instance, automated capsule production and dispersion onto fabrics. Moreover, 125-250 μm revealed as an appropriate capsule size fraction for manufacturing capsule-based self-healing FRPs with a standard woven reinforcement, since capsules could geometrically fit the interstices of the selected fabric. However, depending on the capsule volume fraction, an increase of the stack thickness and a change in the compressibility and permeability properties were expected and further confirmed. More specifically, the packing and longitudinal permeability behavior of a fabric reinforcement stack were found to be affected by the presence of functionalising capsules. These findings suggested that an adaptation of the manufacturing parameters is strongly suggested in order to avoid premature capsule rupture and maintain adequate impregnation kinetics.

Finally, for the manufacturing of the capsule-containing composites, a vacuum infusion-based technique was applied, rather than longer and less reproducible wet lay-up approaches. Due to the presence of capsules, the technique required tuning in terms of lay-out and vacuum pressure difference. Industrially relevant fibre volume fractions of approximately 50 vol% were achieved. We believe this is important progress in terms of how any capsule-based self-healing composite can be manufactured with reproducible features.

The key result of the healing assessment demonstrated that no healing (1-2%) was observed for Mode I interlaminar cracks of composite samples. This lack of healing was attributed to two interdependent reasons: (i) the lack of thick resin layers on the fracture surface, due to interfacial debonding observed as the main fracture mechanism occurring during crack propagation, (ii) a poor swelling capability of the fibre-reinforced matrix in the presence of EPA, lowered by 80-95% compared to the neat resin. As a countercheck, efficiencies up to 100% and 30% were calculated for samples made of unreinforced epoxy resin and resin-rich joints between composites, respectively.

Alternative healing assessments for interlaminar cracks propagated in Mode II and

due to low energy impacts were also carried out, but did not seem suitable tests for an appropriate evaluation of the healing performance.

We concluded that a solvent capsule-based healing system is only suitable for repairing, after static damage, neat resins or fractures that occurred within the matrix rather than at the matrix/fibre interface. It is worth mentioning that interfacial cracks likely also occur in low fibre-volume fraction composites as the crack propagation at the matrix/fibre interface is preferential. Further investigations can be contemplated for the effectiveness of the present solvent-based system for the repair of cracks presenting matrix-rich faces, such as cracks occurring within resin joints between composites and matrix microcracks in static or fatigue loading.

In cases where interfacial debonding is the main failure mode and the crack faces contain fibre-rich zones, other healing systems must be proposed. A literature review indicated epoxy or other monomer capsule-based systems as promising approaches, since they are not based on the swelling capacity of the crack surfaces. Also, a preliminary experimental study showed that thermoplastic particles can also be effective healing agents compatible with the presence of fibres. These healing systems could potentially be integrated into the composites by following guidelines equivalent to those given here for solvent capsules.

A main outcome of the present work is the proof that a healing approach demonstrating a sufficient efficiency for neat polymers does not directly translate into an efficient healing of matrix cracks in fibre-reinforced polymers. Several key factors arise and need to be solved: these mainly include the method of integration of the healing system, the choice and adaptation of the manufacturing technique, the influence of the healing system on a variety of material properties, the choice of a suitable test to quantify healing. Using an equivalent healing concept, the solutions to answer the composite related issues may differ from those optimised for the healing of neat polymer. Even more importantly, the effectiveness of the healing system for neat polymers can be totally compromised in the presence of fibre reinforcement and an alternative approach must then be considered. In general, a successful healing approach for composites should address theses issues from the beginning, and still represents a (partially, at least) unsolved problem. As a result, the selection of a suitable healing concept for composites requires to address a certain number of trade-offs: (i) should we opt for an industrially relevant processing and fibre volume fraction (as the one herein proposed, which is at least suitable for small series) or for more complex and cumbersome manufacturing steps that would significantly lengthen the cycle times (as for some microvascular systems, which require to imprint the vascules and remove them after processing, then to inject a liquid through a pumping system)? This may require performing trade-off cost and cycle time analysis versus the potential gain in maintenance and safety of the final part. (ii) Should we opt for an extrinsic or intrinsic system? Intrinsic systems seem to be preferable, but they may entail a more

difficult process route if the matrix viscosity is too high, and more importantly they may lead to composites with very different properties, as they are in general much less stiff. Also, adhesion to the fibres needs to be checked. If an extrinsic system is selected, as in the present case, the one-component approach based on solvent healing is not appropriate except in very specific cases, so a two-component healing approach seems preferable. However, in that case, an adapted system for hardener/catalyst is needed, and this is still a topic of intense research. (iii) Are we ready to accept that healing is triggered by an external factor like temperature, pressure or light? This may seem complex, but potentially less than having a reservoir of healing agent ready to be pumped to the crack, which also will require some external actuation. (iv) Should we restrict the crack gap to heal to a micro-crack thickness, such as encountered in fatigue, or should we opt for a healing concept involving significant volume expansion to fill the gap? Or should we devise systems to assist crack closure, such as shape memory alloy (SMA) or shape memory polymer (SMP) wires? This is also the subject of intense research in the self-healing community. Many questions remain, although we hope this work contributed to elucidate some critical hurdles towards effective healing properties for fibre-reinforced polymers.

List of Figures

List of Tables

Bibliography

[1] Kessler M. R., White S. R., Self-activated healing of delamination damage in woven composites. *Composites Part A: Applied Science and Manufacturing,* 2001, 32, 683-699.

[2] Kessler M. R., Sottos N. R., White S. R., Self-healing structural composite materials. *Composites Part A: Applied Science and Manufacturing,* 2003, 34, 743-753.

[3] White S. R., Sottos N. R., Geubelle P. H., Moore J. S., Kessler M. R., Sriram S. R., Brown E. N., Viswanathan S., Autonomic healing of polymer composites. *Nature,* 2001, 409, 794-797.

[4] Dry C. M., Sottos N. R., Passive smart self-repair in polymer matrix composite materials. *Proceedings of SPIE*, 1993, Albuquerque.

[5] Chen X., Dam M. A., Ono K., Mal A., Shen H., Nutt S. R., Sheran K., Wudl F., A thermally re-mendable cross-linked polymeric material. *Science*, 2002, 295, 1698-1702.

[6] Caruso M. M., Delafuente D. A., Ho V., Sottos N. R., Moore J. S., White S. R., Solvent-promoted self-healing epoxy materials. *Macromolecules,* 2007, 40, 8830-8832.

[7] Caruso M. M., Blaiszik B. J., White S. R.; Sottos, N. R.; Moore, J. S., Full recovery of fracture toughness using a nontoxic solvent-based self-healing system. *Advanced Functional Materials,* 2008, 18, 1898-1904.

[8] Blaiszik B. J., Caruso M. M., McIlroy D. A., Moore J. S., White S. R., Sottos N. R., Microcapsules filled with reactive solutions for self-healing materials. *Polymer,* 2009, 50, 990-997.

[9] Neuser S., Michaud V., White S. R., Improving solvent-based self-healing materials through shape memory alloys. *Polymer,* 2012, 53, 370-378.

[10] Neuser, S., Michaud, V., Effect of aging on the performance of solvent-based self-healing materials. *Polymer Chemistry*, 2013, 4, 4993-4999.

[11] Jones A. R., Blaiszik B. J., White S. R., Sottos N. R., Full recovery of fiber/matrix interfacial bond strength using a microencapsulated solvent-based healing system. *Composites Science and Technology*, 2013, 79, 1-7.

[12] Neuser, S., Michaud, V., Fatigue response of solvent-based self-healing smart materials. *Experimental Mechanics,* 2014, 54, 293-304.

[13] Neuser S., Manfredi E., Michaud V., Characterisation of solvent-filled polyurethane/urea-formaldehyde core-shell composites. *Materials Chemistry and Physics*, 2014, 143, 1018-1025.

[14] Neuser S., Tailored capsule based self-healing for epoxy matrix composites, Institut de Materiaux, PhD thesis, Ecole Polytechnique Fédérale de Lausanne, 2013.

[15] Laffan M. J., Pinho S. T., Robinson P., McMillan A. J., Translaminar fracture toughness testing of composites: A review. *Polymer Test*ing, 2012, 31, 481–489.

[16] Broutman L. J., Measurement of the fibre-polymer matrix interfacial strength. *ASTM STP,* 452, 1969, vol. Interface in Composites, 27-41.

[17] Goan J. C. and Prosen S. P., Interfacial bonding in graphite fibre-resin composites. *ASTM STP,* 452, 1969, vol. Interface in Composites, 3-26.

[18] Paul J. T. and Thompson J. B., The importance of voids in the filament wound structure. *Proceedings of SPI Technical Conference*, 20th Anniversary, 1965, Chicago.

[19] Chamis C. C., Hanson M. P., Serafini T. T., Criteria for selecting resin matrices for improved composite strength. *Proceedings of the Annual Conference on Reinforced plastics - Ever new,* 28th, 1973, Washington D.C.

[20] O'Brien T. K., Interlaminar fracture toughness: the long and winding road to standardisation. *Composites Part B: Engineering.*, 1998, 29, 57-62.

[21] Sela N., Ishai O., Interlaminar fracture toughness and toughening of laminated composite materials: a review. *Composites*, 1989, 20, 423-435.

[22] Mckenna G. B., Interlaminar effects in fibre- reinforced plastics-A review. *Polymer-plastics technology and engineering,* 1975, 5, 37-41.

[23] Nairn J. A., Matrix microcracking in composites. In *Comprehensive composite materials*, A. Kelly and C. Zweben, ed. Pergamon (Oxford), 2000, 403-432.

[24] Jose S., Ramesh Kumar R., Jana M. K., Venkateswara Rao G., Intralaminar fracture toughness of a cross-ply laminate and its constituent sub-laminates. *Composites Science and Technology*, 2001, 61, 1115–1122.

[25] Hitchen S. A., Kemp R. M. J., The effect of stacking sequence on impact damage in a carbon fibre/epoxy composite. *Composites,* 1995, 26, 207-214.

[26] Heslehurst R. B., Analysis and modeling of damage and repair of composite materials in aerospace. In *Numerical analysis and modeling of composite materials*, J. W. Bull, ed. Blackie Academic & Professional (London), 1996, 27-59.

[27] Nairn J. A., Hu S., Bark J. S., A critical evaluation of theories for predicting microcracking in composite laminates. *Journal of Materials Science*, 1993, 28, 5099-5111.

[28] Yip H. W. C., Shortall J. B., The interfacial bond strength in glass fibre-polyester resin composite systems Part 2. The effect of surface treatment. *The Journal of Adhesion,* 1976, 8, 155-169.

[29] Hughes J. D. H., The carbon fibre/epoxy interface–A review. *Composites Science and Technology,* 1991, 41, 13-45.

[30] Badini C., In *Materiali compositi per l'ingegneria*. C. Badini, ed. Celid (Torino), 2003.

[31] Foreman C., Nondestructive detection and characterisation of damages in honeycomb composite structures. PhD thesis, 2008, Iowa State University.

[32] Byun J.-H., Chou T.-W., Three-dimensional textile composites. A review. Use of composite materials in transportation systems. *American Society of Mechanical Engineers, Applied Mechanics Division*, 1991, 129, 47–55.

[33] Verpoest I., Wevers M., De Meester P., 2.5d-fabrics and 3d-fabrics for delamination resistant composite laminates and sandwich structures. *Sampe Journal,* 1989, 25, 51–56.

[34] Mouritz A. P., Bannister M. K., Falzon P. J., Leong K. H., Review of applications for advanced threedimensional fibre textile composites. *Composites Part A: Applied Science and Manufacturing,* 1999, 30, 1445–1461.

[35] Desplentere F., Lomov S. V., Woerdeman D. L., Verpoest I., Wevers M., Bogdanovich A., Micro-CT characterization of variability in 3D textile architecture. *Composites Science and Technology*, 2005, 65, 1920-1930.

[36] Yuan Y. C., Self-healing in polymers and polymer composites. Concepts, realisation and outlook: A review. *Express Polymer Letters,* 2008, 2(4), 238-250.

[37] Blaiszik B. J., Kramer S. L. B., Olugebefola S. C., Moore J. S., Sottos N. R., White S. R., Self-healing polymers and composites. *Annual Review of Materials Research,* 2010, 40, 179-211.

[38] Bergman S. D., Wudl F., Mendable polymers. *Journal of Materials Chemistry,* 2008, 18, 41-62.

[39] Dry C. M., Procedures developed for self-repair of polymer matrix composite materials. *Composite Structures*, 1996, 35, 263-269.

[40] Motuku M., Vaidya U. K., Janowski G. M., Parametric studies on self-repairing approaches for resin infused composites subject to low velocity impact. *Smart Materials and Structures*, 1999, 8, 623-638.

[41] Bleay S. M., Loader C. B., Hawyes V. J., Humberstone L., Curtis P. T., A smart repair system for polymer matrix composites. *Composites Part A: Applied Science and Manufacturing*, 2001, 32, 1767-1776.

[42] Pang J. W. C., Bond I. P., "Bleeding composites": damage detection and self-repair using a biomimetic approach, *Composites Part A: Applied Science and Manufacturing*, 2005, 36, 183-188.

[43] Pang J. W. C., Bond I. P., A hollow fibre-reinforced polymer composite encompassing self-healing and enhanced damage visibility. *Composites Science and Technology*, 2005, 65, 1791-1799.

[44] Trask R., Bond I., Biomimetic self-healing of advanced composite structures using hollow glass fibres. *Smart Material and Structures*, 2006, 15, 704-710.

[45] Trask R. S., Williams G. J., Bond I. P., Bioinspired self-healing of advanced composite structures using hollow glass fibres. *Journal of the Royal Society Interface*, 2007, 4, 363-371.

[46] Williams G. J., Trask R. S., Bond I. P., A self-healing carbon fibre-reinforced polymer for aerospace applications. *Composites A*, 2007, 38, 1525-1532.

[47] Williams G. J., Bond I. P., Trask R. S., Compression after impact assessment of self-healing CFRPs. *Composites Part A: Applied Science and Manufacturing*, 2009, 40, 1399-1406.

[48] Toohey K. S., Sottos N. R., Lewis J. A., Moore J. S., White S. R., Self-healing materials with microvascular networks. *Nature Materials*, 2007, 6, 581-585.

[49] Toohey K. S., Hansen C. J., Lewis J. A., White S. R., Sottos N. R., Delivery of two-part self-healing chemistry via microvascular networks. *Advanced Functional Materials*, 2009, 19, 1399-1405.

[50] Williams G. J., Trask R. S., Bond I. P., Self-healing composites and sandwich structures. *Smart Materials and Structures*, 2007, 16, 1198–1207.

[51] Williams G. J., Trask R. S., Bond I. P., Self-healing sandwich panels: restoration of compressive strength after impact. *Composites Science and Technology*, 2008, 68, 3171-3177.

[52] Patrick J. F., Sottos N. R., White S. R., Microvascular based self-healing polymeric foam. *Polymer*, 2012, 53, 4231-4240.

[53] Hamilton A. R., Sottos N. R., White S. R., Pressurized vascular systems for self-healing materials. *Journal of the Royal Society Interface*, 2012, 9, 1020-1028.

[54] Esser-Kahn A. P., Thakre P. R., Dong H., Patrick J. F., Vlasko-Vlasov V. K., Sottos N. R., Moore J. S., White S. R., Three-dimensional microvascular ber-reinforced composites. *Advanced Materials*, 2011, 23, 3654-3658.

[55] Cho S. H., Andersson H. M., White S. R., Sottos N. R., Braun P. V., Polydimethylsiloxane-based self-healing materials. *Advanced Materials*, 2006, 18, 997-1000.

[56] Wilson G., Moore J. S., White S. R., Sottos N. R., Andersson H., Autonomic healing of epoxy vinyl esters via ring-opening metathesis polymerisation. *Advanced Functional Materials,* 2008, 18, 44-52.

[57] Zhang J., Guo Q., Huson M., Slota I., Fox B., Interphase study of thermoplastic modified epoxy matrix composites: phase behavior around a single fibre influenced by heating rate and surface treatment. *Composites Part A: Applied Science and Manufacturing*, 2010, 41, 787-794.

[58] Hayes S. A., Zhang W., Branthwaite M., Jones F. R., Self-healing of damage in fibre-reinforced polymer-matrix composites. *Journal of the Royal Society Interface,* 2007, 4, 381-387.

[59] Hayes S. A, Jones F. R., Marshiya K., Zhang W., A self-healing thermosetting composite material. *Composites Part A: Applied Science and Manufacturing*, 2007, 38, 1116-1120.

[60] Luo X., Ou R., Eberly D. E., Singhal A., Viratyaporn W., Mather P. T., A thermoplastic/thermoset blend exhibiting thermal mending and reversible adhesion. *ACS Applied Materials & Interfaces*, 2009, 1, 612-620.

[61] Chen J., Chang F., Temperature-dependent phase behavior in poly (ε-caprolactone)-epoxy blends. *Polymer*, 2001, 42, 2193-2199.

[62] Li G., Meng H., Hu J., Healable thermoset polymer composite embedded with stimuli-responsive fibres. *Journal of the Royal Society Interface*, 2012, 9, 3279-3287.

[63] Kim B. S., Chiba T., Inoue T., A new time-temperature-transformation cure diagram for thermoset/thermoplastic blend: tetrafunctional epoxy/poly(ether sulfone). *Polymer*, 1999, 34, 13, 2809-2815.

[64] Yamanaka K., Inoue T., Structure development in epoxy resin modified with poly(ether sulphone). *Polymer*, 1989, 30, 662-667.

[65] Olmos D., González-Benito J., Visualisation of the morphology at the interphase of glass fibre-reinforced epoxy-thermoplastic polymer composites. *European Polymer Journal*, 2007, 43, 1487-1500.

[66] Cabanelas J. C., Serrano B., Baselga J., Development of cocontinuous morphologies in initially heterogeneous thermosets blended with poly(methyl methacrylate). *Macromolecules*, 2005, 38, 961-970.

[67] Ishii Y., Ryan A. J., Processing of poly(2,6-dimethyl-1,4-phenylene ether) with epoxy resin. 1. Reaction-induced phase separation. *Macromolecules*, 2000, 33, 158-166.

[68] Girard-Reydet E-, Sautereau H., Pascault J. P., Keates P., Navard P., Thollet G., Vigier G., Reaction-induced phase separation mechanisms in modified thermosets. *Polymer*, 1998, 39, 2269-2279.

[69] Yang J., Keller M., Moore J., White S., Sottos N. R., Microencapsulation of isocyanates for self-healing polymers. *Macromolecules,* 2008, 41, 9650-9655.

[70] Coope T. S., Mayer U. F. J., Wass D. F., Trask R. S., Bond I. P., Self-healing of an epoxy resin using scandium(III) triflate as a catalytic curing agent, *Advanced Functional Material*, 2011, 21, 4624-4631.

[71] Coope T. S., Wass D. F., Trask R. S., Bond I. P., Metal triflates as catalytic curing agents in self-healing fibre-reinforced composites. *Macromolecular Materials & Engineering*, 2014, 299, 208-218.

[72] Keller M. W., White S. R., Sottos N. R., A self-healing poly(dimethyl siloxane) elastomer. *Advanced Functional Materials,* 2007, 17, 2399-2404.

[73] Cho S. H., White S. R., Braun P. V., Self-healing polymer coatings. *Advanced Materials*, 2009, 21, 645-649.

[74] Beiermann B. A., Keller M. W., Sottos N. R., Self-healing flexible laminates for resealing of puncture damage. *Smart Materials and Structures,* 2009, 18, 085001.

[75] Yuan Y., Rong M., Zhang M., Chen J., Yang G., Li X., Self-healing polymeric materials using epoxy/mercaptan as the healant. *Macromolecules,* 2008, 41, 5197-5202.

[76] Xiao D., Yuan Y., Rong M., Zhang M., Hollow polymeric microcapsules: preparation, characterisation and application in holding boron trifluoride diethyl etherate. *Polymer,* 2009, 50, 560-568.

[77] Jin H., Mangun C. L., Stradley D. S., Moore J. S., Sottos N. R., White S. R., Self-healing thermoset using encapsulated epoxy-amine healing chemistry. *Polymer,* 2012, 53, 581-587.

[78] Zako M., Takano N., Intelligent material systems using epoxy particles to repair microcracks and delamination damage in GFRP. J*ournal of Intelligent Material Systems and Structures,* 1999, 10, 836-841.

[79] Sauvant-Moynot V., Gonzalez S., Kittel J., Self-healing coatings: An alternative route for anticorrosion protection. *Progress in Organic Coatings,* 2008, 63, 307-315.

[80] Yin T., Rong M. Z., Zhang M. Q., Yang G. C., Self-healing epoxy composites - Preparation and effect of the healant consisting of microencapsulated epoxy and latent curing agent. *Composites Science and Technology,* 2007, 67, 201-212.

[81] Lee J., Hong S., Liu X., Yoon S., Characterisation of dicyclopentadiene and 5-ethylidene-2-norbornene as self-healing agents for polymer composite and its microcapsules. *Macromolecular Research,* 2004, 12, 478-483.

[82] Guadagno L. *et al.*, A composite material which is self-repairing even at low temperature. *Patent WO 2009/113025 A1*, 2009.

[83] Caruso M. M., Blaiszik B. J., Jin H., Schelkopf S. R., Stradley, D. S., Sottos, N. R., White, S. R.; Moore, J. S., Robust, double-walled microcapsules for self-healing polymeric materials. *ACS Applied Materials & Interfaces,* 2010, 2, 1195-1199.

[84] Mookhoek S. D., Blaiszik, B. J., Fischer H. R., Sottos N. R., White S. R., Zwaag S. v. d., Peripherally decorated binary microcapsules containing two liquids. *Journal of Materials Chemistry,* 2008, 18, 5390-5394.

[85] Sun G., Zhang Z., Mechanical properties of melamine-formaldehyde microcapsules. *Journal of microencapsulation,* 2001, 18, 593-602.

[86] Hu J., Chen H. Q., Zhang Z., Mechanical properties of melamine formaldehyde microcapsules for self-healing materials. *Materials Chemistry and Physics,* 2009, 118, 63-70.

[87] Malloggi F., Pannacci N., Attia R., Monti F., Mary P., Willaime H., Tabeling P., Cabane B., Poncet P., Monodisperse colloids synthesised with nanofluidic technology. *Langmuir*, 2010, 26, 2369-2373.

[88] Hennequin Y., Pannacci N., Puldio de Torres C., Tetradis-Meris G., Chapuliot S., Bouchaud E., Tabeling P., Synthesizing microcapsules with controlled geometrical and mechanical properties with microfluidic double emulsion technology. *Langmuir*, 2009, 25, 7857-7861.

[89] Abate A. R., Thiele J., Weitz D. A., One-step formation of multiple emulsions in microfluidics. *Lab on a Chip - Miniaturisation for Chemistry and Biology*, 2011, 11, 253-258.

[90] Utada A. S., Lorenceau E., Link D. R., Kaplan P. D., Stone H. A., Weitz D. A., Monodisperse double emulsions generated from a microcapillary device. *Science,* 2005, 308, 537-541.

[91] Okushima S., Nisisako T., Torii T., Higuchi T., Controlled production of monodisperse double emulsions by two-step droplet breakup in microfluidic devices. *Langmuir,* 2004, 20, 9905-9908.

[92] Tetradis-Meris G., Rossetti D., Pulido de Torres C., Cao R., Lian, G., Janes R., Novel parallel integration of microfluidic device network for emulsion formation. *Industrial & Engineering Chemistry Research*, 48, 8881-8889.

[93] Park S. J., Shin Y. S., Lee J. R., Preparation and characterisation of microspheres containing lemon oil. *Journal of Colloid and Interface Science*, 2001, 241, 502-508.

[94] Brown E. N., Kessler M. R., Sottos N. R., White S. R., *In situ* poly (urea-formaldehyde) microencapsulation of dicyclopentadiene. *Journal of microencapsulation,* 2003, 20, 719-730.

[95] Li H., Wang R., Hu H., Liu W., Surface modification of self-healing poly (urea-formaldehyde) microcapsules using silane-coupling agent. *Applied Surface Science,* 2008, 255, 1894-1900.

[96] Jackson A. C., Bartelt J. A., Marczewski K., Sottos N. R., Braun P. V., Silica-protected micron and sub-micron capsules and particles for self-healing at the microscale. *Macromolecular Rapid Communications*, 2011, 32, 82-87.

[97] Rule J. A., Sottos N. R., White, S. R., Effect of microcapsule size on the performance of self-healing polymers. *Polymer,* 2007, 48, 3520-3529.

[98] Blaiszik B. J., Sottos N. R., White S. R., Nanocapsules for self-healing materials. *Composites Science and Technology,* 2008, 68, 978-986.

[99] Bon S. A. F., Mookhoek S. D., Colver P. J., Fischer H. R., van der Zwaag S., Route to stable non-spherical emulsion droplets. *European Polymer Journal,* 2007, 43, 4839-4842.

[100] Xu S., Nie Z., Seo M., Lewis P., Kumacheva E., Stone H. A., Garstecki P., Weibel D. B., Gitlin I., Whitesides G. M., Generation of monodisperse particles by using microfluidics: control over size, shape and composition. *Angewandte Chemie - International Edition,* 2005, 44, 724-728.

[101] Keller M. W., Sottos N. R., Mechanical properties of microcapsules used in a self-healing polymer. *Experimental Mechanics,* 2006, 46, 725-733.

[102] Brown E. N., Sottos N. R., White S. R., Fracture testing of a self-healing polymer composite. *Experimental Mechanics,* 2002, 42, 372-379.

[103] `http://www.sigmaaldrich.com/switzerland-schweiz.html` (accessed: 11/08/2014).

[104] Jones A., Rule J. D., Moore J. S., White S. R., Sottos N. R., Catalyst morphology and dissolution kinetics of self-healing polymers. *Chemistry of Materials,* 2006, 18, 1312-1317.

[105] Skipor A., Scheifer S., Olson B., Self-healing polymer compositions. *Patent US 7108914 B2*, 2006.

[106] Kamphaus J. M., Rule J. D., Moore, J. S., Sottos N. R., White S. R., A new self-healing epoxy with tungsten (VI) chloride catalyst. *Journal of the Royal Society Interface,* 2008, 5, 95-103.

[107] Wilson G. O., Caruso M. M., Reimer N., White S. R., Sottos N. R., Moore J. S., Evaluation of ruthenium catalysts for ring-opening metathesis polymerisation-based self-healing applications. *Chemistry of Materials,* 2008, 20, 3288-3297.

[108] Wilson G. O., Porter K. A., Weissman H., White S. R., Sottos N. R., Moore J. S., Stability of second generation Grubbs' alkylidenes to primary amines: formation of novel ruthenium-amine complexes. *Advanced Synthesis & Catalysis,* 2009, 351, 1817-1825.

[109] Liu X., Sheng X., Lee J. K., Kessler M. R., Rheokinetic evaluation of self-healing agents polymerised by Grubbs' catalyst embedded in various thermosetting systems. *Composites Science and Technology, 2009, 69*, 2102-2107.

[110] Sriram S. R., Development of self-healing polymer composites and photoinduced ring-opening metathesis polymerisation. PhD thesis, University of Illinois at Urbana-Champaign, 2002.

[111] Rule J. D., Moore J. S., ROMP reactivity of *endo*-and *exo*-dicyclopentadiene. *Macromolecules,* 2002, 35, 7878-7882.

[112] Mauldin T. C., Rule J. D., Sottos N. R., White S. R., Moore J. S., Self-healing kinetics and the stereoisomers of dicyclopentadiene. *Journal of the Royal Society Interface,* 2007, 4, 389-393.

[113] Kessler M. R., White S. R., Cure kinetics of the ring-opening metathesis polymerisation of dicyclopentadiene. *Journal of Polymer Science Part A: Polymer Chemistry,* 2002, 40, 2373-2383.

[114] Aldridge M., Shankar C., Changgua Z., Lang S., Kieffer J., Caruso M., Moore J. S., Combined experimental and simulation study of the cure kinetics of DCPD. *Journal of Composite Materials,* 2010, 44, 2605-2618.

[115] Caruso M. M., Solvent-based self-healing polymeric materials. Department of Chemistry, PhD thesis, University of Illinois at Urbana-Champaign, 2010.

[116] Wool R. P., O'Connor K. M., A theory crack healing in polymers. *Journal of Applied Physics,* 1981, 52, 5953-5963.

[117] Brown E. N., White S. R.; Sottos N. R., Microcapsule induced toughening in a self-healing polymer composite. *Journal of Materials Science,* 2004, 39, 1703-1710.

[118] Yang Y., Zhang H., Zhang J., Wang S., Duan C., He Y., The experiment study of fracture mechanics on self-healing composite material containing microcapsules. *Materials Review,* 2007, 21, 143-147.

[119] Mostovoy S., Crosley P., Ripling E., Use of crack-line-loaded specimens for measuring plane-strain fracture toughness. *Journal of Materials*, 1967, 2, 661-681.

[120] Brown E. N., White S. R., Sottos N. R., Fatigue crack propagation in microcapsule-toughened epoxy. *Journal of Materials Science*, 2006, 41, 6266-6273.

[121] Jones A. S., Rule J. D., Moore J. S., Sottos N. R., White S. R., Life extension of self-healing polymers with rapidly growing fatigue cracks. *Journal of the Royal Society Interface*, 2007, 4, 395-403.

[122] Ye X. J., Zhang J.-L., Zhu Y., Rong M. Z., Zhang M. Q., Song Y. X., Zhang H.-X., Ultrafast self-healing of polymer toward strength restoration. *ACS Applied Materials & Interfaces*, 2014, 6, 3661-3670.

[123] ASTM Standard D7136/D7136M, 2007, Standard Test Method for Measuring the Damage Resistance of a Fibre-Reinforced Polymer Matrix Composite to a Drop-Weight Impact Event.

[124] ASTM Standard D7137/D7137M, 2007, Standard Test Method for Compressive Residual Strength Properties of Damaged Polymer Matrix Composite Plates.

[125] Patel A., Sottos N. R., Wetzel E., White S. R., Autonomic healing of low-velocity impact damage in fibre-reinforced composites. *Composites Part A: Applied Science and Manufacturing*, 2010, 41, 360-398.

[126] Kalista S. J., Ward T. C., Oyetunji Z., Self-healing of poly(ethylene-comethacrylic acid) copolymers following projectile puncture. *Mechanics of Advanced Materials and Structures*, 2007, 14, 391-397.

[127] Kalista S., Ward T., Thermal characteristics of the self-healing response in poly(ethylenecomethacrylic acid) copolymers. *Journal of the Royal Society Interface*, 2007, 4, 405-411.

[128] Varley R. J., van der Zwaag S., Towards an understanding of thermally activated self-healing of an ionomer system during ballistic penetration. *Acta Materialia*, 2008, 56, 5737-5750.

[129] Moll J. L., White, S. R., Sottos N. R., A self-sealing fibre-reinforced composite. *Journal of Composite Materials*, 2010, 44, 2573-2585.

[130] Suryanarayana C., Rao K. C., Kumar D., Preparation and characterisation of microcapsules containing linseed oil and its use in self-healing coatings. *Progress in Organic Coatings*, 2008, 63, 72-78.

[131] Kumar A., Stephenson L., Murray J., Self-healing coatings for steel. *Progress in Organic Coatings,* 2006, 55, 244-253.

[132] Odom S. A., Caruso M. M., Finke A. D., Prokup A. M., Ritchey J. A., Leonard J. H., White S. R., Sottos N. R., Moore J. S., Restoration of conductivity with TTF-TCNQ charge-transfer salts. *Advanced Functional Materials,* 2010, 20, 1721-1727.

[133] Sanada K., Yasuda I., Shindo Y., Transverse tensile strength of unidirectional fibre-reinforced polymers and self-healing of interfacial debonding. *Plastics, Rubber and Composites*, 2006, 35, 67-72.

[134] Sanada K., Itaya N., Shindo Y., Self-healing of interfacial debonding in fibre-reinforced polymers and effect of microstructure on strength recovery. *The Open Mechanical Engineering Journal*, 2008, 2, 97-103.

[135] Sanada K., Effect of microstructure on the performance of unidirectional fibre composites encompassing self-healing of interfacial debonding. *Proceeding of Advances in Heterogeneous Material Mechanics*, 2008, Shanghai.

[136] Yin T., Rong M. Z., Wu J., Chen H., Zhang M. Q., Healing of impact damage in woven glass fabric reinforced epoxy composites. *Composites Part A: Applied Science and Manufacturing,* 2008, 39, 1479-1487.

[137] Blaiszik B. J., Baginska M., White S. R., Sottos N. R., Autonomic recovery of fibre/matrix interfacial bond strength in a model composite. *Advanced Functional Materials*, 2010, 20, 3547-3554.

[138] Estrada G., Vieux-Pernon C., Advani S. G., Experimental characterisation of the influence of tackifier material on preform permeability. *Journal of Composite Materials*, 2002, 36, 2297-2310.

[139] De Freitas M., Reis L., Failure mechanisms on composite specimens subjected to compression after impact. *Composite structures*, 1998, 42, 365-373.

[140] `http://www.swiss-composite.ch/` (accessed: 13/02/2013).

[141] `http://fiji.sc/wiki/index.php/Auto_Threshold#Minimum`

[142] Feng W. W., Yang W. H., On the contact problem of an in ated spherical nonlinear membrane. *Journal of Applied Mechanics, Transactions ASME*, 1973, 40, Ser E(1), 209-214.

[143] Lardner T. J., Pujara P., On the contact problem of a highly in ated spherical nonlinear membrane. *Journal of Applied Mechanics*, 1978, 45, 202-203.

[144] Liu K. K., Williams D. R., Briscoe B. J., Compressive deformation of a single microcapsule. *Physical Review E*, 1996, 54, 6673-6680.

[145] Vernet N., Ruiz E., Advani S. G., Alms J. B., Aubert M., Barari B., Barburski M., Beraud J. M., Berg D. C., Correia N. C., Danzi M., Delavière T., Dickert M., Di Fratta C., Endruweit A., Ermanni P., Francucci G., Garcia J. A., George A., Hahn C., Klunker F., Lomov S. V., Long A., Louis B., Maldonado J., Meier R., Michaud V., Perrin H., Pillai K., Rodriguez E., Trochu F., Verheyden S., Weitgrefe M., Xiong W., Zaremba S., Ziegmann G., Experimental determination of the permeability of textile preforms: Benchmark II. *Composites Part A: Applied Science and Manufacturing,* 2014, 61, 172-184.

[146] Merhi D., Michaud V., Comte E., Månson J.-A. E.. Predicting sizing dependent bending rigidity of glass fibre bundles in sheet molding compounds. *Composites Part A: Applied Science and Manufacturing,* 2006, 37, 1773-1786.

[147] ASTM Standard D5528-13, 2014, Standard Test Method for Mode I Interlaminar Fracture Toughness of Unidirectional Fibre-Reinforced Polymer Matrix Composites.

[148] JIS, Standard K7086, 1993, Testing Methods for Interlaminar Fracture Toughness of Carbon-Fibre-Reinforced Plastics.

[149] Schuecker C., Davidson B. S., Evaluation of the accuracy of the four-point bend end-notched flexure test for mode II delamination toughness determination. *Composites Science & Technology*, 2000, 60, 2137-2146.

[150] Davidson B. D., Sun X. K., Effects of friction, geometry and fixture compliance on the perceived toughness from three- and four-point bend end-notched flexure tests. *Journal of Reinforced Plastics and Composites*, 2005, 24, 1611-1628.

[151] Sun X. K., Davidson B. D., Numerical evaluation of the effects of friction and geometric nonlinearities on the energy release rate in three- and four-point bend end-notched flexure tests. *Engineering Fracture Mechanics*, 2006, 73, 1343-1361.

[152] de Moura M. F. S. F., de Morais A. B., Equivalent crack based analyses of ENF and ELS tests. *Engineering Fracture Mechanics*, 2008, 75, 2584-2596.

[153] de Morais A.B., Novel cohesive beam model for the end-notched flexure (ENF) specimen. *Engineering Fracture Mechanics*, 2011, 78, 3017-3029.

[154] J.-K. Kim, Y.-W. Mai, Engineered interfaces in fiber-rienforced composites, 1998, Elsevier.

[155] Saunders R., Lekakou C., Bader M., Compression in the processing of polymer composites 1. A mechanical and microstructural study for different glass fabrics and resins. *Composites Science and Technology*, 1999, 59, 983-993.

[156] Saunders R., Lekakou C., Bader M., Compression in the processing of polymer composites 2. Modelling of the viscoelastic compression of resin-impregnated fibre networks. *Composites Science and Technology*, 1999, 59, 1483-1494.

[157] Toll S., Packing mechanics of fibre reinforcements. *Polymer Engineering & Science*, 1998, 38, 1337-1350.

[158] Servais C., Michaud V., Månson J.-A. E., The packing stress of impregnated fibre mats. *Polymer Composites,* 2001, 22, 298-311.

[159] Chen B., Chou T.-W., Compaction of woven-fabric preforms in liquid composite molding processes: single-layer deformation. *Composites Science & Technology,* 1999, 59, 1519-1526.

[160] Chen B., Chou T.-W., Compaction of woven-fabric preforms: nesting and multi-layer deformation. *Composites Science & Technology,* 2000, 60, 2223-2231.

[161] Chen B., Lang E. J., Chou T.-W., Experimental and theoretical studies of fabric compaction behavior in resin transfer molding. *Materials Science and Engineering: A*, 2001, 317, 188-196.

[162] Somashekar A. A., Bickerton S., Bhattacharyya D., An experimental investigation of non-elastic deformation of fibrous reinforcements in composites manufacturing. *Composites Part A: Applied Science and Manufacturing,* 2006, 37, 858-867.

[163] Somashekar A, A., Bickerton S., Bhattacharyya D., Exploring the non-elastic compression deformation of dry glass fibre reinforcements. *Composites Science & Technology,* 2007, 67, 183-200.

[164] Kelly P. A., Transverse compression properties of composite reinforcements. In *Composite reinforcements for optimum performance*, P. Boisse, ed. Woodhead Publishing, 2011.

[165] Tanoğlu M., Tuğrul Seyhan A., Compressive mechanical behavior of E-glass/polyester composite laminates tailored with a thermoplastic preforming binder. *Materials Science and Engineering: A*, 2003, 363, 335-344.

[166] Michaud V., Månson, J.-A. E., Impregnation of compressible fiber mats with a thermoplastic resin. Part I: theory. *Journal of Composite Materials*, 2001, 35, 1150-1173.

[167] Michaud V., Månson, J.-A. E., Impregnation of compressible fiber mats with a thermoplastic resin. Part II: experiments. *Journal of Composite Materials*, 2001, 35, 1174-1200.

[168] Cherry J. A., Freeze R. A., In *Groundwater*, ed. Prentice Hall (Englewood Cliffs N. J.), 1979.

[169] Alif N., Carlsson L. A., Gillespie J. W., Mode I, mode II and mixed mode interlaminar fracture of woven fabric carbon/epoxy. In *Composites materials: testing and design*, vol 13, ed. S. J. Hooper, ASTM International, 1997.

[170] Ebeling T., Hiltner A., Baer E., Delamination failure mechanisms in microlayers of polycarbonate and poly(styrene-co-acrylonitrile). *Journal of Applied Polymer Science*, 1998, 68, 793-805.

[171] Chen P. W., Cadisch G., Studart A. R., Encapsulation of aliphatic amines using microfluidics. *Langmuir*, 2014, 30, 2346-2350.

[172] Neuser S., Chen P. W., Studart A. R., Michaud V., Fracture toughness healing in epoxy containing both epoxy and amine loaded capsules. *Advanced Engineering Materials*, 2014, 16, 581-587.

[173] Varley R. J., Craze D. A., Mouritz A. P., Wang C. H., Thermoplastic healing in epoxy networks: exploring performance and mechanism of alternative healing agents. *Macromolecular Materials and Engineering*, 2013, 298, 1232-1242.

[174] Meure S., Wu D.-Y., Furman S., Polyethylene-co-methacrylic acid healing agents for mendable epoxy resins. *Acta Materialia,* 2009, 57, 4312-4320.

[175] Meure S., Wu D.-Y., Furman S., FTIR study of bonding between a thermoplastic healing agent and a mendable epoxy resin. *Vibrational Spectroscopy*, 2010, 52, 10-15.

[176] Pingkarawat K., Bhat T., Craze D. A., Wang C. H., Varley R. J., Mouritz A. P., Healing of carbon fibre–epoxy composites using thermoplastic additives. Polymer Chemistry, 2013, 4, 5007-5015.

[177] Tuli R. A., George G. A., Dargaville T. R., Islam N., Studies on the effect of the size of polycaprolactone microspheres for the dispersion of salbutamol sulfate from dry powder inhaler formulations. *Pharmaceutical Research*, 2012, 29, 2445-2455.

[178] Tuli R. A., Dargaville T. I. M. R., George G. A., Islam N., Polycaprolactone microspheres as carriers for dry powder inhalers: effect of surface coating on aerosolisation of salbutamol sulfate. *Pharmaceutical Technology*, 2012, 101, 733-745.

ERICA MANFREDI

RUE DE TERREAUX 6, 1003 LAUSANNE, SWITZERLAND
+41 78 9154111 (CH), +39 349 4567878 (I)
erica.manfredi@epfl.ch (current job)
erichesca@gmail.com (personal)

Professional Experience

2011-2015 **PhD in Material Science**
Laboratoire de Technologie des Composites et Polymères (LTC), Ecole Polytechnique Fédérale de Lausanne (EPFL), Switzerland

2010 **Internship (6 months)**
Centre of Innovation and Research in Materials & Polymers (CIRMAP), Mons, Belgium

Education

2008-2010 **Master of Science**
Materials Engineering, Politecnico di Torino
- 4-months Erasmus program at Université de Mons, Belgium
- Thesis: "Poly(lactic acid)/non-covalent surface-surface functionalised carbon nanotubes (nano)composites: preparation and characterisation", supervised by Proff. Philippe Dubois and Giulio Malucelli, discussed in October 2010.

2005-2008 **Bachelor degree**
Materials Engineering, Politecnico di Torino
- Thesis: "Synthesis and characterization of a polymeric self-healing composite", Politecnico di Torino, supervised by Prof. Giulio Malucelli

1999-2005 **High school**
Liceo Classico Statale Vittorio Alfieri (Torino)

Publications

- Supramolecular design of high-performance poly(L-lactide)/carbon nanotube nanocomposites: from melt-processing to rheological, morphological and electrical properties, Erica Manfredi, Franck Meyer, Pierre Verge, Jean-Marie Raquez, Jean-Michel Thomassin, Michael Alexandre, Bart Dervaux, Filip DuPrez, Pascal Van Der Voort, Christine Jérôme, Philippe Dubois, *J Mater Chem* 2011, 21, 16190-16196.

- Characterization of solvent-filled polyurethane/urea-formaldehyde core-shell composites, Sam Neuser, Erica Manfredi, Véronique Michaud, *Mat Chem Phys* 2014;143(3):1018-1025.

- Packing and permeability properties of E-glass fibre reinforcements functionalised with capsules for self-healing applications, Erica Manfredi, Véronique Michaud, *Compos Part A-Appl S* 2014;66:94-102.

- Assessment of solvent capsule-based healing for woven E-glass fibre-reinforced polymers, Erica Manfredi, Amaël Cohades, Inès Richard, Véronique Michaud, Smart *Mater Struct* 2015;24(1):015019.

- Polycaprolactone/epoxy blends for thermal mending applications in woven E-glass fibre-reinforced polymers, Erica Manfredi, Amaël Cohades, Alexandre Mordasini, Véronique Michaud, in preparation.

Conferences And Seminars

- MRS Fall 2014 (oral presentation), December 2014, Boston (USA)

- FPCM 2014 (oral presentation), July 2014, Enschede (NL)

- EDMX Research Day (oral presentation), September 2013, Lausanne (CH)

- ICSHM 2013 (oral presentation), June 2013, Ghent (B)

- IOP Self-healing Materials Summer School, September 2012, Vlieland (NL)

- ICSHM 2011 (participation), June 2011, Bath (UK)

Personal Situation

Nationality	Italian
Citizenship	Swiss (B Permit)
Place of birth	Torino
Date of birth	22/07/1986
Driver's licence	A1, B
Marital status	Single